IMPROVING RELIABILITY AND ASSESSING PERFORMANCE OF GLOBAL NAVIGATION SATELLITE SYSTEM PRECISE POINT POSITIONING AMBIGUITY RESOLUTION

GARRETT SEEPERSAD

A DISSERTATION SUBMITTED TO THE FACULTY OF GRADUATE STUDIES
IN PARTIAL FULFILLMENT OF THE REQUIREMENTS FOR THE DEGREE OF
DOCTOR OF PHILOSOPHY

GRADUATE PROGRAMME IN EARTH AND SPACE SCIENCE
YORK UNIVERSITY
TORONTO, ONTARIO

AUGUST, 2018

ABSTRACT

Conventional Precise Point Positioning (PPP) has always required a relatively long initialization period (few tens of minutes at least) for the carrier-phase ambiguities to converge to constant values and for the solution to reach its optimal precision. The classical PPP convergence period is primarily caused by the estimation of the carrier-phase ambiguity from the relatively noisy pseudoranges and the estimation of atmospheric delay. If the underlying integer nature of the ambiguity is known, it can be resolved, thereby reducing the convergence time of conventional PPP.

To recover the underlying integer nature of the carrier-phase ambiguities, different strategies for mitigating the satellite and receiver dependent equipment delays have been developed, and products made publicly available to enable ambiguity resolution without any baseline restrictions. There has been limited research within the scope of interoperability of the products, combining the products to improve reliability and assessment of ambiguity resolution within the scope of being an integrity indicator. This study seeks to develop strategies to enable each of these and examine their feasibility.

The advantage of interoperability of the different PPP ambiguity resolution (PPP-AR) products would be to permit the PPP user to transform independently generated PPP-AR products to obtain multiple fixed solutions of comparable precision and accuracy. The ability to provide multiple solutions would increase the reliability of the solution for, e.g., real-time processing: if there were an outage in the generation of the PPP-AR products, the user could instantly switch streams to a different provider.

The satellite clock combinations routinely produced within the International GNSS Service (IGS) currently disregard that analysis centers (ACs) provide products which enable ambiguity resolution. Users have been expected to choose either an IGS product which is a combined product from multiple ACs or select an individual AC solution which provides products that enable PPP-AR. The goal of the novel research presented was to develop and test a robust satellite clock combination preserving the integer nature of the carrier-phase ambiguities at the user end. mm-level differences were noted, which was expected as the strength lies mainly in its reliability and stable median performance and the combined product is better than or equivalent to any single AC's product in the combination process.

As have been shown in relative positioning and PPP-AR, ambiguity resolution is critical for enabling cm-level positioning. However, what if specifications where at the few dm-level, such as 10 cm and 20 cm horizontal – what role does ambiguity resolution play? The role of ambiguity resolution relies primarily on what are the user specifications. If the user specifications are at the few cm-level, ambiguity resolution is an asset as it improves convergence and solution stability. Whereas, if the user's specification is at the few dm-level, ambiguity resolution offers limited improvement over the float solution. If the user has the resources to perform ambiguity resolution, even when the specifications are at the few dm-level, it should be utilized.

DEDICATION

To: Grandma, Mom, Dad, Dawn, Noah, Glenroy and Alexandra

ACKNOWLEDGEMENTS

As with most journeys in life, this thesis took me along a pathway that I could have never predicted. It could not have been completed successfully without the invaluable support from several people.

Especial thanks to my supervisor, Dr. Sunil Bisnath who provided me with the opportunity to embark on this journey. He never ceased to challenge me, redirected my path after each setback, and always encouraged me to believe in myself as I forged ahead. He also created countless networking opportunities for me through conferences and multiple internships for which I am extremely grateful. Thanks to Dr. Bisnath for his invaluable support with technical advice, financial assistance, and an amicable work environment. I also wish to thank Drs. Jian-Guo Wang, Spiros Pagiatakis and Costas Armenakis for their priceless corridor consultations and insightful feedback.

A memorable guest lecture from the late Dr. Kees de Jong in 2013 at York University, Canada led to an internship at Fugro Intersite, Netherlands. The work relationship with Drs. Kees de Jong, Xianglin Liu and Matthew Goode and Ms. Karin Cambier at Fugro was commendable. The experience obtained from this internship augured well with core of my research. Special thanks to the Etienne van der Kuij of ProTanks Group in Rotterdam, Netherlands for the first-hand knowledge gained in assessing the performance of GNSS within the Rotterdam World Gateway (RWG).

In 2016, I was selected to serve at the Geodetic Surveying Division of the Canadian Federal Government as part of the Research Affiliate Program (RAP). I am deeply indebted to Dr.

Simon Banville, Paul Collins and François Lahaye for their shrewd and skillful supervision. To the pioneers of Precise Point Positioning, Jan Kouba and Pierre Héroux, my direct consultation with them is invaluable. A special thanks to Paul for his innovative techniques in the development of the decoupled clock model which serves as the foundation of this research. I also wish to acknowledge NRCan for providing the base PPP code and PPP expertise.

York University was not just a school, but also a home and my colleagues and I became a family. A special thanks to John Aggrey, Amir Saeidi, Amandeep Mander, Surabhi Guruprasad, Maninder Gill and Siddharth Dave. Thanks to John for his contributions to the development of the YorkU-PPP software. Without his support, YorkU-PPP could not have been the powerful tool that it is today.

While the journey of a PhD takes a lot of self discipline, dedication and hard work none of it would have been possible without the support of my family. Thanks to Grandma, Mom, Dad, Dawn, Noah, Glenroy, Shiva, Alexandra, Taylia, Shana, Ravi, Damian, Vivek and Vachan. I will always be indebted to them for their prayers, sacrifices and encouragements.

TABLE OF CONTENTS

Abstract ii

Dedication iv

Acknowledgements v

Table of Contents vii

List of Tables xi

List of Figures xii

List of Acronyms xvii

List of Symbols xxi

CHAPTER 1 Introduction into PPP GNSS measurement processing 1

1.1 The origins of Precise Point Positioning 2

1.2 Review of PPP ambiguity resolution 9

1.3 GNSS performance parameters 13

1.4 Problem Statement 17

1.5 Thesis Statement 19

1.6 Research Contributions 19

1.7 Thesis Outline 22

CHAPTER 2 Evolution of the PPP user model 25

2.1 Introduction into Point Positioning 25

2.2 Conventional PPP model 26

2.3 PPP-AR model 30

2.3.1 Receiver equipment delay 36
2.3.2 Satellite equipment delay 39
2.4 Slant ionosphere estimation 39
2.5 Multi-GNSS PPP 46
2.6 Multi-frequency PPP 51
2.7 Summary of PPP evolution 54
CHAPTER 3 Examination of the interoperability PPP-AR products 57
3.1 Introduction into PPP-AR product interoperability 57
3.2 PPP-AR Products 60
3.2.1 Decoupled clocks 60
3.2.2 Fractional Cycle Bias 65
3.2.3 Integer Recovery Clock 69
3.2.4 Summary of available PPP-AR products 73
3.3 Dataset and processing parameters used to quantify performance of PPP-AR 76
3.4 Performance of transformed products 78
3.5 Challenges in interoperability of PPP-AR products 83
3.5.1 Axis convention 83
3.5.2 Yaw manoeuvres during satellite eclipse 84
3.6 Summary of the performance of PPP-AR product interoperability 86
CHAPTER 4 Improving reliability of PPP-AR products 89
4.1 Introduction to satellite clock combination 89
4.2 Satellite clock combination of common clocks 91
4.3 Combining clock products that enable PPP-AR 94

4.3.1 Combination process of PPP-AR clock products 95
4.3.2 Combined clock products 96
4.4 Aligning IGS common clocks to clock products that enable PPP-AR 102
4.5 Performance of combined satellite clock products 104
4.6 Summary of the benefits of combining AR products 107
CHAPTER 5 Reassessing the role of ambiguity resolution in PPP 110
5.1 Introduction 110
5.2 Ambiguity resolution 112
5.2.1 Partial Ambiguity resolution 112
5.2.2 Resolving and fixing the ambiguities 114
5.3 Ambiguity validation 117
5.4 Assessment of the role of ambiguity resolution in PPP 119
5.4.1 Convergence 120
5.4.2 Position uncertainty 125
5.4.3 Post-fit and integer-fit residuals 128
5.5 Conclusions 134
CHAPTER 6 Conclusions and Recommendations for Future Research 137
6.1 Research Conclusions 137
6.1.1 Uncombining the PPP representation 138
6.1.2 Interoperability of the PPP-AR products 139
6.1.3 Combining the PPP-AR products 141
6.1.4 Re-examining the role of ambiguity resolution 143
6.2 Research recommendations for the near future 143

6.2.1 Real time PPP-AR with low GNSS receiver and antenna 144
6.2.2 Improving the stochastic model 145
6.2.3 Low-cost, multi-sensor integration 146
6.2.4 A priori atmospheric corrections 148
References 150

LIST OF TABLES

Table 1.1 Summary of error sources in PPP, mitigative strategy and residuals (Seepersad and Bisnath 2014a) 6

Table 2.1: Preferred measurements within YorkU-PPP multi-GNSS model. 56

Table 3.1: Comparison of different public providers of products to enable PPP-AR 75

Table 3.2: Summary of the transformation of the PPP-AR products to the combined DCM format and uncombined representation..... 76

Table 3.3: rms error of the final solution produced by YorkU-PPP from 24-hour datasets using data from 155 sites for DOY 178 to 184, GPS week 1903, of 2016 provided by the IGS. Satellite products were provided by NRCan, CNES and Wuhan University. All units are in millimetres. 79

Table 4.1: Estimated parameters in satellite clock combination and associated constraints. 93

Table 4.2: Fixed terms in the adjustment to remove rank deficiency. 94

Table 5.1: Summary statistics of ambiguity resolved, and ambiguity validated solutions for the station ALGO. Statistics compares the performance of ambiguity validation in relative positioning and PPP-AR. GNSS data from DOY 178 of 2016 was used. All units are in cm. 134

LIST OF FIGURES

Figure 1.1 Fundamental idea underlying the SPS technique as compared to PPP (Seepersad and Bisnath 2014a). 4

Figure 1.2 Range to position and time domain transformations in PPP data processing illustrating the different domains of PPP error sources (Seepersad and Bisnath 2014a).... 5

Figure 1.3: Current research areas in Precise Point Positioning. 8

Figure 1.4: Illustration of the difference between the “float” and “fixed” solution in the horizontal component. NRC1 DOY 179, 2016 located in Ottawa, Canada. 10

Figure 1.5: Evolution of the PPP user model. 11

Figure 1.6 Current research areas within PPP ambiguity resolution. 13

Figure 1.7 Multi-GNSS Experiment (MGEX) product availability (IGS 2018a) 15

Figure 2.1: Conceptual illustration of the integer nature of the ambiguity term affected by receiver and satellite equipment delays. 29

Figure 2.2: Different correction terms transmitted in observation space and state space representation (Wübbena 2012). 33

Figure 2.3: Illustration of the residuals for PRN 4 of P1 and P2 pseudorange measurements, combined P1 and P2 and linearly combined ionosphere-free pseudorange measurements for the site NRC1 DOY 178 of 2016 located in Ottawa, Canada. 46

Figure 2.4: Transition towards the uncombined PPP mathematical model. 56

Figure 3.1: Relative satellite carrier-phase clock correction provided by NRCan on DOY 178 of 2016 for PRN 28 (relative to PRN 5). Linear trend has been removed. All units are in metres. 62

Figure 3.2: Satellite code clock offset provided by NRCan on DOY 178 of 2016 for PRN 28. All units are in metres. 62

Figure 3.3: Satellite widelane correction provided by NRCan on DOY 178 of 2016 for PRN 28. All units are in metres. 63

Figure 3.4: Code dependent equipment delay corrections. Corrections were generated from products provided by NRCan on DOY 178 of 2016 for PRN 28. All units are in metres. 65

Figure 3.5: Relative satellite carrier-phase clock correction provided by Wuhan University utilizing IGS products on DOY 178 of 2016 for PRN 28 (relative to PRN 5). Linear trend has been removed. All units are in metres. 66

Figure 3.6: L1 satellite equipment delay provided by Wuhan University on DOY 178 of 2016 for PRN 28. All units are in metres..... 67

Figure 3.7: Wide lane satellite equipment delay provided by Wuhan University on DOY 178 of 2016 for PRN 28. All units are in metres. 67

Figure 3.8: Uncombined code satellite equipment delay provided by Wuhan University on DOY 178 of 2016 for PRN 28 using IGS Final products. All units are in metres. 69

Figure 3.9: Relative satellite carrier-phase clock correction provided by CNES on DOY 178 of 2016 for PRN 28 (relative to PRN 5). Linear trend has been removed. All units are in metres. 71

Figure 3.10: Wide lane correction provided by CNES on DOY 178 of 2016 for PRN 28. All units are in metres. 71

Figure 3.11: Uncombined satellite code clock provided by CNES on DOY 178 of 2016 for PRN 28. All units are in metres..... 73

Figure 3.12: Uncombined satellite phase clock provided by CNES on DOY 178 of 2016 for PRN 28. All units are in metres..... 73

Figure 3.13: Global distribution of the selected 155 IGS stations observed during DOY 178 to 184, GPS week 1903, of 2016. 78

Figure 3.14: Site NRC1 DOY 178 of 2016 located in Ottawa, Canada, illustrating the differences between the “float” and “fixed” solution in the horizontal component where insets for each figure represents the initial 30 minutes of convergence time. Limits of y-axis represents position error. 81

Figure 3.15: Site NRC1 DOY 178 of 2016 located in Ottawa, Canada, illustrating the differences between the “float” and “fixed” solution in the vertical component where insets for each figure represents the initial 30 minutes of convergence time. Limits of y-axis represents position error. 82

Figure 3.16: Orientation of the spacecraft body frame for GPS Block IIR/IIR-M satellites (a) manufacturer specification system; (b) IGS axis conventions (Montenbruck et al. 2015). 84

Figure 3.17: Geometry of an eclipsing satellite, where β is elevation of the Sun above the orbital plane and μ is the spacecraft’s geocentric orbit angle. “Midnight” denotes the farthest point of the orbit from the Sun whereas “noon” denotes the closest point. From Dilssner et al. (2011). 86

Figure 4.1: Overview of the steps required to combine satellite clocks products that enable PPP-AR..... 95

Figure 4.2: Inconsistent error modelling during a satellite eclipse for PRN 24 with respect to PRN 1, Block IIF on DOY 178 of 2016 between IRC and DCM. 98

Figure 4.3: Convergence of the forward run of DCM L1 satellite offset with respect to the IRC on DOY 178, 2016 with the differences in yaw manoeuvres and axis convention taken into consideration. Each colour represents a different satellite with the integer component removed from each time series. 99

Figure 4.4: Convergence of the DCM L1 satellite offsets with respect to the IRC for DOY 179, 2016 with the differences in axis convention not account for. Each colour represents a different satellite with the integer component removed from each time series. 99

Figure 4.5: Convergence of the DCM L1 satellite offset with respect to the IRC on DOY 179, 2016 with the differences in axis convention account for. Each colour represents a different satellite with the integer component removed from each time series. 100

Figure 4.6: Convergence of the DCM widelane satellite offset with respect to the IRC on DOY 178, 2016. Each colour represents a different satellite with the integer component removed from each time series. 101

Figure 4.7: Time reference parameter of DCM with respect to IRC on DOY 178, 2016. 101

Figure 4.8: Post-fit residuals of the combined clock (IRC and DCM) with respect to the reference clock (IRC) on DOY 178, 2016. 102

Figure 4.9: Convergence of the forward run of IGS L1 satellite offset with respect to the IRC on DOY 178, 2016. Each colour represents a different satellite with an integer component removed from each time series. 103

Figure 4.10: Time reference parameter of IGS with respect to IRC on DOY 178, 2016. 103

Figure 4.11: Post-fit residuals of the combined clock (IRC and IGS) with respect to the reference clock (IRC) on DOY 178, 2016. 104

Figure 4.12: Overview of analysis centres used to generate combined products IGS-AR and IRC+DCM..... 105

Figure 4.13: Examination of the repeatability of the PPP user solution in static mode utilizing different types of clock products. Statistics are based on GPS data from 155 IGS stations were observed during DOY 178 to 184, of 2016. All units are in millimetres. 106

Figure 4.14: Examination of the repeatability of the PPP user solution in kinematic mode utilizing different types of clock products. Statistics are based on GPS data from 155 IGS stations were observed during DOY 178 to 184, of 2016. All units are in millimetres. 107

Figure 5.1: Schematic approach to fixing (Collins et al. 2010). 117

Figure 5.2: Definition of convergence. 122

Figure 5.3: Cumulative histogram illustrating the required convergence of time to attain 20 cm horizontal for the float and fixed solutions. 123

Figure 5.4: Cumulative histogram illustrating the required convergence of time attain 10 cm horizontal for the float and fixed solutions. 124

Figure 5.5 Cumulative histogram illustrating the required convergence of time attain 2.5 cm horizontal for the float and fixed solutions. 125

Figure 5.6: Solution integrity for the horizontal component. 128

Figure 5.7: Performance of ambiguity validated solution at site ALGO DOY 178 of 2016 located in Algonquin Park, Canada. Upper plot illustrates the easting component and the lower plot is the northing component. 130

Figure 5.8: Station distribution used to compare the performance of ambiguity validation in single baseline relative positioning and PPP-AR. 131

Figure 5.9: Comparison of the ambiguity validated solution between long single baseline relative positioning and PPP-AR. For relative positioning ALGO was coordinated with respect to BAIE with a baseline length of 819 km and with respect to NRC1 199 km. GNSS data from DOY 178 of 2016 was used. 133

LIST OF ACRONYMS

AC	Analysis Centre
AR	Ambiguity resolution
BeiDou/BDS	Chinese Navigation Satellite System
CC1	Common Clock model
CDDIS	Crustal Dynamics Data Information System
CDMA	Code Division Multiple Access
CIR	Cascade Integer Resolution
CNES	Centre National d'Etudes Spatiales
CODE	Center for Orbit Determination in Europe
DCB	Differential Code Bias
DCM	Decoupled Clock Model
DGPS	Differential GPS
DOY	Day of year
EWL	Extra widelane
FARA	Fast Ambiguity Resolution Approach
FASF	Fast Ambiguity Search Filter
FCB	Fractional Cycle Biases
FDMA	Frequency Division Multiple Access
GALILEO	European Navigation Satellite System
GBAS	Ground-Based Augmentation System
GEO	Geostationary Orbit
GF	Geometry Free

GFZ	GeoForschungsZentrum, Germany
GLONASS	Russian Navigation Satellite System
GNSS	Global Navigation Satellite System
GPS	United States Navigation Satellite System
GRG	CNES IGS analysis center solution
GRGS	Le Groupe de Recherche de Géodésie Spatiale
ICB	Inter-frequency Channel Bias
IF	Ionosphere-free linear combination
IGN	Institut Geographique National, France
IGR	IGS Rapid
IGS	International GNSS Service
IRC	Integer Recovery Clock
JPL	Jet Propulsion Lab
KASI	Korean Astronomy and Space Science Institute
LAMBDA	Least-squares AMBiguity Decorrelation Adjustment
LSAST	Least-Squares Ambiguity Search Technique
MEO	Medium Earth Orbit
MGEX	Multi-GNSS Experiment
MLAMBDA	Modified LAMBDA
MW	Melbourne-Wübbena
NAS	National Airspace System
NL	Narrowlane linear combination
NNSS	U.S. Navy Navigation Satellite System

NRCan	Natural Resources Canada
NRTK	Network RTK
OMEGA	Optimal Method for Estimating GPS Ambiguities
OSR	Observation Space Representation
PPP	Precise Point Positioning
PPP-AR	Precise Point Positioning Ambiguity Resolved
PPS	Precise Positioning Service
PRN	Pseudorandom noise
PTC	Positive Train Control
QC	Quality Control
RAP	Research Affiliate Program (RAP) of the Canadian Federal Government
RINEX	Receiver Independent Exchange Format
RTCM	Radio Technical Commission for Maritime Services
RTK	Real Time Kinematic
RTKLIB	Real Time Kinematic Library
SAVO	Sequential fixing Ascending Variance Order
SBAS	Satellite-Based Augmentation Systems
SEBLO	Sequential BLewitt fixing Order
SGG-WHU	Wuhan University School of Geodesy and Geomatics
SINEX	Site Independent Exchange Format
SOFOS	Sequential Optimum Fixing Order Search
SPP	Single Point Positioning
SPS	Standard Positioning Service

SSR	State Space Representation
TCAR	Three Carrier Ambiguity Resolution
TEC	Total Electron Content
TTFF	Time to first fix
UPD	Uncalibrated Phase Delay
VTEC	Vertical Total Electron Content
WAAS	Wide Area Augmentation System
WL	Widelane linear combination
YorkU	York University
YorkU-PPP	PPP software developed at York University

LIST OF SYMBOLS

i	identifies frequency-dependant terms
P	measured pseudorange on L_i (m)
Φ	measured carrier-phase on L_i (m)
dt	clock error (m) common to pseudorange and carrier-phase measurements
δt	clock error (m) common to carrier-phase measurements only
ρ	true geometric range (m)
d	code equipment delay (m)
δ	carrier-phase equipment delay (m)
α	measurement combination co-efficient
β	measurement combination co-efficient
λ	wavelength (m)
A	carrier-phase ambiguity (m)
N	carrier-phase ambiguity (cycles)
I	slant ionosphere delay on L_i (m)
μ_i	constant $= \frac{f_1^2}{f_i^2}$ frequency dependent coefficient
u	user position
a_{FCB}	measurement equipment delay generated using FCB model
s	satellites
m	number of visible satellites from user's position
$\overline{dt}$	combined clock error
B_a	AC-specific bias
a	analysis centre
n	number of analysis centres
ψ_a^s	consistency correction

$\vec{X}_a^s$	AC satellite position vector
$\vec{X}_{IGS}^s$	the IGS combined satellite position vector
$\vec{D}_a$	geocentre offset vector provided by the respective AC
$\lvert\ \rvert$	computation of the radius vector with respect to the centre of the Earth
$\overline{\delta}$	combined equipment delay
K	Boolean matrix
c	vacuum speed of light (m/s)
τ	pre-selected ratio threshold

CHAPTER 1 INTRODUCTION INTO PPP GNSS MEASUREMENT PROCESSING

Navigation is a very ancient skill or art, which has become a complex science. It is essentially about travel and finding the way from one place to another and there are a variety of means by which this objective may be achieved (Britting 1971). Navigation has been evolving since the beginning of human history and has always been a critical aspect in our (society's) development. Navigation systems have taken many forms, varying from simple ones such as those making use of landmarks, compasses and stars, to more modern techniques such as the utilization of artificial satellites.

Satellite-based navigation technology was introduced in the early 1960s. The first such system was the U.S. Navy Navigation Satellite System (NNSS), known as TRANSIT, in which the receiver measured Doppler shifts of the signal as the satellite transited with a navigational accuracy of 25-500 m. In 1978, the Global Positioning System (GPS) was introduced. GPS is a satellite-based radio-positioning and time transfer system designed to provide all-weather, 24-hour coverage for military users and reduced accuracy for civilian users. Since then, it has become the backbone of a whole body of navigation and positioning technologies.

Currently, the U.S., Russia, the European Union (E.U.), and China are each operating or in the case of the latter two, developing individual Global Navigation Satellite Systems (GNSS's): GPS, GLONASS, GALILEO and BeiDou, respectively. Evolving GNSSs can provide the worldwide community with several benefits, such as the ability to work in

challenging environments with limited visibility of satellites, increased positioning accuracy, more robust detection and exclusion of anomalies, more accurate timing reference as well as improved estimation of tropospheric and ionospheric parameters.

GNSSs can be augmented with other systems which leads to an improvement in the navigation system's attributes, such as accuracy, precision, reliability, availability and integrity through the integration of external information into the adjustment process. These augmentation systems can be broadly grouped into satellite-based augmentation systems (SBAS) and ground-based augmentation system (GBAS). SBAS supports wide-area or regional augmentation through the use of additional satellite-broadcast messages where as GBAS utilizes terrestrial based radio messages. Additional information on augmentation systems can be found in Hofmann-Wellenhof et al. (2007), Kaplan and Hegarty (2006), Kee et al. (1991), Leick (1995) and Van Diggelen (2009).

1.1 The origins of Precise Point Positioning

The concept of Precise Point Positioning (PPP) is based on standard, single-receiver, single-frequency point positioning using pseudorange measurements, but with the metre-level satellite broadcast orbit and clock information replaced with centimetre-level precise orbit and clock information, along with additional error modelling and dual-frequency pseudorange and carrier-phase measurement filtering (Bisnath et al. 2018).

In 1995, researchers at Natural Resources Canada were able to reduce GPS horizontal positioning error from tens of metres to the few- metre level with code measurements and precise orbits and clocks in the presence of Selective Availability (SA) (Héroux and Kouba

1995). Subsequently, the Jet Propulsion Laboratory introduced PPP as a method to greatly reduce GPS measurement processing time for large static networks (Zumberge et al. 1997). SA entailed intentional dithering of the satellite clocks and falsification of the navigation message (Leick 1995). Since SA was turned off in May 2000 and GPS satellite clock estimates could then be more readily interpolated. Hence, the PPP technique became scientifically and commercially popular for certain precise applications (Kouba and Héroux 2001).

Unlike static relative positioning and RTK, conventional PPP did not make use of double-differencing, which is the mathematical differencing of simultaneous pseudorange and carrier-phase measurements from reference and remote receivers to greatly reduce or eliminate many error sources. Rather, conventional PPP applies precise satellite orbit and clock corrections estimated from a sparse global network of satellite tracking stations in a state-space version of a Hatch filter (in which the noisy, but unambiguous, code measurements are filtered with the precise, but ambiguous, phase measurements) (Bisnath et al. 2018). In conventional PPP, when attempting to combine satellite positions and clocks errors precisely to a few centimetres with ionospheric-free pseudorange and carrier-phase observations, it is important to account for some effects that may not have been considered in Standard Positioning Service (SPS). The GPS Standard Positioning Service (SPS) is a positioning and timing service provided by way of ranging signals broadcasted on the GPS L1 frequency. The L1 frequency, transmitted by all satellites, contains a coarse/acquisition (C/A) code ranging signal, with a navigation data message, that is available for peaceful civil, commercial, and scientific use (US DoD 2001). Figure 1.1

directly compares the approaches of SPS and PPP. In the SPS, metre-level real-time satellite orbit and clock information is supplied to the user by each GPS satellite. For single-frequency users, ionospheric refraction information is also required. For the troposphere a common mapping function for wet and dry troposphere is utilized (Collins 1999a) in contrast to PPP that considers different obliquity factors for the wet and dry components (Seepersad 2012). All of this information is combined with C/A-code pseudorange measurements to produce metre level user position estimates (Bisnath and Collins 2012). Where as in PPP, the same receiver tracking information as in SPP is utilized but cm-level precise orbit and clock information together with additional error modelling and filtering is utilized to enable dm to mm level user position estimation.

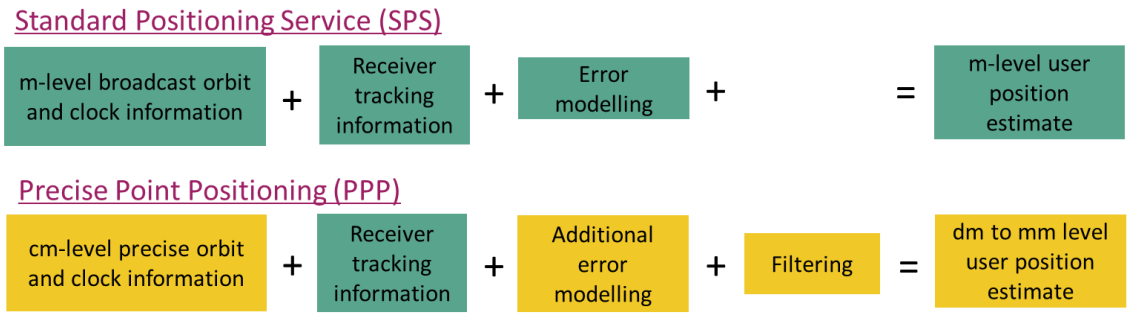

Figure 1.1 Fundamental idea underlying the SPS technique as compared to PPP (Seepersad and Bisnath 2014a).

Also, defining the PPP error budget becomes more challenging as these error sources can be subdivided into errors projected onto the range and localized antenna displacements, illustrated in Figure 1.2. As the signal is transmitted from the satellite to the receiver, error sources affected in the range domain include satellite and receiver clock error, atmospheric, relativistic, multipath and noise and carrier-phase wind-up. Antenna displacement effects

occur at the satellite and receiver and these include effects such as phase centre offset and variation, orbit and at the receiver, site displacement effects such as solid Earth tides and ocean loading. The measurements are continually added in time in the range domain, and errors are modelled and filtered in the position domain, resulting in reduced position error in time (Seepersad and Bisnath 2014a).

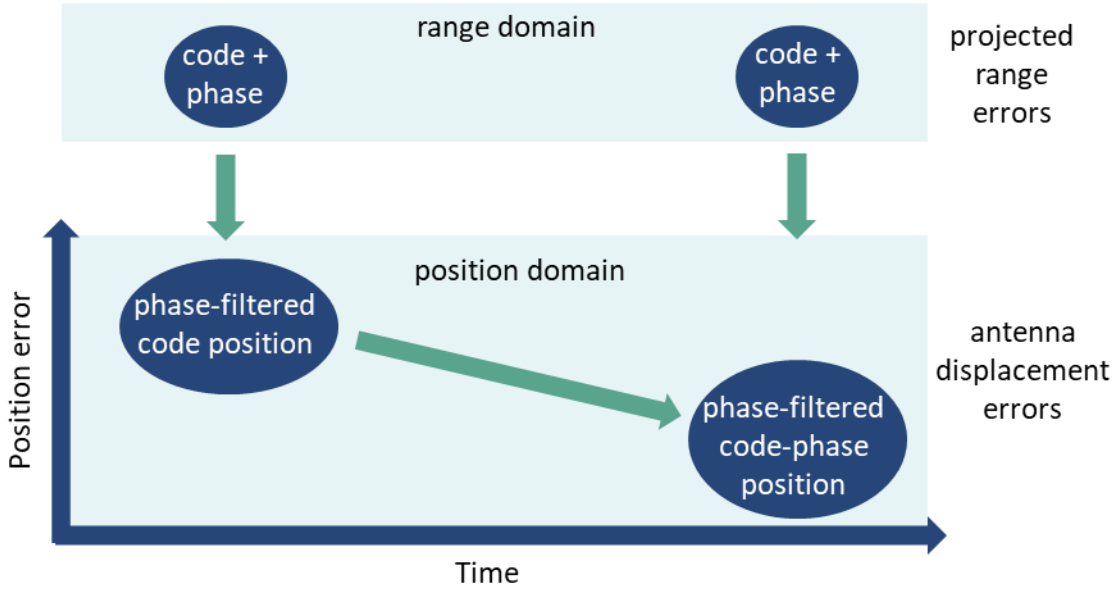

Figure 1.2 Range to position and time domain transformations in PPP data processing illustrating the different domains of PPP error sources (Seepersad and Bisnath 2014a).

It is necessary when processing data with a PPP algorithm to mitigate all potential error sources in the system. As a result of the undifferenced nature of conventional PPP, all errors caused by the space segment, signal propagation and signal reception directly impact the positioning solution. Error mitigation can be carried out by modelling, estimating, eliminated through linear combinations of the measurements or filtering through time averaging. As previously mentioned, there are additional corrections which have to be

applied to pseudorange and carrier-phase measurements such as phase wind-up, antenna phase centre offset and geophysical effects, in addition to other commonly known effects such as relativistic correction in order to have a complete observation model in PPP. Presented in Table 1.1 is a summary of all corrections accounted for and the applied within the mitigation strategy.

Table 1.1 Summary of error sources in PPP, mitigative strategy and residuals (Seepersad and Bisnath 2014a)

Effect	Magnitude	Domain	Mitigation method	Residuals
Ionosphere	10s m	range	linear combination; estimation	few mm
Troposphere	few m	range	modelling; estimation	few mm
Relativistic	10 m	range	modelling	mm
Satellite phase centre; variation	m - cm	position; range	modelling	mm
Code multipath; noise	1 m	range	filtering	10s cm - mm
Solid Earth tide	20 cm	position	modelling	mm
Phase wind-up (iono-free)	10 cm	range	modelling	mm
Ocean loading	5 cm	position	modelling	mm
Satellite orbits; clocks	few cm	position; range	filtering	cm - mm
Phase multipath; noise	1 cm	range	filtering	cm - mm
Receiver phase centre; variation	cm - mm	position; range	modelling	mm

Pole tide	few cm	position	modelling	mm
Receiver clock	10s m	range	estimation	mm
Atmospheric loading	cm - mm	position	modelling	cm - mm
Code biases	60 cm	range	modelling	mm
Ambiguity term	m - cm	range	estimation	dm - mm

PPP is considered a cost-effective technique as it enables sub-centimetre horizontal and few centimetre vertical positioning with a single receiver under ideal conditions with few hours of GNSS data (Seepersad 2012) in contrast to the methods such as relative GNSS, RTK and Network RTK that require more than one receiver. PPP can be used for the processing of static and kinematic data, both in real-time and post-processing. PPP's application has been extended to the commercial sector, as well in areas such as agricultural industry for precision farming, marine applications (for sensor positioning in support of seafloor mapping and marine construction), airborne mapping and vehicle navigation (Bisnath and Gao 2009). In rural and remote areas where precise positioning and navigation is required, and no reference stations are available, PPP proves to be an asset. Based on PPP's performance, it may be extended to other scientific applications such as ionospheric delay estimation, pseudorange multipath estimation, satellite pseudorange bias and satellite clock error estimation (Leandro 2009).

One of the major limitations of conventional PPP has been its relatively long initialization time as carrier-phase ambiguities converge to constant values and the solution reaches its

optimal precision. PPP convergence depends on a number of factors such as the number and geometry of visible satellites, user environment and dynamics, observation quality and sampling rate (Bisnath and Gao, 2009). As these different factors interplay, the period of time required for the solution to reach a pre-defined precision level will vary (Seepersad 2012).

Within academia, industry and governments, there are key areas of focus within the PPP PPP GNSS measurement processing. These research areas include ambiguity resolution, integration of PPP and INS, precise atmospheric models, using multi-GNSS constellations and processing data collected with low-cost (single-frequency) receivers, illustrated in Figure 1.3. The improvements that these different methods to PPP can be categorized in terms of reduction of the initial and re-convergence period of PPP and improvement in solution accuracy.

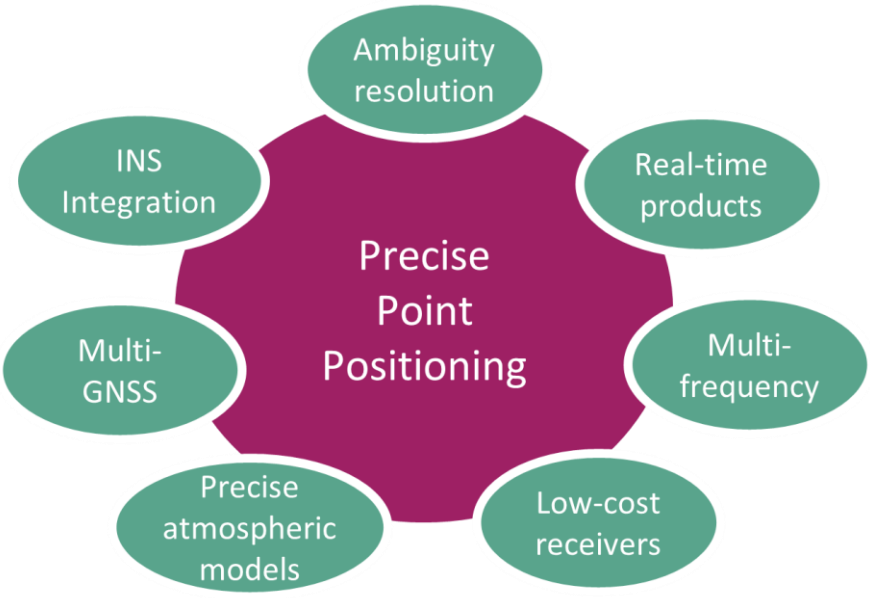

Figure 1.3: Current research areas in Precise Point Positioning.

1.2 Review of PPP ambiguity resolution

From the inception of GPS navigation, the largest hindrances to reliable few metre positioning was a result of the ionosphere delay. As a result of the ionosphere delay, two L-band navigation signals at 1575.42 MHz (L1) and 1227.60 MHz (L2) were deployed. After Selective Availability was turned off in 2000, it permitted more precise interpolation of the satellite clocks. As a result of the more precise modelling of the satellite clock error, delays due to the ionosphere became more prominent. The ionosphere delay led to the formation of the ionosphere-free linear combination using GPS data from a single receiver, as some of the early applications were for post-processing of static geodetic data for, e.g., rapid processing of GNSS tracking station data and crustal deformation monitoring.

With the ionosphere delay mitigated using the ionospheric-free linear combination, conventional PPP's relatively long convergence time fuelled research in single receiver ambiguity resolution (AR) (Laurichesse and Mercier 2007; Collins 2008; Mervart et al. 2008; Ge et al. 2008; Laurichesse et al. 2009; Teunissen et al. 2010; Bertiger et al. 2010; Geng et al. 2012). If the ambiguities could be isolated and estimated as integers, then there would be more information that could be exploited to accelerate convergence to provide cm-level horizontal accuracy within an hour of data collection, as illustrated in Figure 1.4. Resolution of these ambiguities converts the carrier-phases into precise pseudorange measurements, with measurement noise at the centimetre-to-millimetre level compared to the metre-to-decimetre-level of the direct pseudoranges (Blewitt 1989; Collins et al. 2010). Collins et al. (2008) and Laurichesse et al. (2009) saw improvements in hourly position

estimates by 2 cm and Geng et al. (2010a) saw noticeable hourly improvements from 1.5, 3.8 and 2.8 cm to 0.5, 0.5, 1.4 cm for north, east and up, respectively.

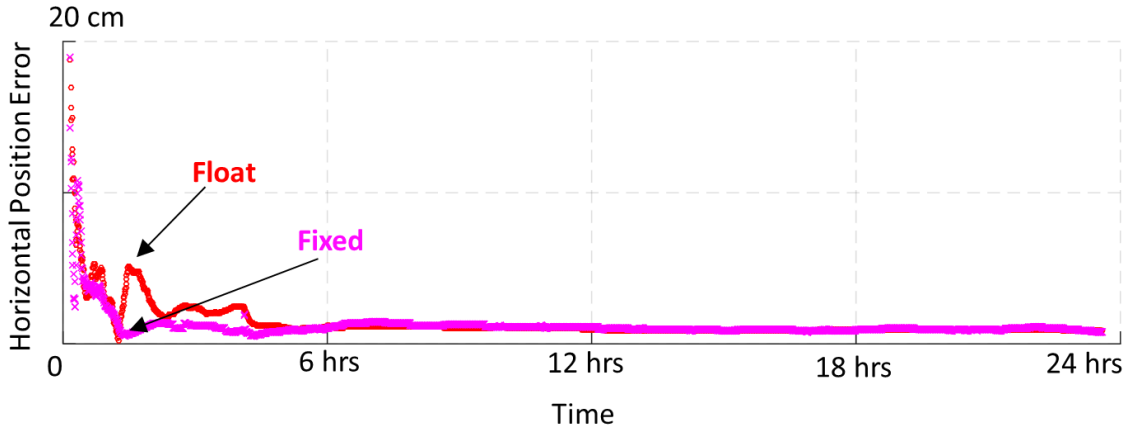

Figure 1.4: Illustration of the difference between the "float" and "fixed" solution in the horizontal component. NRC1 DOY 179, 2016 located in Ottawa, Canada.

By 2010, the advantages of PPP ambiguity resolution (PPP-AR) in regards to improved convergence and position stability was well examined; however, PPP still required over 30 minutes to attain cm-level accuracy (Geng et al. 2010a). During this period, research in multi-GNSS (GPS and GLONASS) positioning and estimation of slant ionosphere delay began to exponentially increase. Similar to GPS only PPP-AR, multi-GNSS positioning resulted in improved convergence time and solution accuracy (Cai and Gao 2007, 2013; Banville et al. 2013; Li and Zhang 2014; Aggrey 2015). Li and Zhang (2014) showed a reduction in convergence time from 20 to 11 minutes to attain a predefined threshold of 10 cm 3D. Li and Zhang (2014) and Jokinen et al. (2013) showed the integration of GPS and GLONASS sped up initial convergence and increased the accuracy of float ambiguity estimates, which contributed to enhanced success rates and reliability of fixing GPS

ambiguities. Estimation of the slant-ionosphere delay permitted instantaneous convergence, if accurate a priori atmospheric corrections were available to the PPP user (Geng et al. 2010a; Collins et al. 2012; Banville 2014). Also, if atmospheric corrections are provided, they assist with improving the reliability of ambiguity-resolved solutions, as uncertainties of the ambiguities will be lower by more than one order of magnitude (to ~0.2 cy 1σ) (Geng et al. 2010a; Collins and Bisnath 2011; Collins et al. 2012; Banville et al. 2014). Naturally, ambiguity resolved triple-frequency was of interest, which promised few minutes convergence, but also required additional linear combinations to be formed (Geng and Bock 2013), while it was possible to perform ambiguity resolution of the uncombined ambiguity terms. The evolution of the PPP user model is presented in Figure 1.5 as the performance converges to become more RTK-like, primarily due to the ability to perform ambiguity resolution within the PPP user model and the ability to introduce a priori atmospheric information.

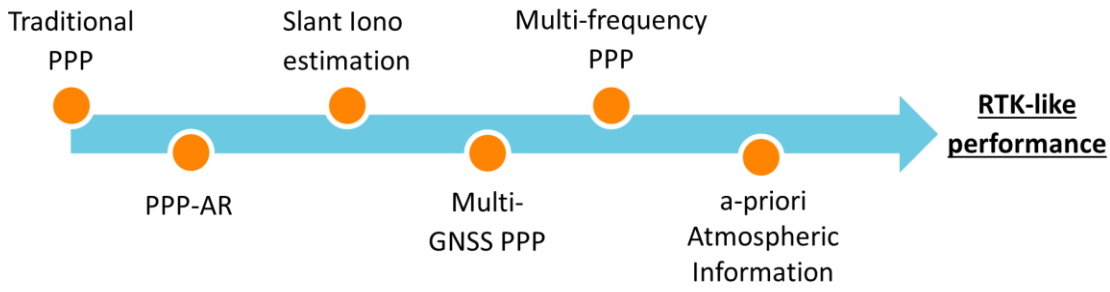

Figure 1.5: Evolution of the PPP user model.

Over the past decade, each of the GNSSs began modernization efforts. The GPS Block IIF is now complete, consisting of 12 satellites transmitting on the L5 band and production of Block III has begun, which will have a 4th civilian signal on L1 (L1C) and promises

enhanced signal reliability, accuracy, and integrity. For GLONASS, the third generation GLONASS-K satellites will change from Frequency Division Multiple Access (FDMA) to Code Division Multiple Access (CDMA), which will also transmit five navigation signals on the GLONASS's L1, L2, and L3 bands. The transition from FDMA to CDMA will eliminate the Inter-frequency Channel Biases (ICBs), which will allow GLONASS to be more consistent with other GNSSs, as well as allowing for easier standardization of GLONASS's satellite equipment delay products to enable ambiguity resolution. The European GNSS, GALILEO, is currently under development, with 14 operating satellites and 4 satellites under commission. Lastly, BeiDou began its transition towards global coverage in 2015. As of writing, 8 satellites have been launched and they are currently undergoing in-orbit validation (CSNO TARC 2018).

Within the scope of ambiguity resolution, the five core areas of research that are presented in Figure 1.6. The core focus within this research is in regard to the publicly available products that enable ambiguity resolution. Currently, publicly available products are limited to GPS only. Other research topics such as GLONASS ambiguity resolution and triple-frequency ambiguity resolution are reviewed in Sections 2.5 and 2.6 respectively.

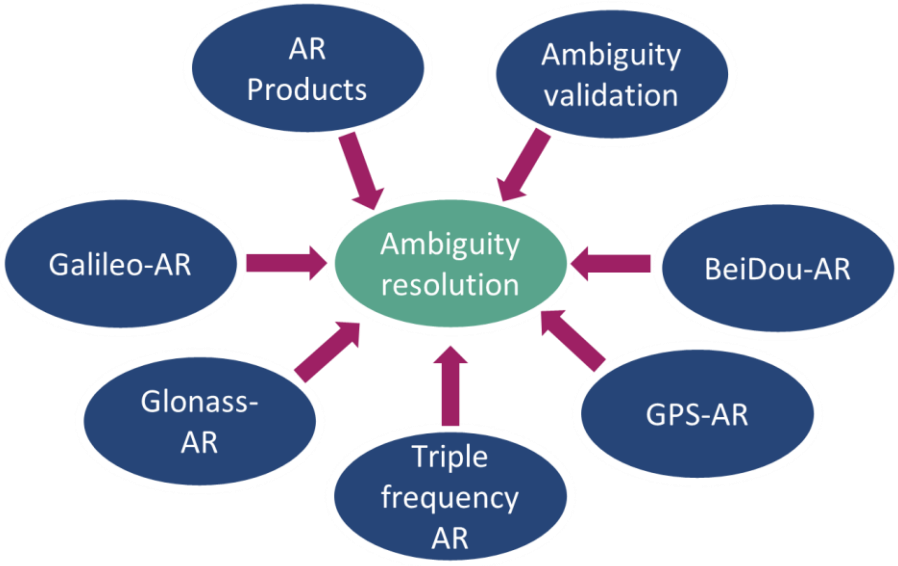

Figure 1.6 Current research areas within PPP ambiguity resolution.

1.3 GNSS performance parameters

The performance of any navigation system is characterized by several factors. Some of the primary factors consists of accuracy, precision, availability, continuity, reliability and integrity (IMO 2001; Grimes 2007; Porretta et al. 2016). The priority given to these different factors are application specific. For applications such as, geodetic control surveying, accuracy is the core requirement (Donahue et al. 2013). Whereas, for safety of life applications, such as automotive, aeronautical and marine navigation integrity and reliability is given the highest priority (RTCA DO-181 1983; IMO 2001; European GNSS Agency 2015). Presented is a review of some of the definitions which have been utilized within the research presented.

Accuracy and Precision: The accuracy of an estimated or measured position of a navigation system at a given time is the degree of conformance of that position with respect to a

reference position, velocity and/or time (RTCA DO-181 1983; Pullen 2011). Accuracy is represented as an averaged root mean square (rms) error with respect to the reference position. Whereas precision represents the standard deviation with respect to the averaged error or mean. Where error represents the difference between the estimated position and reference position and mean represents the average of the time period positions were provided by the navigation system (Anderson et al. 1998).

Availability: The availability of a navigation system is the percentage of time that the services of the system are usable by the navigator. Availability is an indication of the ability of the system to provide usable service within the specified coverage area (IMO 2001; U.S. Coast Guard Navigation Center 2008; Pullen 2011). Non-availability can be caused by schedule and/or unscheduled interruptions (IMO 2001). The description of availability can be broken into different components, such as, operational, service, system and signal availability (Pullen 2011). Where operational availability for e.g. is defined as the typical or maximum periods of time over which the service is unavailable and service availability is the fraction of time (expressed as a probability over all satellite geometries and conditions) that the navigation service is unavailable (Pullen 2011). Renfro et al. (2018) states there will an operational satellite count availability of $\geq$ 95% probability that the constellation will have at least 24 operational satellites. The IGS (2013) states that the operational availability of their real time products has a 95% availability for their rapid, ultra-rapid products and real-time products. Presented in Figure 1.7 is an overview of the availability of each of the contributing analysis centres towards IGS's Multi-GNSS Experiment (MGEX). Figure 1.7 highlights the importance of redundancy within a network

ensure product availability. Additional information about each of the contributing analysis centres can be found at IGS (2018a).

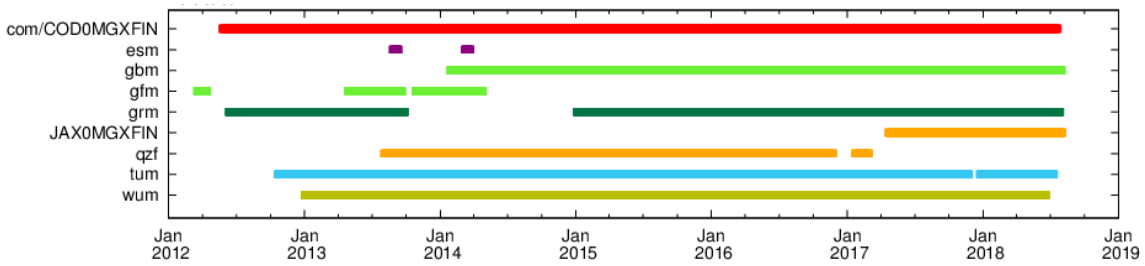

Figure 1.7 Multi-GNSS Experiment (MGEX) product availability (IGS 2018a)

Continuity: The continuity of a system is the ability of the total system (comprising all elements necessary to maintain position navigation system within the defined area) to perform its function without interruption during the intended operation. More specifically, continuity is the probability that the specified system performance will be maintained for the duration of a phase of operation, presuming that the system was available at the beginning of that phase of operation (U.S. Coast Guard Navigation Center 2008). Presented by U.S. Coast Guard Navigation Center (2008), the most stringent requirement for the location determination system to support the Positive Train Control (PTC) system is the ability to determine which of two tracks a given train is occupying with a probability of 99.999%. The minimum centre-to-centre spacing of parallel tracks is 3.5 m. While GPS alone cannot meet the specified continuity of service and accuracy, Nationwide Differential Global Positioning Systems NDGPS (previously called United States Coast Guard DGPS) in combination with map matching, inertial navigation systems, accelerometers, and other devices and techniques will provide both the continuity of service and accuracy required

to meet the stringent requirements set forth for PTC (U.S. Coast Guard Navigation Center 2017). The IGS (2013) describes the continuity of their ultra-rapid products as 4x daily, at 03, 09, 15 and 21 UTC, daily at 17 UTC for their rapid and continuous for their real time.

Reliability: The probability of success or the probability that the system will perform its intended function under specified design limits. More specifically, reliability is the probability that a product will operate within their specifications for a period of time (design life) under the design operating conditions (such as temperature, volt, etc.) without failure. In other words, reliability may be used as a measure of the system's success in providing its function properly (RTCA DO-181 1983; Pham 2006). Reliability of a system can be decomposed into failure prevention (robustness and redundancy) and failure response (resilience). For e.g. the Wide Area Augmentation System (WAAS) focuses on failure prevention by providing reliability and redundancy to meet the overall National Airspace System (NAS) requirements with no single point of failure. The overall reliability of the WAAS signal- in-space approaches 100% (U.S. Coast Guard Navigation Center 2008). Where redundancy is the existence of multiple equipment or means for accomplishing a given function in order to increase the reliability of the total system (IMO 2001).

A system is considered reliable in terms of robustness if it is resilient with respect to input and failure uncertainties, and consequently it has low reliability when even the small amounts of uncertainty entail the possibility of failure (RTCA DO-181 1983). The IGS also focuses on failure prevention by improving reliability and robustness primarily through redundancy. IGS products consist of a combination from multiple analysis centres

(IGS 2007). As of writing there are 12 analysis centres which contribute towards the combination of the IGS products (IGS 2018b). By combining multiple products, the navigation system is less vulnerable to network outages and can maintain availability and continuity of the service.

Integrity: Integrity is the measure of the trust that can be placed in the correctness of the information supplied by a navigation system. Integrity includes the ability of the system to provide timely warnings to users when the system should not be used for navigation (Ochieng et al. 2003; U.S. Coast Guard Navigation Center 2008; Pullen 2011). Where integrity risk is the probability of an undetected, threatening navigation system problem (Parkinson and Axelrad 1988; Ober 1999; Pullen 2011). Overall GNSS system integrity is described by three parameters: the threshold value or alert limit, the time to alarm and the integrity risk. The output of integrity monitoring is that individual (erroneous) observations or the overall GNSS system cannot be used for navigation (IMO 2001). Other definitions of integrity combine the concepts of reliability and integrity under the title Integrity Monitoring (Parkinson and Axelrad 1988; Sturza 1988; Feng et al. 2012; Seepersad and Bisnath 2013; Jokinen et al. 2013a).

1.4 Problem Statement

As previously stated, conventional PPP has always required a relatively long initialization period (few tens of minutes at least) for the carrier-phase ambiguities to converge to constant values and for the solution to reach the sub-dm-level. This situation is primarily caused by the estimation of the carrier-phase ambiguity from the relatively noisy

pseudoranges and the estimation of atmospheric delay. The result is PPP can then take full advantage of the precise but ambiguous carrier-phase observations; however, the length of time it takes to reach the optimal solution is a major disadvantage to the wider use of the technique. If the underlying integer nature of the ambiguity is known, it can be resolved, thereby reducing the convergence time of conventional PPP. The challenge of ambiguity resolution in conventional PPP is due to equipment delays that are absorbed by the ambiguity state term within the least squares estimation process. These equipment delays are due to different filters used with the receivers and satellites as well as delays experienced within the antennas and cables.

To recover the underlying integer nature of the carrier-phase ambiguities, different strategies for mitigating the satellite and receiver dependent equipment delays have been developed, and products made publicly available to enable ambiguity resolution without any baseline restrictions. There has been limited research within the scope of interoperability of the products which enable ambiguity resolution. Interoperability of the products can occur within the network solution or within the user solution. The limitation of product interoperability within the user processing engine is ambiguity re-initialization due to changing of ambiguity resolution product providers. In addition, there has been no publish literature examining the performance of product interoperability. If the products are combined within the network processing engine, this will ensure a continuous precise user solution if one of the providers experiences an outage. As PPP and PPP-AR is being adopted by the mass market, which has less stringent accuracy specifications but higher

integrity requirements, as a result, a reassessment of the role of ambiguity resolution is needed.

1.5 Thesis Statement

The focus of this research is to develop an effective strategy to improve the reliability of the PPP ambiguity resolved user solution. Traditionally, PPP users have been expected to choose between either robust satellite orbit and clock products, which are a combination from multiple analysis centres or select solutions from individual analysis centre that provide PPP-AR products. To address the limitation whereby users were expected to choose between either a robust solution or higher accuracy solution, the following specific objectives are defined:

1. Implementation of ambiguity resolution of the carrier-phase observable;
2. Re-design of the traditional PPP-AR model to an uncombined representation;
3. Examination of the interoperability of multiple PPP-AR products;
4. Development of a combination process for the PPP-AR products; and
5. Re-examination the role of PPP ambiguity resolution.

1.6 Research Contributions

The research presented has been fuelled by the advancements made in ambiguity resolution by Laurichesse and Mercier (2007); Collins (2008); and Ge et al. (2008). To allow PPP GNSS measurement processing to be adopted into mass market applications that involves safety of life for e.g., the operation of autonomous vehicles, there is now increased

requirement on the reliability, robustness and integrity of the user solution. To enable research within the realm of PPP ambiguity resolution it was required to expand of pre-existing PPP infrastructure to facilitate ambiguity resolution. Presented, is an overview of the implementation process to enable ambiguity resolution utilizing PPP-AR products. Receiver dependent equipment delays were mitigated by performing implicit single (satellite-to-satellite) differencing. Implicit differencing was selected to permit estimation of the receiver code clock, phase clock and relative carrier-phase L1-L2 measurement equipment delay. Satellite equipment delays were mitigated by utilizing products from different public providers to examine performance and interoperability.

PPP users have been expected to choose between either robust satellite orbit and clock products, which represents a combination from multiple analysis centres or select solutions from individual analysis centre that provides PPP-AR products. If PPP users selected combined satellite orbit and clock products they would not be able to resolve the ambiguity terms as the satellite equipment delays were not mitigated. If the PPP users opted for products from individual analysis centre that provided PPP-AR products they would be able to attain a more accurate and precise user solution but be vulnerable to network outages which is the motivational factor behind the novel research presented. The novel contributions are comprised of an in-depth analysis of the PPP-AR products in a combined and uncombined representation, mathematical representation of how to utilize the products in the different representations, examination of the performance of the PPP-AR products from different providers, the challenges involved in utilizing the PPP-AR products from

the different providers and the strategies required to allow interoperability of the different products.

As a result of the advancements made in the interoperability of PPP-AR products, permitted another significant novel contribution, development of a technique to combine multiple PPP-AR products. The combination of the PPP-AR products resulted in improved reliability of the user solution and robustness of the products as the user is no longer dependent on a single analysis centre. Combining of the PPP-AR products will be performed within the network processing engine which will ensure a continuous precise user solution

PPP and PPP-AR processing has become routinely utilized within applications such as crustal deformation monitoring, near real-time GNSS meteorology, orbit determination of LEO satellites as well as control and engineering surveys where requires few cm-level positioning accuracy. If PPP-AR is to be adopted in techniques such as lane navigation which requires 10 to 20 cm horizontal positioning accuracy, a re-examination of the role of ambiguity resolution in PPP is needed. Within this scope another novel contribution within this research exists as there has been limited focus on the utilization of ambiguity resolution as an integrity indicator as having a successfully resolved and validated solution indicates to the user increased accuracy, precision and reliability of the user solution thereby increasing the amount of trust that can be placed in the information supplied by the ambiguity resolved PPP data processing engine.

1.7 Thesis Outline

Chapter 2 provides an overview of the evolution of the PPP user model over the past two decades, how to process the measure as well as steps needed to expand the mathematical model to facilitate ambiguity resolution in PPP utilizing an uncombined representation. The standard practice in conventional PPP has been to linearly combine two pseudoranges and two carrier-phases to produce ionosphere-free linear pseudoranges and carrier-phase combinations which eliminates the first order ionosphere delay. Originally, the ionosphere delay was considered a nuisance parameter within the positioning community. As a result, the ionosphere-free linear combination was favoured in contrast to the estimation of the slant ionosphere delay. Nowadays, the PPP model permits multi-frequency, multi-constellation, slant ionosphere estimation and ambiguity resolution. Presented in each section is a review of the steps the PPP user model underwent within its evolution.

Chapter 3 examines the interoperability of high-rate satellite equipment delays which enable PPP-AR. Interoperability of PPP-AR products is important, as it can increase the reliability of the user solution while offering similar performance, in regard to precision and accuracy. Interoperability of the products is possible for the PPP user, as the mathematical model to enable an ambiguity resolved solution is similar. The different PPP-AR products contain the same information and would allow for a one-to-one transformation, allowing interoperability of the PPP-AR products. The PPP user will be able to transform independently generated PPP-AR products to seamlessly integrate within their PPP user solution. The seamless integration of the transformed products will allow the PPP user to have multiple solutions, which will increase the reliability of the solution,

for, e.g., real-time processing. During real-time PPP processing, if there were an outage in the generation of the PPP-AR products, the user can instantly switch streams to a different provider. A novel component of the research presented is the examination of the interoperability of PPP-AR products with real data, as well as the presentation of the products in combined and uncombined representation.

Chapter 4 investigates the feasibility of combining the products from multiple providers of PPP-AR products. While satellite clock combinations are routinely utilized within the IGS, they currently disregard the fact that some ACs provide satellite clock products that account for the satellite equipment delays. Users have been expected to choose either a robust combined solution or select individual AC solutions that provide PPP-AR products that allow the user to compute an ambiguity resolved solution. The objective of this investigation was to develop and test a robust satellite clock combination, while preserving the underlying integer nature of the clocks and therefore the carrier-phase ambiguities to the user end to enable PPP-AR. The novelty of the research presented with this chapter is the development of a process to combine multiple products which enable robust PPP-AR.

Chapter 5 re-examines the role of ambiguity resolution in multi-GNSS PPP with the advent of quad-constellation, triple-frequency and external atmospheric constraints being provided to the PPP user. The focus and novelty of this chapter is in the quest to answer the question: Is ambiguity resolution in PPP needed for accuracy and/or for integrity? First, a re-examination of the significance between the float and ambiguity resolved PPP user solution is undertaken. Is the improvement significant enough for applications such as precision agriculture and autonomous vehicles to justify the additional cost and

computational complexity of producing a PPP-AR solution? A novel component within the realm of PPP-AR is the analysis of ambiguity resolution as a metric to examine the integrity of the user solution.

Finally, Chapter 6 summarizes all the findings and provides recommendations for research in the near future.

CHAPTER 2 EVOLUTION OF THE PPP USER MODEL

Over the past two decades, the PPP user model has constantly been evolving. With each iteration, improvements were made primarily in regards to accuracy and most notably convergence. The standard practice in conventional PPP has been to linearly combine two pseudoranges and two carrier-phases to produce ionosphere-free linear pseudoranges and carrier-phase combinations, which eliminates the first order ionosphere delay. Originally, the ionosphere delay was considered a nuisance parameter within the positioning community. As a result, the ionosphere-free linear combination was favoured in contrast to the estimation of the slant ionosphere delay. Nowadays, the PPP model permits multi-frequency, multi-constellation, slant ionosphere estimation and ambiguity resolution. Presented in each of the following sections is a review of the steps the PPP user model underwent within its evolution.

2.1 Introduction into Point Positioning

Single point positioning (SPP), also referred to as absolute positioning or point positioning, is the most basic GPS solution obtained with epoch-by-epoch least-squares estimation. For SPP, GPS provides two levels of services, the Standard Positioning Service (SPS) with the access for civilian users and the Precise Positioning Service (PPS) with the access for the authorized users. Traditionally, in SPS, only the L1 C/A-code was available. As part of the modernization efforts, civilians would now gain access to the L2 C/A-code. The achievable

real-time SPS 3D positioning accuracy is ~ 10 m at the 95% confidence level. The SPS model is presented in equation (2.1).

$$P^{s}_{u,C1} = \rho^{s}_{u} + dt_{u,C1} + dt^{s}_{C1} + d_{iono} + d_{tropo} \quad (2.1)$$

$P^{s}_{u,C1}$ represents the C/A-code modulated on the L1 frequency. ρ^{s}_{u} is the non-dispersive delay between satellite (s) and user position (u) including geometric delay. $dt_{u,C1}$ and dt^{s}_{C1} represents the receiver and satellite clock errors, respectively, with respect to GPS time. d_{iono} and d_{tropo} represent the delays caused by ionosphere and troposphere refraction, respectively.

2.2 Conventional PPP model

Similar to SPP, PPP is a positioning technique which only requires a single receiver, but has the functionality to provide few centimetre-level results in static mode and decimetre-level results in kinematic mode (Seepersad 2012). To transition from SPP to PPP, two core components are required:

1) Precise satellite orbits and clocks

Broadcast orbits have an accuracy of ~100 cm in contrast to precise orbits which ranges from 5 cm, real-time to 2.5 cm, post-processed. The broadcast clocks have a precision of ~2.5 ns in contrast to the precise clocks ranging from ~1.5 ns, real-time to ~20 ps, post-processed, (Dow et al. 2009).

2) Pseudorange and carrier-phase measurements

The pseudorange and carrier-phase measurements are strongly reliant on each other and are critical to enable precise positioning. The pseudoranges act as a reference frame (or datum) to the precise but ambiguous carrier-phase measurements. Whereas, the precise nature of the carrier-phase measurements smooths the relatively noisy pseudorange measurements.

Presented in equations (2.2) and (2.3) are the pseudorange measurements modulated on the L1 and L2 frequencies respectively, measured in units of metres. In equations (2.4) and (2.5) are the carrier-phase measurements modulated on the L1 and L2 frequencies respectively. The carrier-phase measurements are measured in units of cycles that is converted to distance. Assuming that PPP related errors such as carrier-phase wind-up, relativity, antenna phase centre offset and geophysical effects have been properly mitigated for the observation equations can be written as follows.

$$P^s_{u,P1} = \rho^s_u + dt_{u,P1} + dt^s_{P1} + d_{iono} + d_{tropo} + d^s_{P1} + d_{u,P1} \tag{2.2}$$

$$P^s_{u,P2} = \rho^s_u + dt_{u,P2} + dt^s_{P2} + d_{iono} + d_{tropo} + d^s_{P2} + d_{u,P2} \tag{2.3}$$

$$\Phi^s_{u,L1} = \rho^s_u + dt_{u,L1} + dt^s_{L1} - d_{iono} + d_{tropo} + A^s_{u,L1} + \delta^s_{L1} + \delta_{u,L1} \tag{2.4}$$

$$\Phi^s_{u,L2} = \rho^s_u + dt_{u,L2} + dt^s_{L2} - d_{iono} + d_{tropo} + A^s_{u,L2} + \delta^s_{L2} + \delta_{u,L2} \tag{2.5}$$

where d_{iono} represents delays due to ionospheric refraction, d_{tropo} represents the delays due to tropospheric refraction and A^s_u is the non-integer phase ambiguity on L1 or L2 in units

of metres. d and δ refer to the equipment delays present within the pseudorange and carrier-phase measurements, respectively. These equipment delays are due to different filters used with the receivers and satellites as well as delays experienced within the antennas and cables (Hauschild and Montenbruck 2014).

To formulate the conventional PPP model, the ionosphere-free linear combination (IF) of the pseudorange ($P^s_{u,IF}$) and carrier-phase measurements ($\Phi^s_{u,IF}$) are formed, which is presented in (2.6) and (2.7) . In conventional PPP, the ionosphere-free linear combination is routinely formed because the ionosphere delay is typically considered a nuisance parameter, thus preferred to be eliminated.

$$P^s_{u,IF} = \rho^s_u + dt_{u,IF} + dt^s_{IF} + d_{tropo} \tag{2.6}$$

$$\Phi^s_{u,IF} = \rho^s_u + dt_{u,IF} + dt^s_{IF} + d_{tropo} + A^s_{u,IF} \tag{2.7}$$

where $A^s_{u,IF}$ is the ionosphere-free carrier-phase ambiguity term.

The equipment delays ($d_{u,IF}, d^s_{IF}, \delta^s_{IF}, \delta_{u,IF}$) were assimilated within the clock terms ($dt^s_{IF}, dt_{u,IF}$), presented in equation (2.8) and (2.9).

$$dt_{u,IF} = dt_u + d_{u,IF} + \delta_{u,IF} \tag{2.8}$$

$$dt^s_{IF} = dt^s + d^s_{IF} + \delta^s_{IF} \tag{2.9}$$

As a result of the unmodelled equipment delays within the satellite and receiver, $A^s_{u,IF}$ is no longer integer natured because the unmodelled equipment delays ($\delta^s_{u,IF}, d^s_{u,IF}$) are absorbed within the ambiguity parameters (Collins et al. 2010). The implications for not accounting for these delays are presented in the following equation.

$$A^s_{u,IF} = \lambda_{IF} N^s_{u,IF} + \delta^s_{u,IF} + d^s_{u,IF} \tag{2.10}$$

Where $A^s_{u,IF}$ represents the real-valued ambiguity term that is comprised of the integer natured carrier-phase ambiguity term ($N^s_{u,IF}$), which is expressed in cycles and scaled by the ionosphere-free wavelength (λ_{IF}) and the equipment delays ($\delta^s_{u,IF}, d^s_{u,IF}$) which are expressed in units metres. Equation (2.10) and Figure 2.2 illustrates the importance of accounting for $d^s_{u,IF}$ and $\delta^s_{u,IF}$, because of the co-dependency that exists between the pseudorange and carrier-phase measurements as a result of the shared clock terms, also referred to as common clocks ($dt^s_{,IF}, dt_{u,IF}$) (Collins et al. 2008). If information about the user and satellite equipment delays were accounted for, the ambiguity term would be integer natured thereby permitting ambiguity resolution. For the GPS ionosphere-free linear combination, it is not practical to attempt to fix the

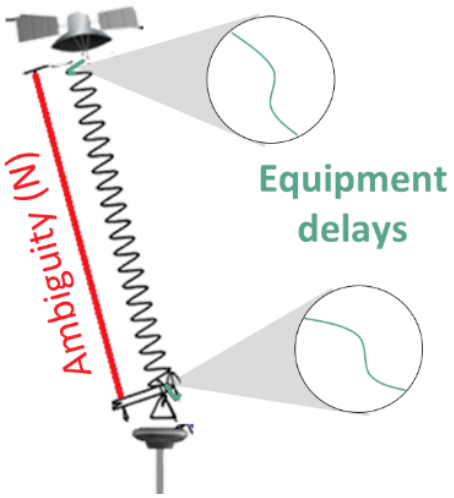

Figure 2.1: Conceptual illustration of the integer nature of the ambiguity term affected by receiver and satellite equipment delays.

ambiguity term as the wavelength (λ_{IF} =0.006 m) is too short relative to the noise of the linear combination (Collins 1999b). The ionosphere-free observation equations expressed in (2.6) and (2.7) are presented in equation (2.11) in matrix/scalar form in a combined and uncombined representation. For simplicity, the troposphere delay, d_{tropo} is grouped within the geometric range, ρ_u^s.

$$\begin{bmatrix} p_{IF}^s \\ \Phi_{IF}^s \end{bmatrix} = \begin{bmatrix} \alpha_{IF} & \beta_{IF} & 0 & 0 \\ 0 & 0 & \alpha_{IF} & \beta_{IF} \end{bmatrix} \begin{bmatrix} p_1^s \\ p_2^s \\ \Phi_1^s \\ \Phi_2^s \end{bmatrix} = \begin{bmatrix} 1 & 1 & 1 & 0 & 0 \\ 1 & 1 & \mu_2 & 0 & 0 \\ 1 & 1 & -1 & 1 & 0 \\ 1 & 1 & -\mu_2 & 0 & 1 \end{bmatrix} \begin{bmatrix} \rho_u^s \\ dt_u^s \\ I_{u,1}^s \\ \lambda_1 N_{u,1}^s \\ \lambda_2 N_{u,2}^s \end{bmatrix} \tag{2.11}$$

where u_i is the frequency dependent coefficient $\mu_i = \frac{f_1^2}{f_i^2}$.

To recover the underlying integer nature of the carrier-phase ambiguities, different strategies for mitigating the satellite and receiver dependent equipment delays are described in the following section.

2.3 PPP-AR model

In relative positioning techniques such as RTK, the integer nature of the carrier-phase ambiguities is uncovered by differencing simultaneous observations from multiple stations visible to the same satellites. Typically the raw measurements are differenced explicitly (Leick 1995; Hofmann-Wellenhof et al. 1997). Differencing of simultaneous observations can be thought of as an optimal correction method (Collins and Bisnath 2011), as the error

sources are not modelled. PPP-AR requires the equipment delays within the GPS measurements to be mitigated, which would allow for resolution of the integer nature of the carrier-phase measurements (Laurichesse and Mercier 2007; Collins 2008; Mervart et al. 2008; Ge et al. 2008; Teunissen et al. 2010; Bertiger et al. 2010; Geng et al. 2012; Lannes and Prieur 2013). These equipment delays are due to different filters used with the receivers and satellites as well as delays experienced within the antennas and cables (Hauschild and Montenbruck 2014). Recall equations (2.2) to (2.5) and apply A_u^s to the carrier-phase measurements in equations (2.14) and (2.15) it is shown that by resolving these ambiguity terms converts the carrier-phases into precise pseudorange measurements, with measurement noise at the centimetre-to-millimetre level compared to the metre-to-decimetre-level of the direct pseudoranges (Blewitt 1989; Collins et al. 2010).

$$P_{u,P1}^s = \rho_u^s + dt_{u,P1} + dt_{P1}^s + d_{iono} + d_{tropo} + d_{P1}^s + d_{u,P1} \tag{2.12}$$

$$P_{u,P2}^s = \rho_u^s + dt_{u,P2} + dt_{P2}^s + d_{iono} + d_{tropo} + d_{P2}^s + d_{u,P2} \tag{2.13}$$

$$\Phi_{u,L1}^s - A_{u,L1}^s = \rho_u^s + dt_{u,L1} + dt_{L1}^s - d_{iono} + d_{tropo} + \delta_{L1}^s + \delta_{u,L1} \tag{2.14}$$

$$\Phi_{u,L2}^s - A_{u,L2}^s = \rho_u^s + dt_{u,L2} + dt_{L2}^s - d_{iono} + d_{tropo} + \delta_{L2}^s + \delta_{u,L2} \tag{2.15}$$

If the ambiguities could be isolated and estimated as integers, then there would be more information that could be exploited to accelerate convergence to give cm-level horizontal accuracy within an hour of data collection. The satellite equipment delays, which are necessary to resolve the ambiguity terms can be transmitted in two formats. They can be

transmitted through an observation space representation (OSR) or state space representation (SSR). OSR and SSR is a data transmission format for corrections to enable higher accuracy positioning of a GNSS receiver. OSR corrections are typically utilized in Network RTK (NRTK) and Differential GNSS (DGNSS), as the range measurements of the GNSS user are improved by applying a range correction as measured by a nearby reference station directly to the GNSS measurements. SSR corrections are required for PPP and PPP-AR, as the assumption when utilizing PPP is, there will not be any localized infrastructure available to the GNSS user. SSR decomposes the errors into meaningful states. A network of reference stations is needed to decorrelate the different GNSS error components (Wübbena et al. 2005). Figure 2.2 illustration of the different correction terms transmitted in observation space and state space representation. SSR corrections are preferred in contrast to OSR primarily because it is bandwidth efficient. By decomposing the range terms into state dependent terms, the state terms can be transmitted at variable rates such as satellite orbits are transmitted every 30 seconds and satellite clocks transmitted every 10 seconds (Schmitz 2012).

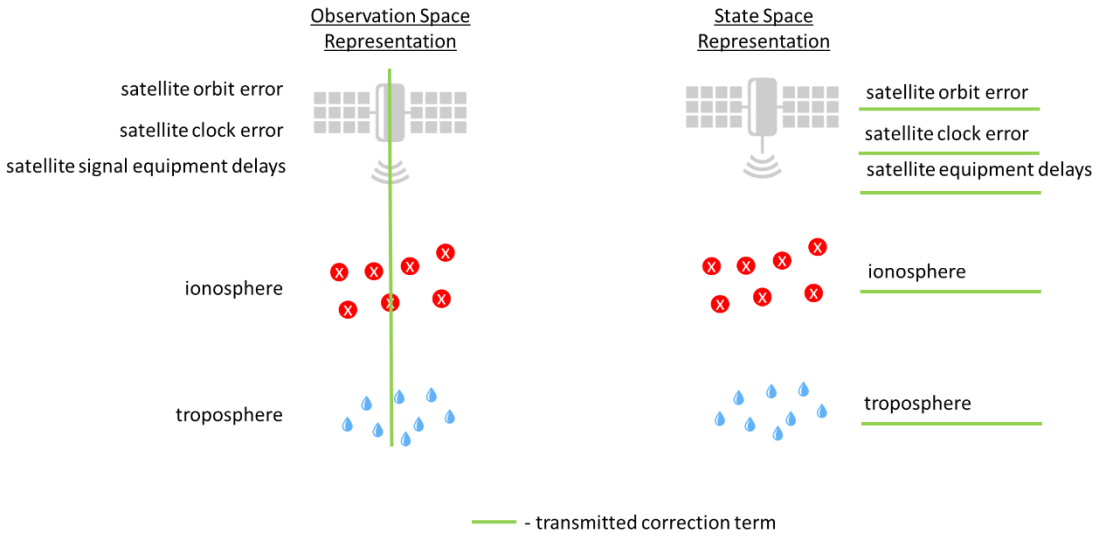

Figure 2.2: Different correction terms transmitted in observation space and state space representation (Wübbena 2012).

The concept of fixing ambiguities using state space representations was originally presented in Blewitt (1989), Goad (1985) and Bock et al. (1985). Their research focused on relative positioning for processing ultra-long baselines, up to 2000 km. Blewitt (1989) adopted a state space representation where undifferenced measurements in the form of ionosphere-free linear combinations of the pseudorange and carrier-phase measurements was processed to form double-differenced estimates. The fractional component of the satellite equipment delay was needed to enable ambiguity resolution in baseline processing. Results presented by Bock et al. (1985, 1986, 2000) and Abbot and Counselman (1987) show improved baseline precision due to ambiguity resolution with the fractional component of the satellite equipment delay mitigated. Dong and Bock (1989) demonstrated ambiguity resolution for baseline lengths up to a few hundred kilometres. Note, as the baseline length increases beyond 20 km, the performance of relative positioning and PPP-

AR becomes equivalent (Bertiger et al. 2010), as localized atmospheric errors are no longer eliminated through double-differencing. Similar performance was noted within the context of PPP; Ge et al. (2008) saw a 30% improvement in the east component when compared to the IGS weekly solutions; Collins et al. (2008) and Laurichesse et al. (2009) saw improvements in hourly position estimates by 2 cm; and Geng et al. (2010a) saw noticeable hourly improvements from 1.5, 3.8 and 2.8 cm to 0.5, 0.5, 1.4 cm for north, east and up, respectively.

Traditionally, PPP and RTK has always represented different GNSS processing techniques. PPP has always been a single receiver data processing technique, utilizing undifferenced GNSS measurements, while relying on precise orbit and clock with a focus on SSR of error components. Where as, RTK always required at least two receivers, has been typically constrained to short baseline (less than 20 km) as a strategy to eliminate localized atmospheric effects, while enabling ambiguity resolution, with a focus on OSR error components. The advent of PPP-AR provided the bridging gap between PPP and RTK as it enabled ambiguity resolution within a single localized GNSS receiver by capitalizing on correction terms provided from a network of GNSS receivers. In literature, PPP-AR has sometimes been referred to as PPP-RTK (Wübbena et al. 2005; Teunissen and Khodabandeh 2015). An appropriate description of the concept PPP-AR is, it is a state space relative positioning technique, as all error terms are mitigated relative to a global distribution of receivers. As previously mentioned, to enable PPP-AR, the equipment delays present within the carrier-phase and pseudorange measurements need to be accounted for. Currently, there are four common approaches to PPP ambiguity resolution:

1. Common Clock model (CC1)
2. Decoupled Clock Model (DCM)
3. Fractional Cycle Biases (FCB) model
4. Integer Recovery Clock (IRC) model

The CC1 adopted an uncombined approach of the measurements, whereas, DCM, IRC and FCB reformulated the ionosphere-free code and carrier-phase observation equations. The DCM, IRC and FCB models utilized the Melbourne-Wübbena linear combination (Φ^s_{MW}) presented in equation (2.16). The Melbourne-Wübbena linear combination is described as a geometry-free linear combination because the range components are eliminated by differencing the narrowlane code (P_{NL}) and widelane phase (Φ_{WL}). The strength of the Melbourne-Wübbena linear combination is in its ability to isolate the widelane ambiguity term. Additional details about fundamentals of linear combinations can be found in Leick (1995), Hofmann-Wellenhof et al., (1997) and Collins (1999b).

$$\begin{bmatrix} P^s_{IF} \\ \Phi^s_{IF} \\ \Phi^s_{MW} \end{bmatrix} = \begin{bmatrix} \alpha_{IF} & \beta_{IF} & 0 & 0 \\ 0 & 0 & \alpha_{IF} & \beta_{IF} \\ -\alpha_{NL} & -\beta_{NL} & \alpha_{WL} & -\beta_{WL} \end{bmatrix} \begin{bmatrix} P^s_1 \\ P^s_2 \\ \Phi^s_1 \\ \Phi^s_2 \end{bmatrix}; \begin{bmatrix} P^s_1 \\ P^s_2 \\ \Phi^s_1 \\ \Phi^s_2 \end{bmatrix} = \begin{bmatrix} 1 & 1 & 1 & 0 & 0 \\ 1 & 1 & \mu_2 & 0 & 0 \\ 1 & 1 & -1 & 1 & 0 \\ 1 & 1 & -\mu_2 & 0 & 1 \end{bmatrix} \begin{bmatrix} \rho^s_u \\ dt^s_{u,IF} \\ I^s_{u,1} \\ \lambda_1 N^s_{u,1} \\ \lambda_2 N^s_{u,2} \end{bmatrix} \quad (2.16)$$

As previously mentioned, it is not practical to attempt to fix the GPS ionosphere-free ambiguity term as the wavelength (λ_{IF} =0.006 m) is too short relative to the noise of the linear combination. As a result of the relatively short ionosphere-free wavelength, $A^s_{u,IF}$ is

decomposed into the L1 ($N^s_{u,1}$) and widelane ($N^s_{u,WL}$) ambiguity terms. As a result of the decomposition of the $A^s_{u,IF}$ term, it becomes possible to resolve the ionosphere-free ambiguity term, equation (2.17). The widelane ambiguity has a wavelength ~86 cm, which amplifies the $N^s_{u,1}$ ambiguity to have a wavelength equivalent to the narrowlane of ~11 cm.

$$A^s_{u,IF} = \lambda_{IF}(17N^s_{u,1} + 60N^s_{u,WL}) \tag{2.17}$$

Presented in equation (2.18) are the linear combinations P^s_{IF}, Φ^s_{IF} and Φ^s_{MW} with the decomposed ambiguity terms $\lambda_1 N^s_{u,1}$ and $\lambda_{WL} N^s_{u,WL}$.

$$\begin{bmatrix} P^s_{IF} \\ \Phi^s_{IF} \\ \Phi^s_{MW} \end{bmatrix} = \begin{bmatrix} 1 & 1 & 0 & 0 \\ 1 & 0 & 1 & \frac{60}{137} \\ 0 & 0 & 0 & 1 \end{bmatrix} \begin{bmatrix} \rho^s_u \\ dt^s_{u,IF} \\ \lambda_1 N^s_{u,1} \\ \lambda_{WL} N^s_{u,WL} \end{bmatrix} \tag{2.18}$$

2.3.1 Receiver equipment delay

When processing undifferenced pseudorange and carrier-phase measurements, the datum (reference frame) within the adjustment is the pseudorange clocks, as the carrier-phase measurements are uniquely ambiguous. The receiver clock ($dt_{u,IF}$) is referred to as the datum, as it is a commonly estimated term between the pseudorange and carrier-phase measurements, equation (2.16). The datum allows the solution to capitalize on the accuracy of the pseudorange measurements and precision of the carrier-phase measurements. Collins (2008) describes the conventional PPP model as sub-optimal in the context of ambiguity

resolution, because the estimated ambiguities contain pseudorange and carrier-phase equipment delays, which degrade the accuracy of the estimated clock parameters.

The first step in enabling PPP-AR requires accounting for the equipment delays generated by the receiver or changing the datum used for the carrier-phase measurements. The equipment delays lack unique separation between the clocks and ambiguities, as such, the solution becomes under-determined.

To remove this singularity, the different PPP-AR techniques adopted implicit (sometimes incorrectly referred to as "undifferenced") (Laurichesse and Mercier 2007; Collins 2008; Zhang et al. 2011) and explicit (Gabor and Nerem 2002; Ge et al. 2008; Bertiger et al. 2010; Geng et al. 2010a; Geng and Bock 2013) single-differencing strategies. Single-differencing (between two satellites and one receiver) changes the datum of carrier-phase measurements from the pseudorange clock to the ambiguity terms.

Implicitly differenced observations are closer to the physical observables within the GNSS receivers, while explicit differencing typically implies differencing of the raw observations. Ge et al. (2008) differenced the ambiguity terms. Explicit differencing eliminates the receiver clock and equipment delay, while implicit differencing permits the estimation of these terms. Implicit and explicitly differenced GNSS observations result in the same estimates of the desired parameters, as long as the models chosen for the implicitly differenced (undifferenced) observation biases satisfy the assumptions of the fundamental differencing theorem. The fundamental differencing theorem states that linear biases can be accounted for either by reducing the number of observations so that the biases cancel, or by adding an equal number of unknowns to model the biases. Both approaches give

identical results, under certain circumstances. Implicitly differenced observations are preferred because they permit greater insight into physical and geometrical meaning of the observable states within the GNSS receiver (Wells et al. 1987).

Presented in equation (2.19) is the implicit differencing strategy adopted within the DCM and IRC strategies (Laurichesse and Mercier 2007; Collins 2008).

$$\begin{bmatrix} P_{IF}^{s} \\ \Phi_{IF}^{ps} \\ \Phi_{MW}^{ps} \end{bmatrix} = \begin{bmatrix} 1 & 1 & 0 & 0 & 0 & 0 \\ 1 & 0 & 1 & 0 & 1 & \frac{60}{137} \\ 0 & 0 & 0 & 1 & 0 & 1 \end{bmatrix} \begin{bmatrix} \rho_{u}^{s} \\ dt_{u,IF}^{s} \\ \phi t_{u,IF}^{ps} \\ \phi_{u,WL}^{ps} \\ \lambda_{1} N_{u,1}^{ps} \\ \lambda_{WL} N_{u,WL}^{ps} \end{bmatrix} \tag{2.19}$$

Presented in equation (2.20) is the implicit differencing strategy adopted within the FCB approach presented in Ge et al. (2008), where the Melbourne-Wübbena combination is formed independently of the least-squares adjustment and treated as a "correction term", thus appearing on the left-hand side of the equation. Fixing of the L1 ambiguity term only occurs if the fixed widelane is introduced. Fixing of the ionosphere-free ambiguity term only occurs when both parameters are fixed.

$$\begin{bmatrix} P_{IF}^{s} \\ \Phi_{IF}^{ps} \end{bmatrix} - \begin{bmatrix} 0 \\ \lambda_{WL} \left[N_{u,WL}^{s} - N_{u,WL}^{p} \right] \end{bmatrix} = \begin{bmatrix} 1 & 1 & 0 \\ 1 & 1 & 1 \end{bmatrix} \begin{bmatrix} \rho_{u}^{s} \\ dt_{u}^{s} \\ \lambda_{1} \left[N_{u,1}^{s} - N_{u,1}^{p} \right] \end{bmatrix} \tag{2.20}$$

The notation $N_{u,1}^{s} - N_{u,1}^{p}$ is used to emphasize the explicit differencing of the ambiguity terms.

2.3.2 Satellite equipment delay

Integer ambiguity resolution of carrier-phase measurements from a single receiver can be implemented by applying additional satellite (correction) products, where the fractional component of the satellite hardware delay has been separated from the integer ambiguities in a network solution (Laurichesse and Mercier 2007; Collins 2008; Mervart et al. 2008; Ge et al. 2008; Teunissen et al. 2010; Bertiger et al. 2010; Geng et al. 2012; Lannes and Prieur 2013). The satellite equipment delays or PPP-AR products are typically provided to the user in two formats, either assimilated within the clocks or provided as a fractional-cycle phase bias. Presented in Chapter 3 is an examination of each of the public providers of PPP-AR products.

2.4 Slant ionosphere estimation

As mentioned in Section 2.3, with the conventional PPP model, ionosphere-free linear combination was typically formed as the ionosphere delay was considered as a nuisance parameter. Capitalizing on the infrastructure built around the conventional PPP model and expanding on previous literature on ultra-long baseline positioning (Bock et al. 1985; Goad 1985; Blewitt 1989), the Melbourne-Wübbena linear combination was introduced to enable PPP-AR. The ionosphere-free ambiguity term was decomposed into the widelane and L1 ambiguity terms. With PPP-AR still requiring 10's of minutes to converge and re-convergence still problematic, the PPP model was further evolved to permit access to the slant ionosphere component. The consequence of using ionosphere-free linear combinations, prevents direct access to the ionosphere component thereby preventing

ionosphere constraining. If the slant ionosphere term is estimated, but no a priori information about the ionosphere is available (no constraints are imposed on the ionosphere parameters), it is equivalent to the ionosphere-free combination.

Ionospheric corrections generated using a regional or even a global network of stations can also be beneficial for reducing the convergence time in PPP. There have been two options discussed in literature for mitigating ionosphere information in the absence of dedicated reference stations: 1) a peer-to-peer approach, and 2) decomposition of the ionosphere and utilization of vertical TEC (VTEC) using external sources.

When constraining slant ionosphere delays in the PPP solution, benefits in terms of precisions are expected if the quality of the external corrections is superior to that of code noise (Banville et al. 2014). If the a priori estimate of the ionosphere is precise enough, then ambiguity fixing becomes achievable with only a few minutes of data being collected which enables cm-level accuracy (Geng 2010; Collins et al. 2012; Li 2012; Ge et al. 2012; Banville et al. 2014). Availability of slant ionosphere knowledge also allows for quick re-convergence to ambiguity-fixed solutions following a discontinuity in measurements (Geng 2010; Collins and Bisnath 2011; Collins et al. 2012), as well as improving initialization (Ge et al. 2012; Yao et al. 2013; Banville et al. 2014; Lou et al. 2016; Liu et al. 2017).

In the literature, there are two common approaches that allow ionospheric constraining while utilizing the ionosphere-free linear combinations. Geng (2010) computed the slant ionosphere term external to the least-squares adjustment, under the assumption that the other terms state terms were precisely estimated. Rather than forming the Melbourne-

Wübbena combination external of the least-squares solution (equation (2.20)), Ge et al. (2008) and Geng (2010) formed the widelane linear combination external to the least-squares adjustment and applied the estimated slant ionosphere as a correction term. The successfully resolved ambiguity term is introduced as a correction term in a similar approach as in equation (2.20) with the key difference being the widelane ambiguity term was resolved faster due to the a priori knowledge of the ionosphere.

Collins et al. (2012) adopted a more formal representation, whereby the estimation of the slant ionosphere term was included within the least-squares adjustment. To permit the estimation of the slant ionosphere term, the Melbourne-Wübbena linear combination was decomposed into its constituents, the narrowlane code and widelane phase as presented in equation (2.21). The DCM was rebranded into the Extended Decoupled Clock Model (EDCM). Collins et al. (2012) stated two benefits to processing the widelane and narrowlane combination simultaneously with the ionosphere-free observables. The first is that the station and satellite widelane equipment delays can be treated as non-constant, clock-like parameters identical to the code and phase clocks. Additionally, the least-squares system is less vulnerable to incorrectly fixed widelane ambiguities biasing the solution. Residual testing can be used to restart estimation of both the widelane and ionosphere-free ambiguities if bad fixes on either observable are suspected. Both effects provide for a more robust solution, with as few a priori assumptions as possible (Collins et al. 2012).

$$\begin{bmatrix} P_{IF}^{s} \\ \Phi_{IF}^{ps} \\ P_{NL}^{s} \\ \Phi_{WL}^{ps} \end{bmatrix} = \begin{bmatrix} 1 & 1 & 0 & 0 & 0 & 0 & 0 \\ 1 & 0 & 1 & 0 & 0 & 1 & \frac{60}{137} \\ 1 & 0 & 1 & 1 & \sqrt{\mu_2} & 0 & 0 \\ 1 & 0 & 1 & 0 & \sqrt{\mu_2} & 0 & 1 \end{bmatrix} \begin{bmatrix} \rho_u^s \\ dt_{u,IF}^s \\ \phi t_{u,IF}^{ps} \\ \phi_{u,WL}^{ps} \\ I_u^s \\ \lambda_1 N_{u,1}^{ps} \\ \lambda_{WL} N_{u,WL}^{ps} \end{bmatrix} \tag{2.21}$$

The optimality of linear combinations can be defined based on several criteria, such as noise reduction, ionosphere delay reduction, or wavelength amplification (Collins 1999b). In recent literature, the role of linear combinations is not clearly acknowledged, as over the decades, it has become "common knowledge" within the GNSS field. Typically, linear combinations are formed to reduce the number of parameters to be estimated, thereby eliminating the terms that are not of interest-nuisance parameters. As previously mentioned, this is why the ionosphere-free linear combination became the industry standard over the past two decades, as the ionosphere delay was not of interest within the positioning community. The pursuit of AR led to introduction of a third linear combination, then with interest in ionosphere constraining, a fourth linear combination. With the introduction of multi-GNSS and multi-frequency PPP, some researchers were forming more linear combinations than the number of underlying measurements (discussed in more detail in Section 2.6).

At this juncture in PPP's evolution, it became more intuitive to adopt a more elegant strategy of processing GNSS data using the raw uncombined observations, where the slant ionosphere delays are estimated as unknown parameters (Wells et al. 1987; Schaffrin and Bock 1988; Odijk 2002; Zhang et al. 2011; Li 2012). If mathematical correlations are

properly accounted for, it can be shown that combined measurements are equivalent to the processing of the uncombined measurements (Banville et al. 2014).

Presented in equation (2.22) is the mathematical model used to process dual-frequency uncombined measurements which is a scalable implementation to utilize uncombined measurements in the presence of multi-constellations and multi-frequencies.

$$\begin{bmatrix} P_1^s \\ P_2^s \\ \Phi_1^{ps} \\ \Phi_2^{ps} \end{bmatrix} = \begin{bmatrix} 1 & 1 & 0 & 0 & 1 & 0 & 0 \\ 1 & 1 & 0 & 0 & \mu_2 & 0 & 0 \\ 1 & 0 & 1 & 0 & -1 & 1 & 0 \\ 1 & 0 & 1 & 1 & -\mu_2 & 0 & 1 \end{bmatrix} \begin{bmatrix} \rho_u^s \\ dt_u^s \\ \delta t_u^{ps} \\ \delta_{\Phi 12} \\ I_{u,1}^{ps} \\ \lambda_1 N_{u,1}^{ps} \\ \lambda_2 N_{u,2}^{ps} \end{bmatrix} + \begin{bmatrix} d_1 \\ d_2 \\ \delta_1 \\ \delta_2 \end{bmatrix} \tag{2.22}$$

Within the least-squares solution, it is favoured to present the model in an uncombined representation as it is easily scalable and the estimated state terms directly represent the physical observable atmospheric effects and receiver dependent equipment delays. The benefits of utilizing the combined measurements is primarily due to reduction of the computational load as well as for simplicity in a priori and a posteriori quality control. Presented in equations (2.23) and (2.24) are the transformation matrices that can be utilized to convert measurements, residuals and ambiguities between combined and uncombined representations.

Uncombined to combined:

$$\begin{bmatrix} P_{IF}^s \\ \Phi_{IF}^s \\ p_{NL}^s \\ \Phi_{WL}^s \end{bmatrix} = \begin{bmatrix} \alpha_{IF} & \beta_{IF} & 0 & 0 \\ 0 & 0 & \alpha_{IF} & \beta_{IF} \\ -\alpha_{NL} & -\beta_{NL} & 0 & 0 \\ 0 & 0 & \alpha_{WL} & -\beta_{WL} \end{bmatrix} \begin{bmatrix} P_1^s \\ P_2^s \\ \Phi_1^s \\ \Phi_2^s \end{bmatrix} \tag{2.23}$$

Combined to uncombined:

$$\begin{bmatrix} P_1^s \\ P_2^s \\ \Phi_1^s \\ \Phi_2^s \end{bmatrix} = \begin{bmatrix} \frac{f_1 - f_2}{f_1} & 0 & \frac{f_1}{f_2} & 0 \\ -\frac{f_1 - f_2}{f_2} & 0 & \frac{f_2}{f_1} & 0 \\ 0 & \frac{f_1 + f_2}{f_1} & 0 & -\frac{f_1}{f_2} \\ 0 & \frac{f_1 + f_2}{f_2} & 0 & -\frac{f_1}{f_2} \end{bmatrix} \begin{bmatrix} P_{IF}^s \\ \Phi_{IF}^s \\ P_{NL}^s \\ \Phi_{WL}^s \end{bmatrix} \tag{2.24}$$

To illustrate the equivalence of the combined and uncombined processing, the P_1 and P_2 pseudorange residuals are presented in Figure 2.3, in which subplot (a) and (b) are the residuals of P_1 and P_2 from the uncombined processing. In Figure 2.3 (c), the residuals were recombined using the measurement combination co-efficients α_{IF} and β_{IF} . In Figure 2.3 (d) are the ionospheric-free pseudorange residuals which were produced through conventional PPP processing. The recombined residuals had a standard deviation of 91.8 cm, where as the ionospheric-free pseudorange residuals from conventional processing had a standard deviation of 91.9 cm, indicating the equivalence between the uncombined and combined processing. There is strength in both approaches, such that, in conventional PPP

the residuals can be transformed into an uncombined representation to detect faults on a specific signal.

(a) P_1 pseudorange residuals

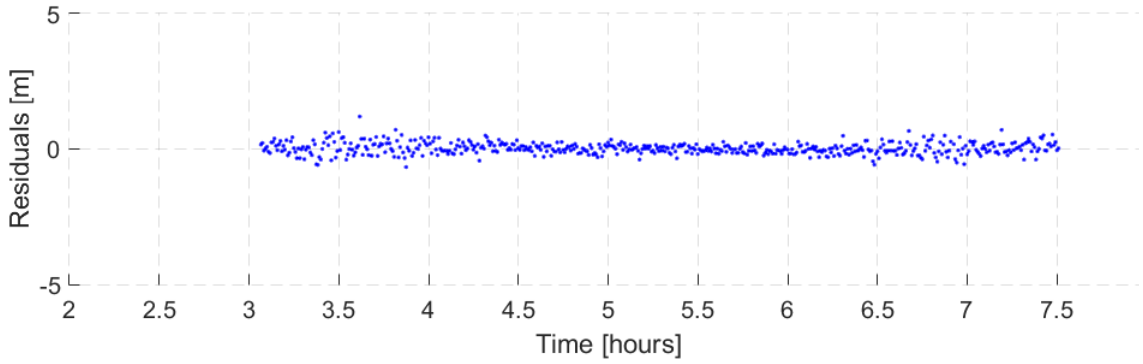

(b) P_2 pseudorange residuals

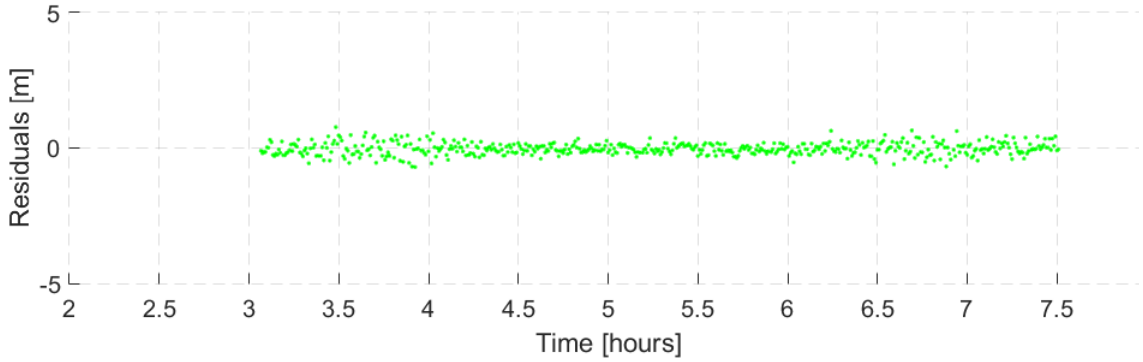

(c) Combined P_1 and P_2 pseudorange residuals

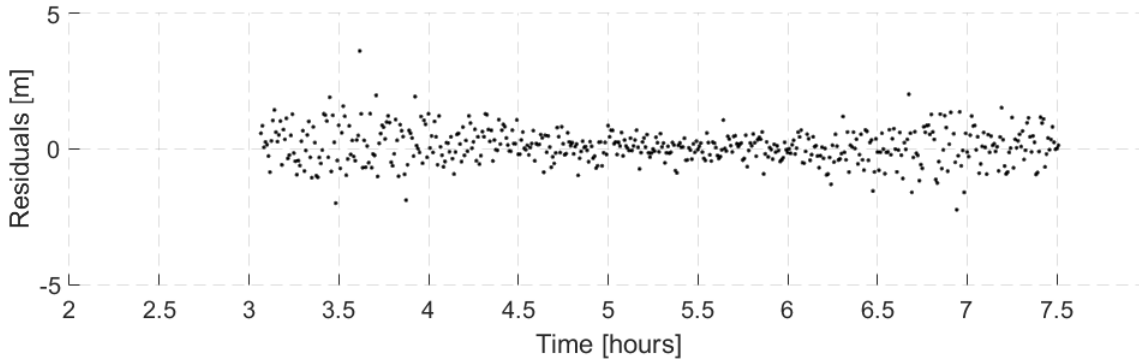

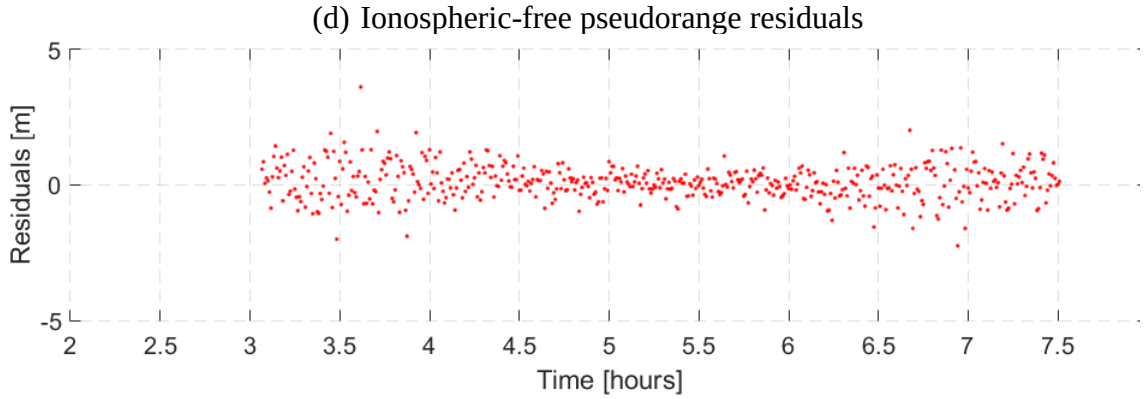

Figure 2.3: Illustration of the residuals for PRN 4 of P1 and P2 pseudorange measurements, combined P1 and P2 and linearly combined ionosphere-free pseudorange measurements for the site NRC1 DOY 178 of 2016 located in Ottawa, Canada.

2.5 Multi-GNSS PPP

Alongside PPP research into the utility of slant ionosphere estimation, research into multi-GNSS (initially GPS and GLONASS) positioning was achieving its maturity as GLONASS re-attained its operational status in October 2011 and the second generation of BeiDou satellites were launched in 2009, with each successive year new geostationary orbit (GEO) and medium Earth orbit (MEO) satellites. The benefits of providing the PPP user with a multi-GNSS solution has always shown its strength in environments such as urban canyons, mountainous areas and open-pit mines, where the visibility of signals is hindered, and available signals become contaminated with multipath and noise. The integration of multiple constellations provides additional independently generated signals, enhanced satellite geometry and improves the quality of solutions in PPP processing.

Research quantifying the improvements of a multi-GNSS PPP solution is not in short supply. (2011), Defraigne and Baire (2011), Wang et al. (2012), Cai and Gao (2013), Tu

et al. (2013), Choy et al. (2013), Chuang et al. (2013), Li and Zhang (2014), Aggrey (2015) and Mohammed et al. (2016) all illustrate similar results of initial convergence times being reduced, but with insignificant improvement in regards to accuracy of the solution after filter convergence with GLONASS. Cai and Gao (2013) showed improvement in the position accuracy from GPS-only solutions of 39%, 30% and 60% in the easting, northing and up components. Even though Choy et al. (2013)'s sample size consisted of only a few stations, similar results were noted. The performance of the combined GPS and GLONASS PPP in kinematic mode, showed improvement of 43% and 25% in the horizontal and vertical components, respectively, and the inclusion of GLONASS did not improve the accuracy of the converged solution filter. Wang et al. (2012) focused on investigating the trend and periodic residual characteristic of combined GPS and GLONASS observations. Their results showed that the positional accuracy of GPS was better than that of GLONASS by 38 %, 17% and 1% in the northing, easting and up components, respectively. Li and Zhang (2014) noted that the average convergence time can be reduced by 46 % from 23 to 12 minutes in static mode and by 60 % from 41 to 18 minutes in kinematic mode, respectively.

As a multi-GNSS solution led to reductions in filter convergence, the next intuitive step was to look at the contribution of GLONASS in regards to GPS-AR. GPS-AR with float GLONASS ambiguities was the focus of the research presented by Li and Zhang (2014) and Jokinen et al. (2013b). Their research showed that the integration of GPS and GLONASS sped up convergence and increased the accuracy of float ambiguity estimates, which contributed to enhanced success rates and reliability of fixing ambiguities. Li and

Zhang (2014) showed that the average time to the first-fixed solution can be reduced by 27% from 22 to 16 minutes in static mode and by 42% from 34 to 20 minutes in kinematic mode, respectively. Jokinen et al. (2013b) research showed that on average improvements were not as significant as Li and Zhang (2014), as the convergence time of GPS-AR only improved by 5% with the inclusion of GLONASS. Jokinen et al. (2013b) noted that improvements were dataset dependent, where specific datasets within their sample size showed improvements as much as 10 minutes.

As discussed in Section 2.3, the primary challenge in PPP-AR relates to the estimation of the satellite equipment delays within a network of reference stations. While PPP-AR has been well achieved for GPS, estimation of satellite equipment delays for GLONASS is difficult because (1) satellites do not share the same frequencies as they are Frequency Division Multiple Access signals; and even worse, (2) pseudorange hardware biases of receivers vary in an irregular manner with manufacturers, antennas, domes, firmware, etc., which especially complicates GLONASS PPP-AR over heterogenous receivers (Wanninger 2012).

The addition of the BeiDou, Galileo and GLONASS systems to standard GPS-only processing reduced convergence time almost by 70%, while the positioning accuracy is improved by about 25%. Some outliers in the GPS-only solutions were removed when multi-GNSS observations were processed simultaneous. The availability and reliability of GPS-only PPP decreases dramatically as the elevation cut-off increases. However, the availability and reliability of the multi-GNSS PPP is less sensitive and few centimetres are still achievable in the horizontal components even with 40° elevation cut-off. At 30° and

40° elevation cut-offs, the availability rates of GPS-only solution drop significantly to 70 and 40 %, respectively (Li et al. 2015).

Banville (2016b) proposed a strategy which benefited from the frequency spacing of GLONASS frequencies on the L1 and L2 bands, allowing for an ionosphere-free ambiguity with a wavelength of approximately 5 cm to be defined; therefore, avoiding the problematic widelane ambiguity resolution. Based on 12 independent baselines with a mean inter-station distance of about 850 km over a 1-week period, it was demonstrated that close to 95% of the estimated double-differenced ionosphere-free ambiguities are within 0.15 cycles of an integer, thereby suggesting that long-baseline ambiguity resolution can be achieved for GLONASS. Applying between station ambiguity constraints was found to improve longitudinal repeatability in static mode by more than 20% for sessions between 2 and 6 hours in duration. In kinematic mode, only limited improvements were made to the initial convergence period since the short wavelength of GLONASS ionosphere-free ambiguities requires the solution to be nearly converged before successful ambiguity resolution can be achieved.

Geng and Bock (2016) proposed a general approach where external ionosphere products were introduced into GLONASS PPP to estimate precise FCBs. Geng and Bock (2016) described the approach as being less impaired by pseudorange equipment delays of different types of receivers. One month of GLONASS data from 550 European stations were processed. From a network of 51 inhomogeneous receivers, including four receiver types with various antennas and spanning about 800 km in both longitudinal and latitudinal directions, it was found that 92% of all fractional parts of GLONASS widelane ambiguities

agreed within ±0.15 cycles with a standard deviation of 0.09 cycles if global ionosphere maps (GIMs) are introduced, compared to only 52% within ±0.15 cycles and a larger standard deviation of 0.22 cycles otherwise. Hourly static GLONASS PPP-AR at 40 test stations can reach position estimates of approximately 1 and 2 cm in rms error with respect to the reference stations for the horizontal and vertical components, respectively. These solutions are comparable to hourly GPS PPP-AR. Integrated GLONASS and GPS PPP-AR can further achieve an rms error of approximately 0.5 cm in horizontal and 1–2 cm in vertical components. It was noted that the performance of GLONASS PPP-AR across inhomogeneous receivers depend on the accuracy of ionosphere products (Geng and Bock 2016; Geng and Shi 2017).

Li et al. (2017) examined PPP-AR using the observations acquired from a quad-constellation, comprised of GPS, BDS, GLONASS, and Galileo (GCRE) utilizing the FCB approach. The BDS satellite-induced code biases were corrected for GEO, IGSO, and MEO satellites before the UPD estimation. An average time to first fix (TTFF) of 9 minutes with 7° cutoff elevation angle can be achieved for GCRE PPP AR, which is much shorter than that of GPS (18 minutes), GR (12 minutes), GE (15 minutes) and GC (13 minutes). With observation length of 10 minutes, the positioning accuracy of the GCRE fixed solution is 1.8, 1.1, and 1.5 cm, while the GPS-only result is 2.3, 1.3, and 9.7 cm for the east, north, and vertical components, respectively. When the cutoff elevation angle is increased to 30°, the GPS-only PPP AR results are very unreliable, while 13 minutes of TTFF is still achievable for GCRE four-system solutions.

2.6 Multi-frequency PPP

With a growing number of multi-GNSS satellites available to the GNSS users, there were also additional signals being made available. The new signals included additional civilian signals and frequencies. The availability of additional signals and frequencies occurred as the older satellites are being replaced by the newer satellites with expanded and improved capabilities. The GPS civilian L2C signal that was introduced with Block IIR-M, provided dual-frequency capabilities to civilian users. Once L2C becomes fully operational, it will remove the necessity for codeless or semi-codeless receivers. The availability of a second civilian signal will open up the GNSS market to other chip manufacturers, increasing competition in a previously stagnant market, thereby reducing the cost of accuracy (Leveson 2006). Even more notable is the introduction of the L5 signal, which began transmitting in May 2010 with the introduction of Block IIF satellites. Some of the benefits of the L5 signal in contrast to the L1 and L2 includes: improved signal structure for enhanced performance, higher transmitted power than L1/L2 signal (~3 dB, or 2× as powerful), wider bandwidth which provides a 10× processing gain, sharper autocorrelation (in absolute terms, not relative to chip time duration) and a higher sampling rate at the receiver and longer spreading codes (Leveson 2006).

Planned modernization of GLONASS include an additional signal transmitted on the L5 frequency, and a switch from Frequency-Division Multiple Access (FDMA) to Code-Division Multiple Access (CDMA), which would increase potential interoperability with other GNSS. Galileo, the European GNSS, is still under development (De Bakker 2016). The Galileo system will transmit navigation signals on four different carrier frequencies:

L1/E1, L5/E5a, E5b and E6, two of which (E5a and E5b) can also be tracked together as one extra wide-band (Alt-BOC) signal.

For the three or four frequency carrier-phase measurements case, such as the modernized GPS, BeiDou navigation satellite system (BDS) and GALILEO, the linear combinations become much more complicated. Based on the pre-defined extra-widelane (EWL) and WL linear combinations, Forssell et al. (1997) and Jung et al. (2000) presented the Three Carrier Ambiguity Resolution (TCAR) method and the Cascade Integer Resolution (CIR) method for GALILEO and GPS, respectively. Han and Rizos (1999) presented the definition of the carrier-phase linear combination for the triple-frequency case and discussed the AR strategies without and with distance constraints by applying the Least-squares AMBiguity Decorrelation Adjustment (LAMBDA) method to the GF GNSS model. Richert and El-Sheimy (2007) studied the optimal GPS and GALILEO linear combinations for differential positioning over medium to long baselines. Feng (2008) introduced the optimal ionosphere reduced linear combinations for the geometry-based TCAR. Cocard et al. (2008) systematically investigated the GPS triple-frequency integer phase combinations with an analytical method and found that the sum of the integer coefficients of the combinations was an important indicator for systematic classification of sets of combinations. Zhang and He (2015) examined the BeiDou triple-frequency linear combinations based on the relevant methods of Richert and El-Sheimy (2007) and Cocard et al. (2008). Hatch (2006) presented a GF and refraction-corrected method for long baseline AR. Li et al. (2010) also studied the GF and IF combinations for estimating the narrowlane ambiguity without distance constraints. Li et al. (2012) presented the optimal triple-frequency IF combination and the

GF and IF combination for long baseline AR and precise positioning and shown that the GALILEO (E1, E6, E5a) has the best performance of long baselines AR, a similar study that was presented by Wang and Rothacher (2013).

Geng and Bock (2016) used a hardware simulator to generate triple-frequency signals which were collected with a high-grade receiver to collect 1 Hz data. Measurement noise and multipath was varied to examine the potential benefit of triple-frequency data under different conditions. When the carrier-phase precisions on L1, L2 and L5 were set to 1.5, 6.3 and 1.5 mm, respectively, widelane ambiguity resolution attained a correctness rate of over 99% within 20 s. As a result, the correctness rate of narrow-lane ambiguity resolution achieves 99% within 65 s, in contrast to only 64% within 150s in dual-frequency PPP. It was noted that widelane ambiguity resolution was still reliable if the L2 carrier-phase precision was degraded to 6 mm. For the simulated high multipath data sets with new ambiguities for all satellites introduced every 120s, it was found that ambiguity-fixed solutions are achieved at 78% of all epochs in triple-frequency PPP, whilst almost no ambiguities are resolved in dual-frequency PPP.

Laurichesse and Blot (2016) utilized data from the IGS Real Time service where by satellite carrier-phase equipment delays were computed for the triple-frequency measurements. For the test, 10 triple-frequency satellites were in view for the GPS and BeiDou constellations. A series of widelane-only combinations were formed. By using the triple-frequency biases, 20 cm accuracy is reached in 2 minutes, compared to 5 minutes with the use of the dual-frequency biases.

2.7 Summary of PPP evolution

The standard practice in PPP was to linearly combine two pseudoranges and two carrier-phases to produce ionosphere-free linear pseudoranges and carrier-phase combinations which eliminated the ionosphere delay (to the first order). As such, the linear combination was favoured in contrast to the estimation of the slant ionosphere delay. The PPP model ionosphere free pseudoranges and carrier-phases is referred to as the conventional PPP model, which provides the user a float-only (ambiguity unresolved) solution. After, the PPP model evolved as research begun to focus on mitigating convergence time.

The first step in its evolution was with the research interest in capturing the underlying integer natured ambiguities. If the ambiguities were isolated and estimated as integers, then there would be more information that could be exploited to accelerate convergence to permit cm-level horizontal accuracy. This required expansion of the model to include the Melbourne-Wübbena linear combination and decomposition of the ionosphere ambiguity into a widelane and L1 ambiguity with an approximate wavelength of 86.2 and 10.7 cm, respectively.

With the resolution of the ambiguities, it was soon realized that capturing the integer-natured ambiguities were not the only key required to unlocking instantaneous cm-level PPP convergence. As with relative positioning, it was a two-step process. Firstly, it requires the elimination of the atmospheric terms, which permitted fast convergence of the float ambiguity term. Secondly it requires the elimination of the hardware delays, which enabled access to the integer ambiguity term. As a result of the need to access the atmospheric term

drove researchers to examine strategies to access the ionosphere term on a software foundation build around the ionosphere-free linear combination. The easier solution, given the foundation restrictions, was to decompose the Melbourne-Wübbena linear combination into its constituents, the narrowlane code and the widelane phase. With a priori slant ionosphere information being introduced, instantaneous cm-level convergence was attainable.

With a growing number constellations and frequencies, the foundation built around the ionosphere-free linear combination needed to be changed, as ad hoc linear combinations of the measurements were being formed. As this juncture, uncombined measurements were adopted into the PPP user model, as it facilitated easier scalability in the PPP user infrastructure. With triple-frequency measurements, improved convergence was noted as additional knowledge about the ionosphere was made available from a signal with a stronger transmission. With the introduction of multi-constellations, an abundance of independent measurements were made available, thereby improving geometry. The additional measurements allowed faster convergence of the float ambiguity, thereby improving time to provide an ambiguity resolved solution. Also creating new research in avenues such as how to select an optimal subset of measurements. Presented in Figure 2.4 is an overview of the described evolution of the PPP user model and presented in Table 2.1

is the preferred measurements within YorkU-PPP multi-GNSS and multi-frequency model for the RINEX 2 and 3 standard.

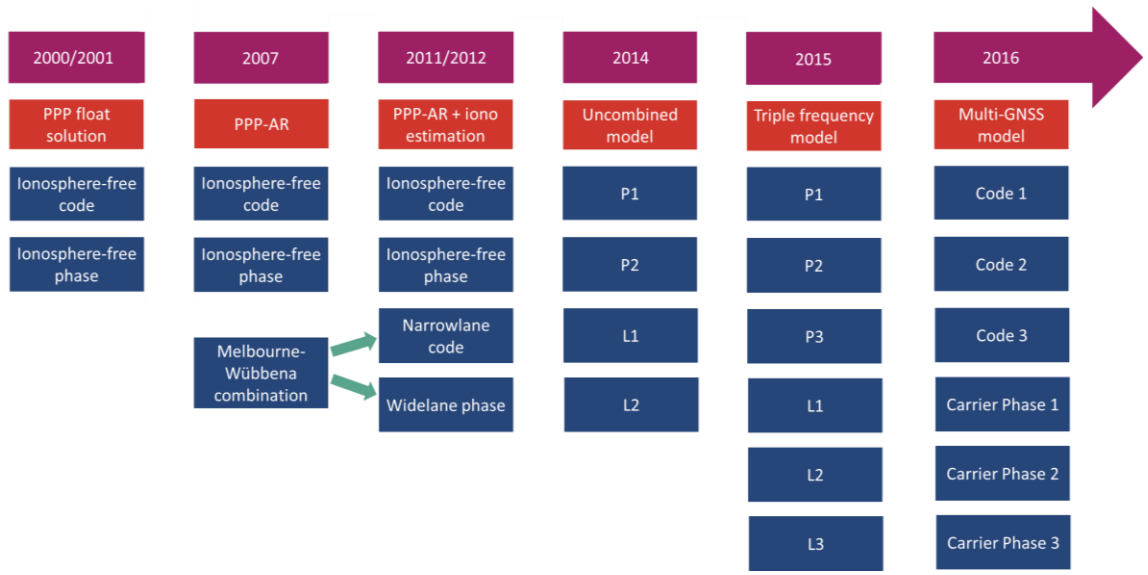

Figure 2.4: Transition towards the uncombined PPP mathematical model.

Table 2.1: Preferred measurements within YorkU-PPP multi-GNSS model.

		GPS		GLONASS		GALILEO		BEIDOU	
		RINEX 2	RINEX 3	RINEX 2	RINEX 3	RINEX 2	RINEX 3	RINEX 2	RINEX 3
Code	1	P1	C1W	P1	C1P	C1	C1Z	-	C1X
	2	P2	C2W	P2	C2P	C7	C8X	-	C7X
	3	C5	C5X	-	C3X	C6	C6X	-	C6X
Carrier phase	1	L1	L1W	L1	L1P	L1	L1Z	-	L1X
	2	L2	L2W	L2	L2P	L7	L8X	-	L7X
	3	L5	L5X	-	L3X	L6	L6Z	-	L6X

CHAPTER 3 EXAMINATION OF THE INTEROPERABILITY PPP-AR PRODUCTS

The equivalence in the performance of the different PPP-AR strategies has been shown extensively in literature with limited focus on integrity and reliability of ambiguity resolution in PPP. One strategy for improving availability, continuity and reliability is by allowing the user interoperability of the different providers of PPP-AR products. Examined within this chapter are the different public providers of the products that enable ambiguity resolution, the transformations needed to utilize the PPP-AR products in different formats, analysis of the performance of each of the products and some of the challenges that hinder interoperability.

3.1 Introduction into PPP-AR product interoperability

While the different strategies (FCB, DC, IRC) make different assumptions, there are fundamental similarities between them. For the PPP user, the mathematical model is similar; the different PPP-AR products contain the same information and as a result should permit one-to-one transformations between them, allowing interoperability of the PPP-AR products (Teunissen and Khodabandeh 2015; Seepersad and Bisnath 2017). The advantage of interoperability of the different PPP-AR products would be to permit the PPP user to transform independently generated PPP-AR products to obtain multiple fixed solutions of comparable precision and accuracy. The ability to provide multiple solutions would increase availability and continuity, thereby increasing reliability of the solution. For, e.g.,

real-time processing: if there were an outage in the generation of the PPP-AR products, the user could instantly switch streams to a different provider.

The following sections examine the transformation matrix used to transform the combined (IRC and FCB) products to the DCM format (dt_{IF}^{s}, δt_{IF}^{s}, δ_{WN}^{s}), as well as the transformation of all three products to an uncombed observable dependent format (d_1^s, d_2^s, δ_1^s, δ_2^s). The novelty of the research presented is focused on the transformation of the IRC and FCB products to the DCM format which was first published Seepersad and Bisnath (2015), as well as the performance of the transformed products. Aspects of the transformation have been published in literature. Laurichesse (2014) focused on the transformation of the IRC products into an uncombined representation to integrate within the RTCM SSR standard. Teunissen and Khodabandeh (2015) presented the derivation and transformation of different models that enables PPP-AR to an uncombined representation. One of the limitations of the research presented by Teunissen and Khodabandeh (2015) was the assumption that the IRC and DCM products were identical due to the mathematical equivalence of the models. Banville (2016a) presented transformations of IRC, DCM and FCB into an uncombined representation as well. As mentioned by Banville (2016a), one of the benefits of an uncombined representation, it becomes simpler for the PPP user to adopt a standardized model to enable PPP-AR. Such a standardized approach also simplifies the approach of combining multiple PPP-AR products, which would improve reliability and consistency of the products, is examined in more detail in Chapter 4.

For the convenience of the reader, the PPP-AR model from equations (2.21) and (2.22) is recalled, which illustrates the application of the PPP-AR products in the DCM combined format, equation (3.1) and the uncombined format, equation (3.2). For simplicity, all products are transformed into units of metres. The notations used to represent the PPP-AR products, while relative in nature, is presented utilizing absolute notation as the research focus is on the user implementation of the products.

Combined representation

$$\begin{bmatrix} P_{IF}^{s} \\ \Phi_{IF}^{ps} \\ P_{NL}^{s} \\ \Phi_{WL}^{ps} \end{bmatrix} = \begin{bmatrix} 1 & 1 & 0 & 0 & 0 & 0 & 0 \\ 1 & 0 & 1 & 0 & 0 & 1 & \frac{60}{137} \\ 1 & 0 & 1 & 1 & \sqrt{\mu_2} & 0 & 0 \\ 1 & 0 & 1 & 0 & \sqrt{\mu_2} & 0 & 1 \end{bmatrix} \begin{bmatrix} \rho_u^s \\ dt_u \\ \phi t_u \\ \phi_{u,MW} \\ I_u^{ps} \\ \lambda_{NL} N_{u,1}^{ps} \\ \lambda_{WL} N_{u,WL}^{ps} \end{bmatrix} + \begin{bmatrix} 1 & 0 & 0 \\ 0 & 1 & 0 \\ 0 & 1 & 1 \\ 0 & 1 & 0 \end{bmatrix} \begin{bmatrix} dt^s \\ \delta t^s \\ \delta^s \end{bmatrix} \tag{3.1}$$

Uncombined representation

$$\begin{bmatrix} P_1^s \\ P_2^s \\ \Phi_1^{ps} \\ \Phi_2^{ps} \end{bmatrix} = \begin{bmatrix} 1 & 1 & 0 & 0 & 1 & 0 & 0 \\ 1 & 1 & 0 & 0 & \mu_2 & 0 & 0 \\ 1 & 0 & 1 & 0 & -1 & 1 & 0 \\ 1 & 0 & 1 & 1 & -\mu_2 & 0 & 1 \end{bmatrix} \begin{bmatrix} \rho_u^s \\ dt_u \\ \delta t_u \\ \delta_{\Phi 12} \\ I_{u,1}^{ps} \\ \lambda_1 N_{u,1}^{ps} \\ \lambda_2 N_{u,2}^{ps} \end{bmatrix} + \begin{bmatrix} 1 & 1 & 0 & 0 & 0 \\ 1 & 0 & 1 & 0 & 0 \\ 1 & 0 & 0 & 1 & 0 \\ 1 & 0 & 0 & 0 & 1 \end{bmatrix} \begin{bmatrix} dt^s \\ d_1^s \\ d_2^s \\ \delta_1^s \\ \delta_2^s \end{bmatrix} \tag{3.2}$$

3.2 PPP-AR Products

Currently, there are three main public providers of products that enable PPP-AR. These include School of Geodesy and Geomatics at Wuhan University (SGG-WHU) (Li et al. 2015; Wuhan University 2017), which provides global post processed FCB products, Natural Resources Canada (NRCan) (Collins 2008; NRCan 2015), which provides post-processed DCM products, and Centre national d'études spatiales (Laurichesse et al. 2009; CNES 2015), which provides post-processed and real-time IRC products. The original format and units of the products are identified within each of the following sections and all figures and transformation matrices presented assume the products are in units of metres.

3.2.1 Decoupled clocks

The underlying concept of the DCM presented by Collins et al. (2008) is that the carrier-phase and pseudorange measurements are not synchronized with each other at the equivalent levels of precision. The timing of the different observables must be considered separately, if they are to be processed together rigorously. Also, the decoupled clock products make no assumption about the temporal variability of the equipment delays, unlike the other PPP-AR products, as such, they are transmitted in an unfiltered format.

The early DCM was based on ionosphere-free pseudorange and carrier-phase observation equations, as well as the Melbourne-Wübbena combination: equation (2.19) (Collins 2008). Later, the Melbourne-Wübbena combination was decomposed into the narrowlane code and widelane phase constituents to facilitate slant ionosphere estimation and constraining: equation (2.21) (Collins et al. 2010). Both of the models utilized the same

DCM products, where reformulation of the model occurred to enable slant ionosphere estimation and constraining.

Presented in Figure 3.1, Figure 3.2 and Figure 3.3 are each of the three correction terms that comprise the DCM products. The satellite products consist of carrier-phase clock error (δt^s_{DCM}), relative code clock offset (Δdt^s_{DCM}) and widelane correction ($\delta^s_{DCM,MW}$). DCM products are provided as timing parameters; therefore, δt^s_{DCM} is units of seconds and Δdt^s_{DCM} and $\delta^s_{DCM,MW}$, which are relative to the phase clocks, are provided in units of nanoseconds.

Illustrated in Figure 3.1 is the relative satellite carrier-phase clock error (δt^{ps}_{DCM}) for PRN 28 with respect to satellite PRN 5. “relative” is utilized in this context because of the explicit differencing of the clock terms between to PRN 28 and PRN 5, which eliminates the time scale factor because of the reference clock selected by the Analysis Centre (AC). The linear trend, representing the clock drift, was removed to better illustrate the underlying clock error.

The satellite code clock offset Δdt^s_{DCM} represents the difference between the code clock (dt^s_{DCM}) and phase satellite clocks (δt^s_{DCM}) is presented in Figure 3.2. Δdt^s_{DCM} is stored in units of nanoseconds at a 30 second data rate. The Δdt^s_{DCM} makes no assumption on the temporal variability of the equipment delays unlike the other PPP-AR products.

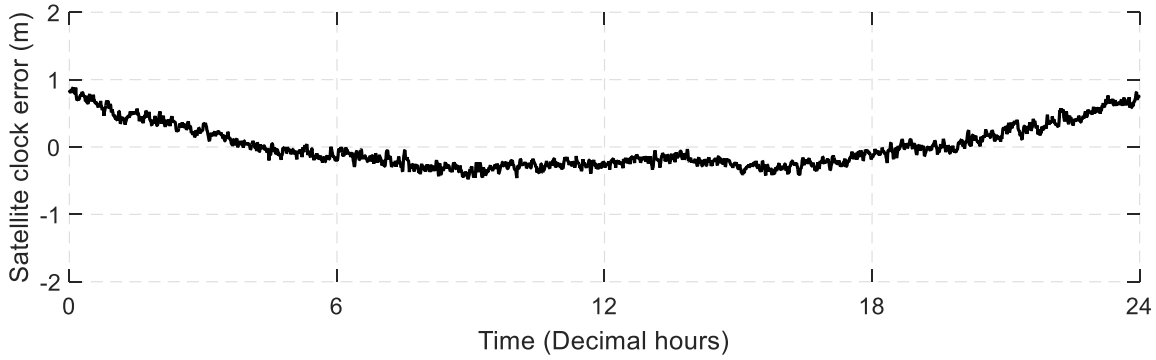

Figure 3.1: Relative satellite carrier-phase clock correction provided by NRCan on DOY 178 of 2016 for PRN 28 (relative to PRN 5). Linear trend has been removed. All units are in metres.

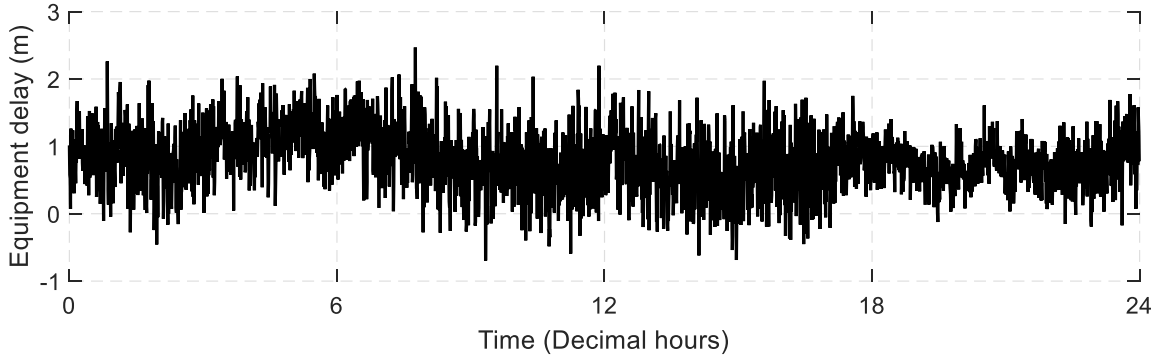

Figure 3.2: Satellite code clock offset provided by NRCan on DOY 178 of 2016 for PRN 28. All units are in metres.

Presented in Figure 3.3 is the satellite widelane correction ($\delta^{s}_{DCM,WL}$) for PRN 28. The satellite widelane correction is comprised of the code and phase equipment delay as a result of the Melbourne-Wübbena linear combination formed within the network solution. The satellite widelane corrections are more stable in time in contrast to the satellite code clock offset. The DCM also makes no assumptions about the temporal variability of the satellite

widelane correction, in contrast to the other providers that treat the terms are daily constants. $\delta^{s}_{DCM,MW}$ is also stored in units of nanoseconds at a 30 second data rate.

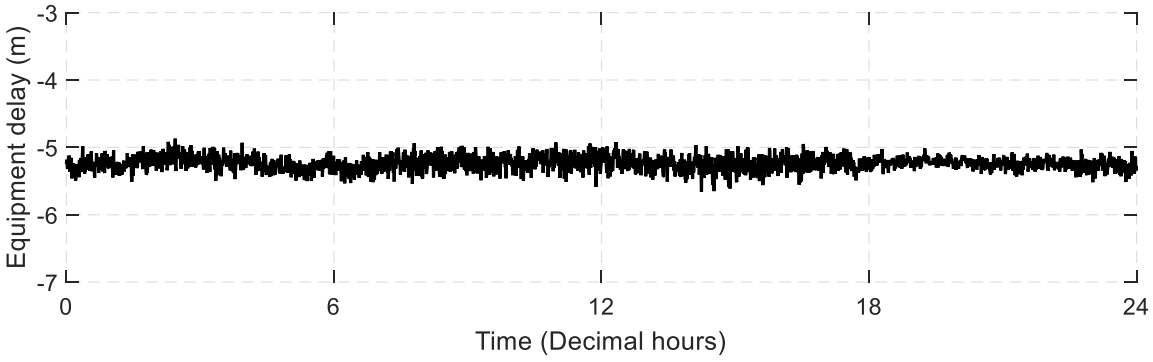

Figure 3.3: Satellite widelane correction provided by NRCan on DOY 178 of 2016 for PRN 28. All units are in metres.

The original YorkU-PPP architecture was designed within the research presented within Seepersad (2012) and Aggrey (2015). Building on the previously established architecture from NRCan CSRS-PPP (NRCan 2015), the engine was extended to include the concepts presented in Collins (2008), as such, code and carrier-phase measurements clocks are treated independently of each other and implicit single-differencing is performed. Presented in equation (3.3) is the application of the DCM products to be utilized in the mathematical model presented in equation (3.1).

$$\begin{bmatrix} dt^{s} \\ \delta t^{s} \\ \delta^{s} \end{bmatrix} = \begin{bmatrix} 1 & 1 & 0 \\ 1 & 0 & 0 \\ 0 & 0 & 1 \end{bmatrix} \begin{bmatrix} \delta t^{s}_{DCM} \\ \Delta dt^{s}_{DCM} \\ \delta^{s}_{WL} \end{bmatrix} \tag{3.3}$$

where all units are in metres.

Presented in equation (3.4) is the transformation of the DCM products to an observable dependent representation. The transformation presented in equation (3.4) was also presented by Banville (2016a). The transformation presented by Teunissen and Khodabandeh (2015) transforms the DCM/IRC products in phase dependent equipment delays, where as in equation (3.4) the phase delays are integrated within the common clock term. In this representation, the satellite clock term (dt^s) is the DCM phase clock, as such the phase equipment delays (δ_1 and δ_2) are zero. The code dependent equipment delays are present within the Δdt^s_{DCM} and δ^s_{WL} terms. The terms Δdt^s_{DCM} and δ^s_{WL} need to be transformed into a code dependent delays, d_1 and d_2.

$$\begin{bmatrix} dt^s \\ d_1 \\ d_2 \\ \delta_1 \\ \delta_2 \end{bmatrix} = \begin{bmatrix} 1 & 0 & 0 \\ 0 & -\frac{1}{\alpha_{WL}} & \frac{f_2}{f_1} \\ 0 & -\frac{1}{\beta_{WL}} & \frac{f_1}{f_2} \\ 0 & 0 & 0 \\ 0 & 0 & 0 \end{bmatrix} \begin{bmatrix} \delta t^s_{DCM} \\ \Delta dt^s_{DCM} \\ \delta^s_{DCM,WL} \end{bmatrix} \tag{3.4}$$

where $\Delta dt^s_{DCM} = dt^s_{DCM} - \delta t^s_{DCM}$

Presented in Figure 3.4 is Δdt^s_{DCM} and δ^s_{WL} for PRN 28 transformed into a code dependent equipment delay, d_1 and d_2. Transformation of the productions into a measurement dependent correction would easily facilitate integration within the Radio Technical Commission for Maritime Services (RTCM) SSR standard (as discussed in Section 2.3).

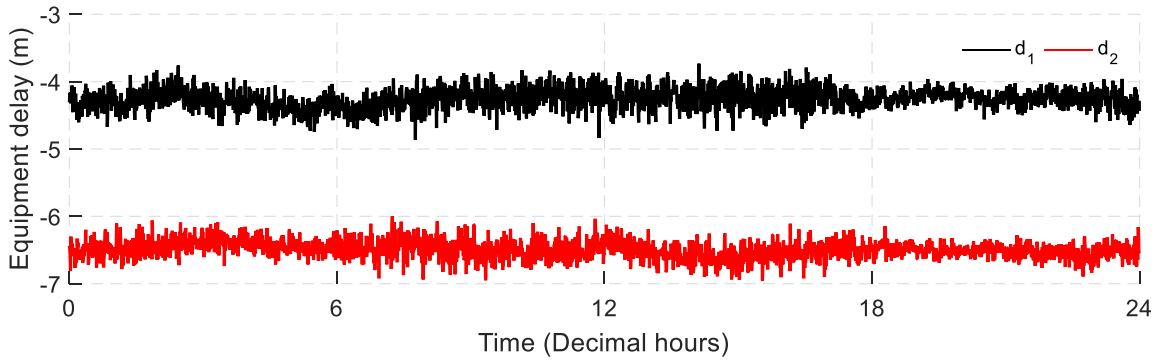

Figure 3.4: Code dependent equipment delay corrections. Corrections were generated from products provided by NRCan on DOY 178 of 2016 for PRN 28. All units are in metres.

3.2.2 Fractional Cycle Bias

FCB was introduced by Ge et al. (2008), where it has also been referred to as Uncalibrated Phase Delay (UPD). The FCB method estimates the equipment delay by averaging the fractional parts of the steady-state float ambiguity estimates to be removed from common satellite clock estimates (Ge et al. 2008). The FCB products consist of a common clock (dt^s_{FCB}), L1 satellite equipment delay ($a^s_{FCB,1}$) and widelane equipment delay ($a^s_{FCB,WL}$). The difference in symbology between DCM (δ) and FCB (a), is due to the term being provided as a correction to the estimated float ambiguity term rather than as a timing correction. $a^s_{FCB,1}$ is the L1 satellite equipment delay, which has been scaled by the narrowlane wavelength of 10.7 cm. In the literature (Geng et al. 2010a), the $a^s_{FCB,1}$ is sometimes referred to as the narrowlane equipment delay, but it is important not to be misconstrueded with the narrowlane linear combination.

Ge et al. (2008), Geng (2010) and Li et al. (2015) opted to provide daily widelane corrections and lower rate L1 corrections, as the satellite equipment delay were sufficiently stable in time and space. Geng (2010) describes the widelane satellite equipment delays as very stable over several days, or even a few months. The widelane FCBs provided by SOPAC are transmitted once every 48 hours (Geng et al. 2013).

FCB products utilized within this study were obtained from SGG-WHU. Currently SGG-WHU produces 14 sets of FCB products, corresponding to different precise products such as those from CODE, ESA, GFZ, GRGS, IGR, and IGS. The FCBs are estimated daily (Li et al. 2015) when the precise products become available. The FCB products can be downloaded from ftp://gnss.sgg.whu.edu.cn/product/FCB and have the prefix "SGG" and the naming convention includes the AC used for generating the FCBs. FCBs generated using the final IGS products were selected as this set of FCB products capitalized on the accuracy and reliability of the combined products IGS. Presented in Figure 3.5 is the relative satellite clock error, dt^{ps} for PRN 28 with respect to satellite PRN 5.

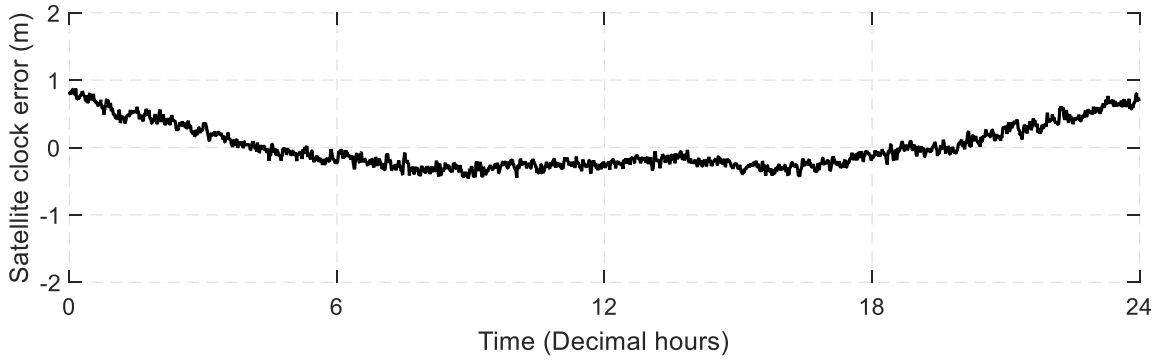

Figure 3.5: Relative satellite carrier-phase clock correction provided by Wuhan University utilizing IGS products on DOY 178 of 2016 for PRN 28 (relative to PRN 5). Linear trend has been removed. All units are in metres.

Presented in Figure 3.6 is the L1 satellite equipment delay, which are provided in units of cycles at a 15-minute data rate and presented in Figure 3.7 is the widelane satellite equipment delay, which is also provided in units of cycles but are provided as daily constant values. The L1 and widelane satellite equipment delays appear smaller in magnitude in contrast to the DCM products, because the integer component of the delay is removed and only the fractional component is provided.

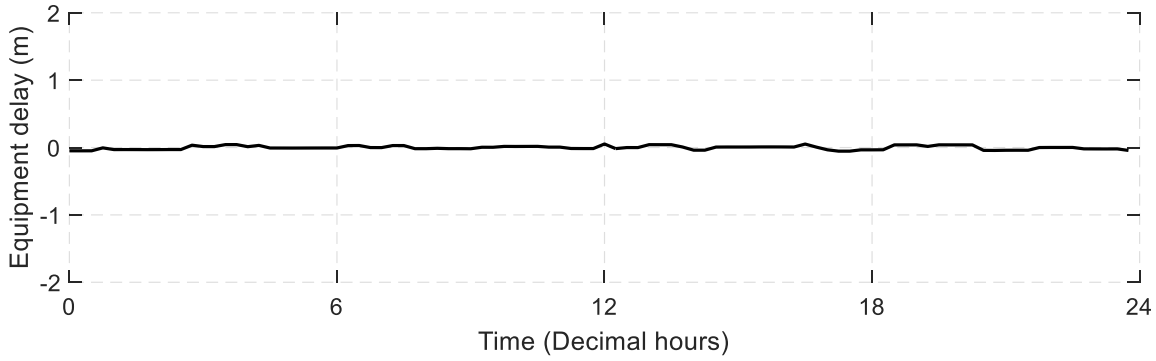

Figure 3.6: L1 satellite equipment delay provided by Wuhan University on DOY 178 of 2016 for PRN 28. All units are in metres.

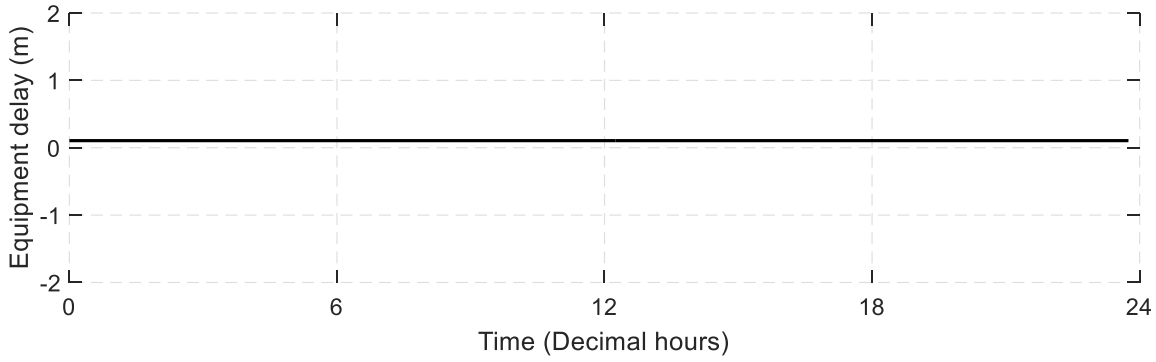

Figure 3.7: Wide lane satellite equipment delay provided by Wuhan University on DOY 178 of 2016 for PRN 28. All units are in metres.

To transform the FCB products into a DCM format is presented in equation (3.5)

$$\begin{bmatrix} dt^s \\ \delta t^s \\ \delta^s \end{bmatrix} = \begin{bmatrix} 1 & 0 & 0 \\ 1 & \lambda_{NL} & 0 \\ 0 & 0 & \lambda_{WN} \end{bmatrix} \begin{bmatrix} dt^s_{FCB} \\ a^s_{FCB,1} \\ a^s_{FCB,WL} \end{bmatrix} \tag{3.5}$$

where, on the RHS and dt^s_{FCB} are in units of metres. $a^s_{FCB,1}$ and $a^s_{FCB,WL}$ are in units of cycles. All transformed terms are in units of metres.

Presented in equation (3.6) is the transformation of the FCB products to an observable dependent representation. In this representation, the satellite clock term (dt^s) is the common clock term. The equipment delays ($a^s_{FCB,1}$ and $a^s_{FCB,WL}$) are transformed into a code dependent delays, d_1 and d_2. The phase equipment delays (δ_1 and δ_2) are set to zero. The transformed FCB product presented in equation (3.6) is similar to that of the transformed DCM product such that the phase equipment delays (δ_1 and δ_2) are set to zero. Banville (2016a) and Teunissen and Khodabandeh (2015) transformed the products to phase equipment delays. Also, Banville (2016a) utilized Differential Code Bias (DCBs) within the transformation.

$$\begin{bmatrix} dt^s \\ d_1 \\ d_2 \\ \delta_1 \\ \delta_2 \end{bmatrix} = \begin{bmatrix} 1 & 0 & 0 \\ 0 & \frac{-f_2}{f_1\alpha_{WL}} & \frac{-f_2}{f_1} \\ 0 & \frac{-f_1}{f_2\beta_{WL}} & \frac{-f_1}{f_2} \\ 0 & 0 & 0 \\ 0 & 0 & 0 \end{bmatrix} \begin{bmatrix} dt^s_{FCB} \\ a^s_{FCB,1} \\ a^s_{FCB,WL} \end{bmatrix} \tag{3.6}$$

Presented in Figure 3.8 is the transformation of the FCB products PRN 28 transformed to code dependent equipment delays, d_1 and d_2.

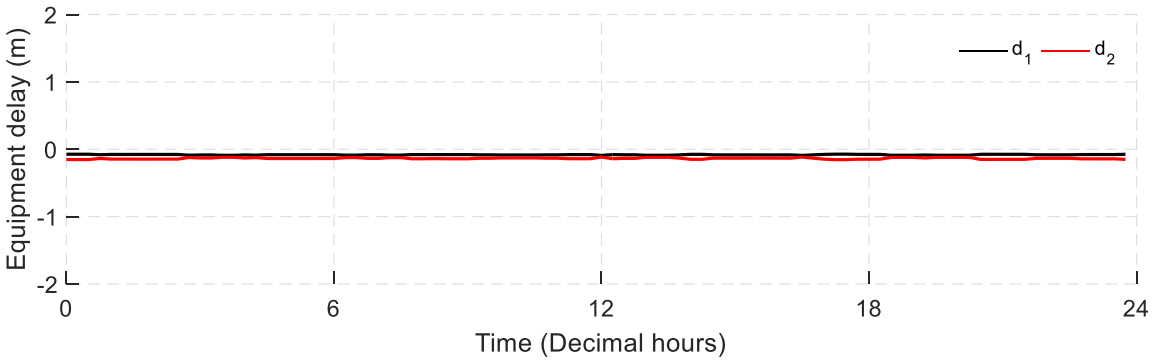

Figure 3.8: Uncombined code satellite equipment delay provided by Wuhan University on DOY 178 of 2016 for PRN 28 using IGS Final products. All units are in metres.

3.2.3 Integer Recovery Clock

The IRC model was first presented by Laurichesse and Mercier (2007). The products by CNES consists of widelane satellite equipment delays and the carrier-phase satellite clocks. The widelane satellite equipment delays are estimated as unconstrained in the network work solution with white noise added at each epoch using the Melbourne-Wübbena combination. The notable difference between the FCB and IRC approaches is the L1

satellite equipment delays are assimilated within the carrier-phase satellite clocks. The carrier-phase satellite clocks are then aligned to the satellite pseudorange clocks within a narrowlane cycle. The alignment of the carrier-phase clocks allows the clocks to be used for the pseudorange and carrier-phase measurements. It is worth noting, real-time applications would require rigorous quality control to account for the integer offset between the pseudorange and carrier-phase measurements. As such, it would be more practical (as with the DCM approach) to allow these integer offsets to exist within the PPP user solution, rather than it being accounted for in real-time within the network solution.

In 2014, real-time IRC products from CNES were made available in an archived SINEX BIAS format (Schaer 2016), which consisted of a common satellite clock and a satellite equipment delays that are provided for each observable (Laurichesse 2014). The IRC orbits and clocks can be downloaded from IGS, IGN, KASI or CDDIS and the widelane corrections from ftp://ftpsedr.cls.fr/pub/igsac/. Orbits, clocks and widelane correction files have the prefix “grg”.

Illustrated in Figure 3.9 is the relative satellite carrier-phase clock error (δt_{IRC}^{ps}) for PRN 28 with respect to satellite PRN 5 and presented in Figure 3.10 is the widelane satellite equipment delay, which is also provided in units of cycles but are provided as daily constant values.

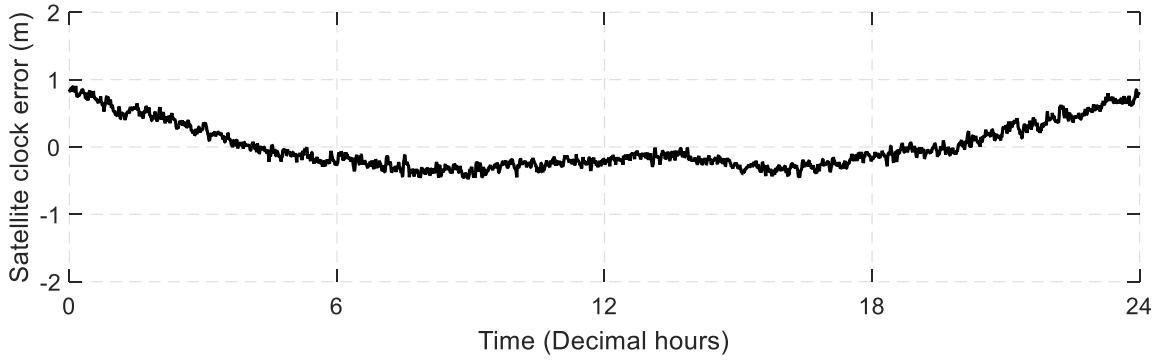

Figure 3.9: Relative satellite carrier-phase clock correction provided by CNES on DOY 178 of 2016 for PRN 28 (relative to PRN 5). Linear trend has been removed. All units are in metres.

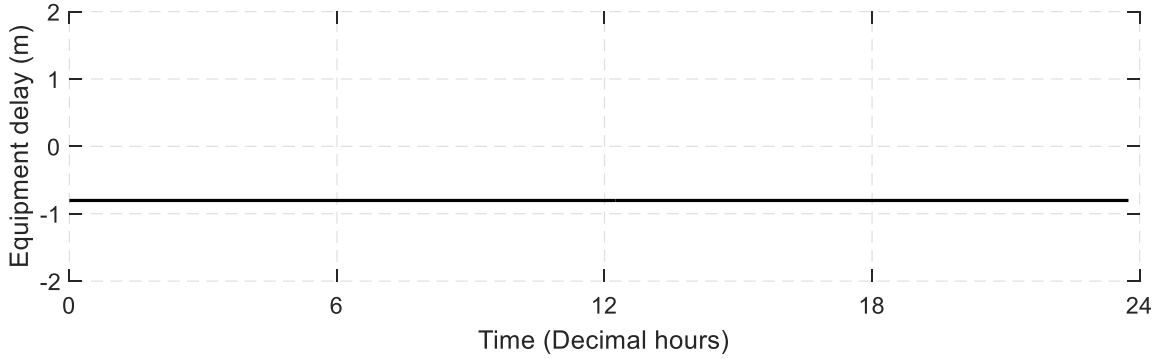

Figure 3.10: Wide lane correction provided by CNES on DOY 178 of 2016 for PRN 28. All units are in metres.

Presented in equation (3.7) is the transformation of the IRC products into a DCM format.

$$\begin{bmatrix} dt^s \\ \delta t^s \\ \delta^s \end{bmatrix} = \begin{bmatrix} 1 & 0 \\ 1 & 0 \\ 0 & \lambda_{WN} \end{bmatrix} \begin{bmatrix} \delta t^s_{IRC,IF} \\ \delta^s_{IRC,WL} \end{bmatrix} \tag{3.7}$$

where, on the RHS, $\delta t^s_{IRC,IF}$ is in units of metres and $\delta^s_{IRC,WL}$ is in units of cycles.

Presented in equation (3.8) is the transformation of the IRC products to an observable dependent representation. In this representation, $\delta t^s_{IRC,IF}$ the satellite clock term is the common clock term (dt^s). The P1-P2 differential code biases ($d^s_{DCB_{P1P2}}$) was transformed into code equipment delays (d_1 and d_2). The $\delta^s_{IRC,WL}$ is transformed into the phase equipment delays (δ_1 and δ_2) but require the code dependent delays to be removed from within $\delta^s_{IRC,WL}$. Code delays were introduced into $\delta^s_{IRC,WL}$ as a natural effect of forming the Melbourne-Wübbena combination. An equivalent transformation was presented by Laurichesse (2014) and Banville (2016a). The DCM/IRC products in Teunissen and Khodabandeh (2015) where transformed into a similar format of phase dependent equipment delays but did not utilize the DCBs within their transformation.

$$\begin{bmatrix} dt^s \\ d_1 \\ d_2 \\ \delta_1 \\ \delta_2 \end{bmatrix} = \begin{bmatrix} 1 & 0 & 0 \\ 0 & \beta_{IF} & 0 \\ 0 & -\alpha_{IF} & 0 \\ 0 & -\beta_{IF} & \frac{f_2}{f_1} \\ 0 & \alpha_{IF} & \frac{f_1}{f_2} \end{bmatrix} \begin{bmatrix} \delta t^s_{IRC,IF} \\ d^s_{DCB_{P1P2}} \\ \delta^s_{IRC,WL} \end{bmatrix} \tag{3.8}$$

Presented in Figure 3.11 and Figure 3.12 is the transformed IRC products for PRN 28 from combined to uncombined code and phase equipment delays. The P1-P2 differential code biases ($d^s_{DCB_{P1P2}}$) were obtained from the Center for Orbit Determination (2016).

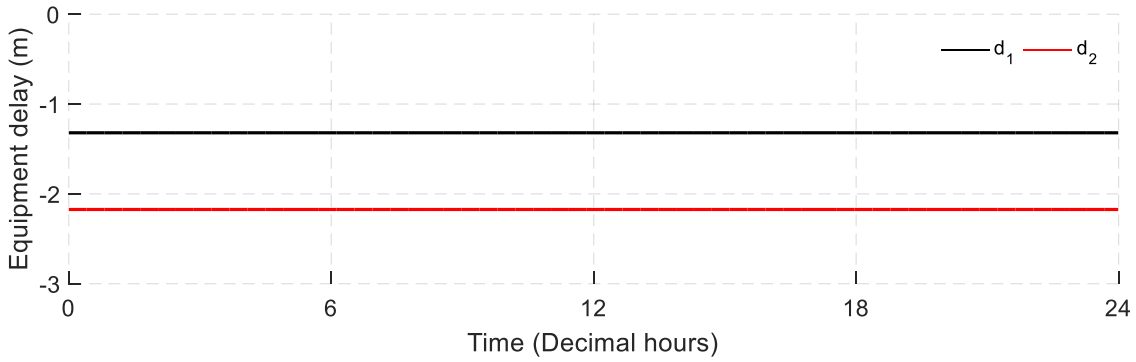

Figure 3.11: Uncombined satellite code clock provided by CNES on DOY 178 of 2016 for PRN 28. All units are in metres.

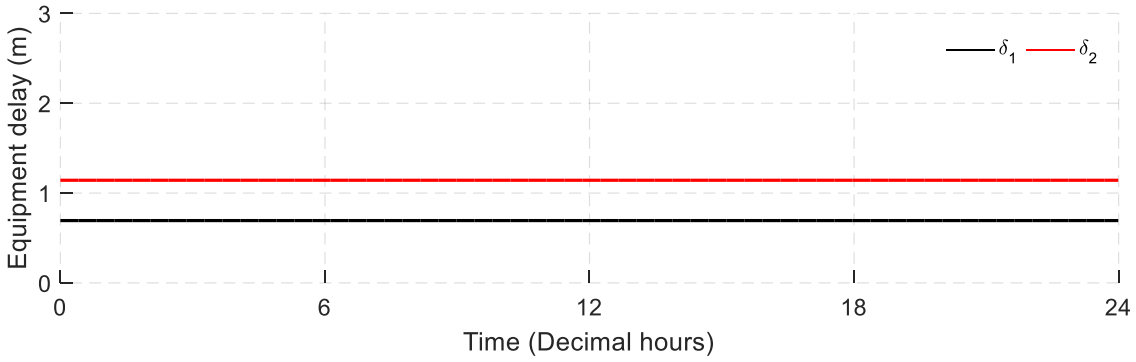

Figure 3.12: Uncombined satellite phase clock provided by CNES on DOY 178 of 2016 for PRN 28. All units are in metres.

3.2.4 Summary of available PPP-AR products

Presented in this section is an overview of the three main public providers of products which enable PPP-AR. The criteria examined included the different format of the products transmitted, data rate and different assumptions made which have been summarized in Table 3.1. Similar tables were presented in literature over the years (Geng 2010; Shi 2012;

Kamali 2017), but have became outdated as research advancements have been made over the years and refinement of the products presented to the user.

In Table 3.2 is an overview of the transformation matrix that can be used to transform the different PPP-AR products to the different formats to allow easier integration within the PPP user's software format. The table focuses on two types of transformations, 1) Transforming the different products into the DCM format and 2) Transforming the combined products into an uncombined measurement dependent format.

Transformation of the different products into the DCM format is novel, as it has only been published in Seepersad and Bisnath (2015) and Seepersad and Bisnath (2017). The significance of the work focuses on the integration of the different products within an infrastructure built around the DCM. Such a transformation addresses any misconceptions that the AC and PPP user must utilize the same PPP-AR model and products. The PPP user is allowed to adopt any PPP-AR model and any AR product type as long as consistent error models are utilized within the AC and the PPP user engine. Also presented are the transformations to an uncombined measurement dependent representation. Presenting the products in an uncombined representation is important as it facilitates easier integration within the RTCM SSR standard and allows the PPP user to adopt any PPP-AR model they prefer. Such a flexibility would eventually lead to standardization of the PPP-AR user model.

Table 3.1: Comparison of different public providers of products to enable PPP-AR

	Fractional Cycle Bias model	**Decoupled Clock model**	**Integer Recovery Clock model**
PPP-AR Products	dt^s_{IF} - code clock $a^s_{FCB,WL}$ - widelane $a^s_{FCB,1}$ - narrowlane	$\delta t^s_{DCM,IF}$ - phase clock $dt^s_{DCM,IF}$ - code clock $\delta^s_{DCM,WL}$ - widelane clock	$\delta t^s_{IRC,IF}$ - phase clock $\delta^s_{IRC,WL}$ - widelane clock
Provided product units	$dt^s_{FCB,IF}$ - seconds $a^s_{FCB,WL}$ - cycles $a^s_{FCB,1}$ - cycles	$\delta t^s_{DCM,IF}$ - seconds $dt^s_{DCM,IF}$ - nanoseconds δ^s_{WL} - nanoseconds	$\delta t^s_{IRC,IF}$ - seconds $\delta^s_{IRC,WL}$ - cycles
Data rate	dt^s - 30 secs $a^s_{FCB,1}$ - 15 mins $a^s_{FCB,WL}$ - daily	$\delta t^s_{DCM,IF}$ - 30 secs $dt^s_{DCM,IF}$ - 30 secs $\delta^s_{DCM,WL}$ - 30 secs	$\delta t^s_{IRC,IF}$ - 30 seconds $\delta^s_{IRC,WL}$ - daily
General assumptions	Constant $a^s_{FCB,WL}$ are estimated daily by averaging arc-dependent estimates.	No constraints or smoothing applied	$\delta t^s_{IRC,IF}$ aligned to the satellite pseudorange clocks within a narrowlane cycle. $\delta^s_{IRC,WL}$ are daily averages.
Products used	Post-processed	Post-processed	Post-processed
Network solution	Global. IGS final products.	Global. EMR rapid products.	Global. GRG final products.
NL correction	$a^s_{FCB,1}$		
WL correction	$a^s_{FCB,WL}$	$\delta^s_{DCM,WL}$	$\delta^s_{IRC,WL}$
Source	ftp://gnss.sgg.whu.edu.cn/product/FCB	By request, nrcan.geodeticinformationservices.rncan@canada.ca	Orbits and clocks from IGS, IGN, KASI or CDDIS and the widelane corrections from ftp://ftpsedr.cls.fr/pub/igsac/

Table 3.2: Summary of the transformation of the PPP-AR products to the combined DCM format and uncombined representation

	Decoupled clocks	Fractional Cycle Bias	Integer Recovery Clock

$$\begin{bmatrix} dt^s_{IF} \\ \delta t^s_{IF} \\ \delta^s_{WN} \end{bmatrix} = \begin{bmatrix} 1 & 0 & 0 \\ 0 & 1 & 0 \\ 0 & 0 & 1 \end{bmatrix} \begin{bmatrix} dt^s_{DCM,IF} \\ \delta t^s_{DCM,IF} \\ \delta^s_{DCM,WL} \end{bmatrix} \quad \begin{bmatrix} 1 & 0 & 0 \\ 1 & \lambda_{NL} & 0 \\ 0 & 0 & \lambda_{WN} \end{bmatrix} \begin{bmatrix} dt^s_{FCB,IF} \\ a^s_{FCB,1} \\ a^s_{FCB,WL} \end{bmatrix} \begin{bmatrix} 1 & 0 \\ 1 & 0 \\ 0 & \lambda_{WN} \end{bmatrix} \begin{bmatrix} \delta t^s_{IRC,IF} \\ \delta^s_{IRC,WL} \end{bmatrix} \tag{3.9}$$

$$\begin{bmatrix} d_1 \\ d_2 \\ \delta_1 \\ \delta_2 \end{bmatrix} = \begin{bmatrix} -\frac{1}{\alpha_{WL}} & \frac{f_2}{f_1} \\ -\frac{1}{\beta_{WL}} & \frac{f_1}{f_2} \\ 0 & 0 \\ 0 & 0 \end{bmatrix} \begin{bmatrix} \Delta d^s_{DCM,IF} \\ \delta^s_{DCM,WL} \end{bmatrix} \begin{bmatrix} \frac{-f_2}{f_1\alpha_{WL}} & \frac{-f_2}{f_1} \\ \frac{-f_1}{f_2\beta_{WL}} & \frac{-f_1}{f_2} \\ 0 & 0 \\ 0 & 0 \end{bmatrix} \begin{bmatrix} a^s_{FCB,1} \\ a^s_{FCB,WL} \end{bmatrix} \begin{bmatrix} \beta_{IF} & 0 \\ -\alpha_{IF} & 0 \\ -\beta_{IF} & \frac{f_2}{f_1} \\ \alpha_{IF} & \frac{f_1}{f_2} \end{bmatrix} \begin{bmatrix} d^s_{DCB_{P1P2}} \\ \delta^s_{IRC,WL} \end{bmatrix} \tag{3.10}$$

3.3 Dataset and processing parameters used to quantify performance of PPP-AR

GNSS data from 155 globally distributed stations were processed from DOY 178 to 184 of 2016 provided by the IGS, which is illustrated in Figure 3.13. Satellite products provided by the different ACs presented in Section 3.2 were utilized. The data were processed using the YorkU-PPP software (Seepersad 2012; Aggrey 2015). YorkU-PPP was developed based on the processing engine used by the online CSRS-PPP service (NRCan 2013). Dual-frequency receivers tracking either the C/A or P(Y) - code on L1 were used. For receivers that do not record the P_1 observable, the DCM_{P1C1} correction was applied. The DCM_{P1P2} was

utilized when transforming an uncombined representation. DCBs are important to be accounted for as they represent the systematic errors between two GNSS code observations at the same or on different frequencies and the signals need to be aligned to IGS's standard based on L1-P1/L2-P2 GPS data. The DCBs were obtained from Center of Orbit Determination in Europe (2016). Dual-frequency uncombined observations were processed with a priori standard deviations of 1.0 m and 6 mm for pseudorange and carrier-phase observations, respectively. An elevation cut-off angle of 10° was selected. Slant ionosphere delays and uncalibrated equipment delays were also estimated epoch-by-epoch in the PPP filter. The reference stations were analyzed in static mode. Receiver clocks were estimated epoch-by-epoch. The zenith tropospheric delays were also estimated each epoch with a random walk coefficient of 2 cm/sqrt(hour). The station coordinates were initialized using a pseudorange only solution with an initial constraint of 10 m. The IGS absolute antenna model file was used and ocean loading coefficients were obtained from Scherneck (2013) for each of the sites processed. To facilitate partial ambiguity resolution, only the candidates with an elevation angle greater than 20° was considered. The Modified LAMBDA method (MLAMBDA) was utilized to resolve the ambiguity candidates (Chang et al. 2005), which is discussed in more detail in Section 5.2. The transformed FCB, DCM and IRC products were processed with their original satellite orbit files to maintain consistency between satellite orbits, clocks and equipment delays.

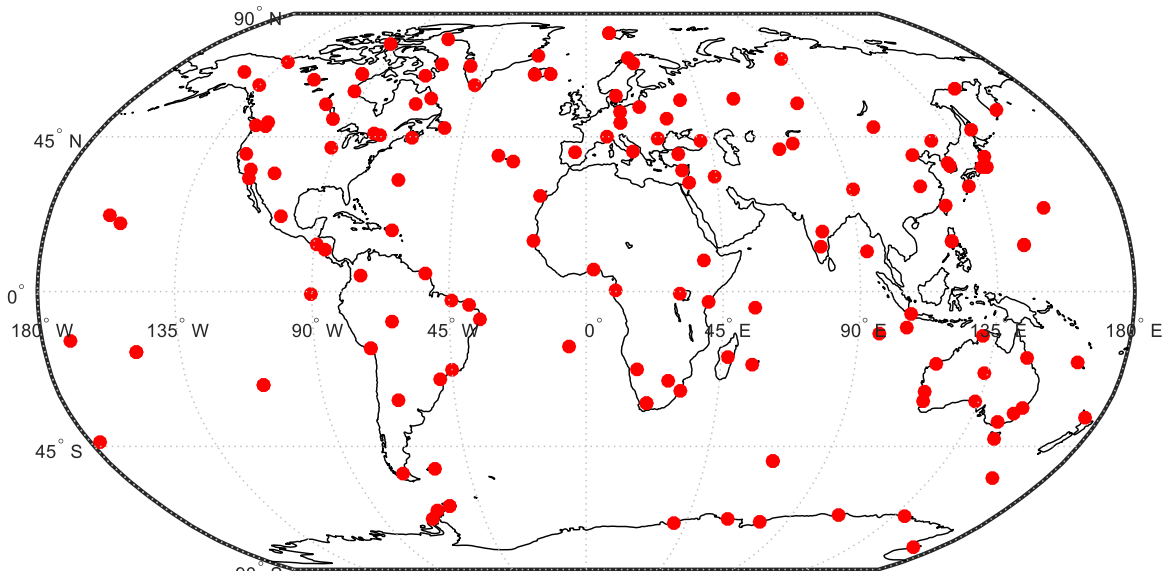

Figure 3.13: Global distribution of the selected 155 IGS stations observed during DOY 178 to 184, GPS week 1903, of 2016.

3.4 Performance of transformed products

Presented in Table 3.3 is the rms error of the final solution of 24-hour datasets using data from 155 IGS sites utilizing the satellite products provided by NRCan, CNES, and Wuhan University. All products were transformed to an uncombined representation. Equivalent performance (at the few mm level) was noted utilizing the DCM, IRC and FCB products. Of the three solutions, FCB products had the highest accuracy which is attributed to the products being generated using final IGS orbit and clock products. To confirm the high accuracy performance of the FCB products were due to being generated using final IGS orbit and clock products, the FCBs generated using GRG orbit and clock products were also examined. The performance of the FCB and IRC products using GRG orbit and clock products were comparable.

Table 3.3: rms error of the final solution produced by YorkU-PPP from 24-hour datasets using data from 155 sites for DOY 178 to 184, GPS week 1903, of 2016 provided by the IGS. Satellite products were provided by NRCan, CNES and Wuhan University. All units are in millimetres.

	DCM		IRC		FCB	
	Float	Fixed	Float	Fixed	Float	Fixed
Northing	5	5	5	4	5	4
Easting	6	3	5	3	5	3
Horizontal	8	6	7	5	7	5
Vertical	11	10	11	10	9	9
3D	13	12	13	11	11	10

Data were selected from the GPS site, NRC1 located in Ottawa, Canada on DOY 178 of 2016. NRC1 was selected because similar performance was observed within the week of processing and it illustrated similar trends to other GPS sites examined. Presented in Figure 3.14 (a) – (c) is the horizontal component and Figure 3.15 (a) – (c) the vertical component for the IRC, DCM and FCB products. The subplots within Figure 3.14 and Figure 3.15 illustrates both the "float" and "fixed" solution, where fixed represents the ambiguity resolved solution and float the unresolved solution. A stringent convergence threshold of 5 cm was set to examine the time the solution took to converge.

The horizontal position error, Figure 3.14 (a) – (c) from all three solutions had an overshoot of 55 – 60 cm after 30 seconds of data processing. Convergence of the float solution to the

predefined threshold (5 cm) was 14 minutes and fixing the ambiguities improved convergence by only 1 minute. Similar convergence was noted in the horizontal component for all four solutions.

The strength of applying ambiguity resolution is illustrated in the time to attain a steady state. All three solutions illustrated different convergence trends before attaining a steady state: DCM products took 2.2 hours, IRC and FCB product took 1 hour. The ambiguity resolved solution improved the time attain a steady state as the time was reduced to 10 minutes.

The vertical position error, Figure 3.15 (a) – (c), had an overshoot of 36, 45 and 60 cm for the DCM, IRC and FCB products, respectively. The same predefined threshold for the vertical component was maintained. Convergence times were 18, 16 and 13 mins for the DCM, IRC and FCB products, respectively. Applying ambiguity resolution did not improve the time to attain a steady state in the vertical component: 4.5, 3,5.8 and 2 hours for the DCM, IRC (GRG), IRC (CNT) and FCB products, respectively. Slower convergence was noted in the vertical component due the strong correlation between the atmospheric effects and the vertical component. Any unmodelled components of the atmospheric effects required time averaging or a priori information to be provided to the user as discussed in Collins and Bisnath (2011) and Shi and Gao (2014).

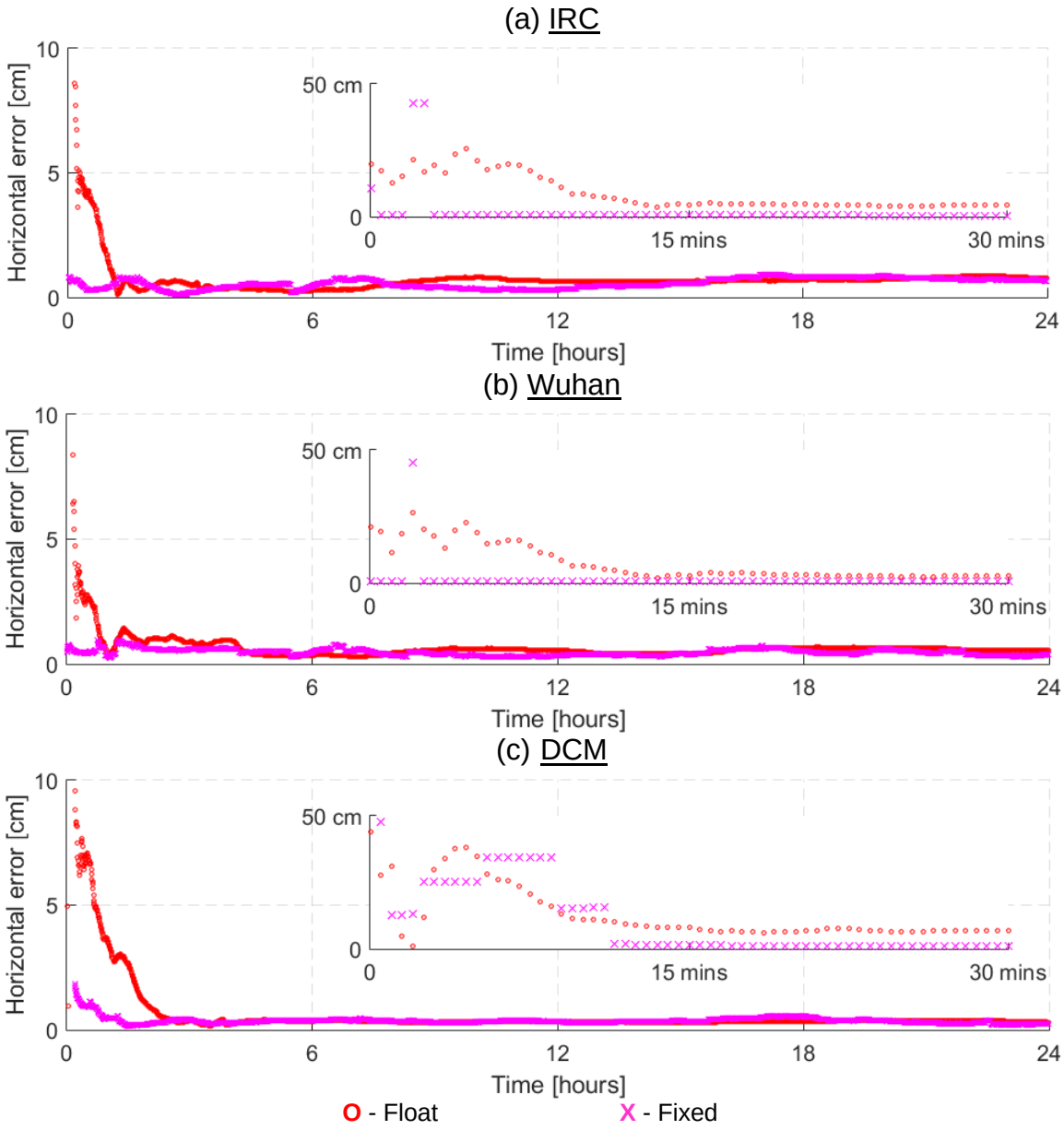

Figure 3.14: Site NRC1 DOY 178 of 2016 located in Ottawa, Canada, illustrating the differences between the "float" and "fixed" solution in the horizontal component where insets for each figure represents the initial 30 minutes of convergence time. Limits of y-axis represents position error.

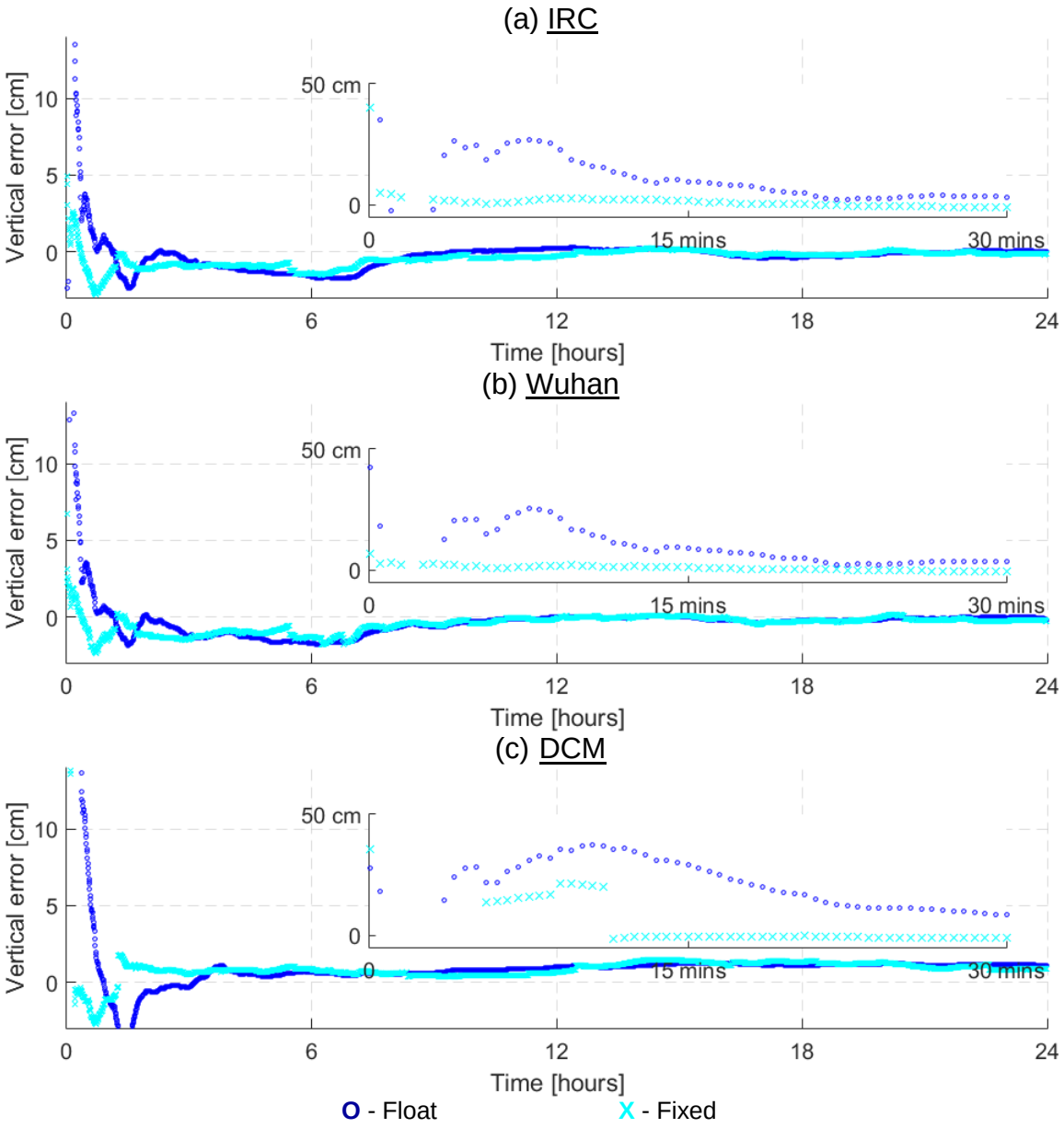

Figure 3.15: Site NRC1 DOY 178 of 2016 located in Ottawa, Canada, illustrating the differences between the "float" and "fixed" solution in the vertical component where insets for each figure represents the initial 30 minutes of convergence time. Limits of y-axis represents position error.

3.5 Challenges in interoperability of PPP-AR products

Interoperability of the different PPP products is a challenging task due to the public availability of different quality products, limited literature documenting the conventions adopted within the network solution of the providers, and unclear definitions of the corrections. Presented in Table 3.1 was a summary of the different qualities of the products that were utilized within the study. As mentioned before, ACs are allowed a certain level of flexibility to improve and innovate through the development of new processing strategies, such as different axis conventions (Section 3.5.1) and different modelling of yaw manoeuvres (Section 3.5.2). In the combination process, it is important that the different strategies (models) utilized by the ACs are taken into consideration within the user's estimation process. The general assumption when PPP products are estimated within the network, assumed that the PPP user will follow similar conventions when utilizing the products from the network. Consequences of different conventions adopted may result in incorrect ambiguities being resolved.

3.5.1 Axis convention

For example, IRC adopted the IGS axis convention, whereas the internal DCM products followed the manufacturer specification. Presented in Figure 3.16 is the orientation of the spacecraft body frame for GPS Block IIR/IIR-M satellites adopted within the IGS axis convention, subplot (a), and provided in the manufacturer specifications, subplot (b). The difference between the manufacturer specifications and IGS axis convention is the orientation of the X and Y axes.

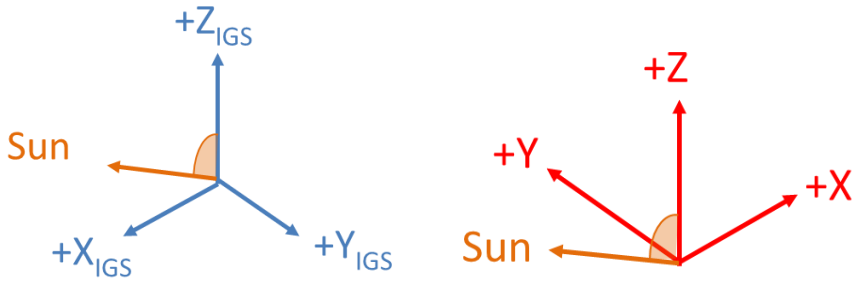

(a) IGS axis convention **(b) Manufacturer specifications**

Figure 3.16: Orientation of the spacecraft body frame for GPS Block IIR/IIR-M satellites (a) manufacturer specification system; (b) IGS axis conventions (Montenbruck et al. 2015).

3.5.2 Yaw manoeuvres during satellite eclipse

Another critical component to be accounted for to ensure interoperability of the PPP-AR products is the difference in the modelling of yaw manoeuvres. Yaw manoeuvres occur when the actual yaw angle differs from the nominal yaw angle. The nominal yaw angle is the orientation angle by which a satellite would maintain optimal solar visibility throughout its orbit, provided it could spin arbitrarily fast. The actual yaw angle is the orientation that the satellite is able to maintain due to its limited rate of yaw.

All satellites fail to maintain their nominal orientation when their orbits pass close to the Earth-Sun axis. These are the eclipsing orbits with turns at both orbit noon and orbit midnight. During a satellite eclipse, Block II GPS satellites behaved unpredictably because of hardware sensitivity, spinning beyond the nominal amount upon entering the Sun's shadow. The Block IIR and Block IIF generations of satellites were designed to be able to maintain their nominal attitude even during orbit noon and orbit midnight (Bar-Sever 1996;

Dilssner et al. 2011). For Block IIR, the yaw manoeuvre is constrained by a maximum yaw rate of 0.2 deg/sec (Kouba 2009) and Block IIF is constrained by a maximum yaw rate of 0.11 deg/sec (Dilssner 2010). The attitude model of the GPS satellites affects the computation of measurement geometry through variations of the transmitter phase centre location and carrier-phase measurement wind-up. It also affects the modelling of the solar radiation pressure force acting on the GPS satellites due to the changes in illumination geometry (Kuang et al. 2016).

The uncertainty of the yaw manoeuvre is higher during midnight orbit as the satellite crosses the Earth's shadow. During the shadow crossing, the satellite's view of the Sun is obstructed partially from the region known as the penumbra or fully by the Earth from the region known as the umbra. A GPS satellite goes through eclipse season approximately every 6 months and the length of the eclipse season varies from 4 to 8 weeks. A typical orbit geometry during eclipse season is depicted in Figure 3.17. Eclipse season typically begins for a GPS satellite when β goes below 13.5°, where β is elevation of the Sun above the orbital plane. The time the satellite spends in the Earth's shadow increases as β approaches 0°, for a time period of up to a maximum of approximately 55 minutes (Bar-Sever 1996; Kouba 2009; Dilssner et al. 2011). Typically, the nominal attitude model fits actual GPS measurements well. During eclipsing season when β typically goes below 4°, the physical GPS satellite yaw attitude rate cannot keep up with what is expected from the nominal model. Dilssner et al. (2011) observed that the orbit noon turn of the Block IIF satellites manifests in the wrong direction for a small negative β angle as much as -0.9°.

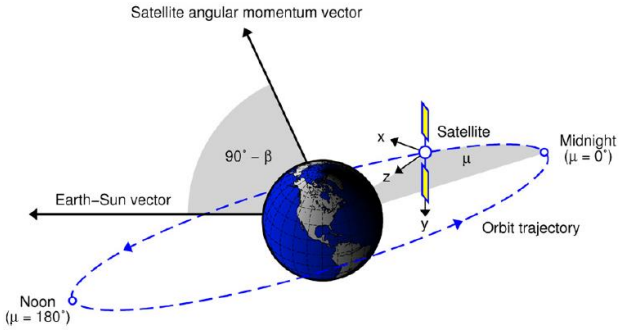

Figure 3.17: Geometry of an eclipsing satellite, where β is elevation of the Sun above the orbital plane and μ is the spacecraft's geocentric orbit angle. "Midnight" denotes the farthest point of the orbit from the Sun whereas "noon" denotes the closest point. From Dilssner et al. (2011).

To account for differences in yaw maneuvering during orbit noon and orbit midnight, knowledge of the actual yaw attitude models from the different ACs is required. As such, there is a proposal to extend the current RINEX clock format to include additional information such as yaw angle and phase/code biases (Donahue et al. 2016). The yaw information would allow for a phase wind-up correction to be applied to each solution for improved consistency, while the phase/code bias information accommodates the different PPP-AR products.

3.6 Summary of the performance of PPP-AR product interoperability

Interoperability of PPP-AR products is important, as it can increase the reliability of the user solution while offering similar performance, in regard to precision and accuracy. Interoperability of the products is possible for the PPP user, as the mathematical model, to enable an ambiguity resolved solution is similar. The different PPP-AR products contain the same information and would allow for a one-to-one transformation, allowing

interoperability of the PPP-AR products. The PPP user will be able to transform independently generated PPP-AR products to seamlessly integrate within their PPP user solution. The seamless integration of the transformed products will allow the PPP user to have multiple solutions, which will increase the reliability of the solution, for e.g., real-time processing. During real-time PPP processing, if there was an outage in the generation of the PPP-AR products, the user can instantly switch streams to a different provider.

The three main public providers of products that enable PPP-AR were examined, which included School of Geodesy and Geomatics at Wuhan University, Natural Resources Canada and Centre National d'Etudes Spatiales. Equivalent performance was noted utilizing the different methods. Of the four solutions, FCB products had the highest accuracy. The improved performance noted with the FCB products in contrast to DCM and IRC is attributed to the products being generated using final IGS orbit and clock products which are a combined product from multiple ACs. Where as, DCM products are generated using rapid orbit and clocks and IRC products utilize final GRG orbit and clocks. To confirm the improved performance of FCBs generated from IGS final products, the FCBs generated using GRG orbit and clock products were also examined and comparable performance was observed between the FCBs and IRC products.

As the results in Section 3.4 indicated, interoperability of PPP-AR products is feasible. While feasible, there were challenges when processing the different PPP-AR products. These challenges were due to the same conventions not being followed between the network and user solution, for e.g. different satellite antenna convention. When different satellite antenna convention was used, fractional cycles was introduced when carrier-phase

wind-up correction was applied. Another critical component to be accounted for is the difference in the modelling of yaw manoeuvres. Difficulties in determining the exact moment when an eclipsing satellite exits the umbra, results in modelling inconsistencies between ACs. If network-defined periods of orbit noon, orbit midnight and yaw angles are not provided, it is recommended that the PPP user not attempt to resolve ambiguities of satellites exiting the umbra if differences in yaw modelling exists between the network and user.

CHAPTER 4 IMPROVING RELIABILITY OF PPP-AR PRODUCTS

While satellite clock combinations are routinely utilized within the IGS, they currently disregard the fact that some ACs provide satellite clock products that account for the satellite equipment delays. Users have been expected to choose between either a robust combined solution or select individual AC solutions that provide PPP-AR products that allow the user to compute an ambiguity resolved solution. The objective of this investigation was to develop and test a robust satellite clock combination, while preserving the underlying integer nature of the clocks and therefore the carrier-phase ambiguities to the user end to enable PPP-AR.

4.1 Introduction to satellite clock combination

In recent years, CNES, an AC of the IGS, began providing satellite clock corrections preserving the integer nature of carrier-phase ambiguities. These products are sometimes referred to as “integer clocks” as they preserve the underlying integer nature of the ambiguities by including the high-rate satellite equipment delay corrections within the products. As previously mentioned, utilizing these types of products would allow for PPP with ambiguity resolution and therefore a more rapid convergence and improved stability of the position estimates. Other ACs, such as NRCan, also generate such products primarily for internal use. Even though all IGS ACs follow a set of guidelines and standards to assure a certain level of consistency, flexibility is allowed to improve and innovate through the development of new processing strategies (as discussed in Section 3.5). Hence, many ACs

utilize their own software packages and methodologies, and all have their solutions based on an independent selection of ground stations. Theoretically, a combination of the AC products is not rigorous since solutions are correlated as a result of similar reference stations used within the network adjustment process. However, on a practical level, given AC-specific characteristics, a combined solution is more robust against outliers and failures within individual AC solutions. The strength of a combined product is always in its reliability and stable median performance, which is better than or equivalent to any single AC product (Kouba and Springer 2001).

Satellite clock combinations were first proposed by the IGS in 1993 (Springer and Beutler 1993) and became an official product of the IGS starting in January 1994 (Beutler et al. 1995, 1999) as a post-processed product. Real-time or near-real-time products are even more prone to robustness issues due to unpredictable factors such as communication outages. The real-time combined product was proposed at the 2002 IGS workshop: "Towards Real-Time" and the pilot project was launched in 2011 (Caissy et al. 2012).

Satellite clock combinations produced by the IGS currently disregard the integer-preserving characteristics of the clock products. Users can either opt for the robustness of the combined solution or select individual AC solutions that provide PPP-AR products, which allows users to compute an ambiguity resolved solution. The motivation of this work is to develop and test a PPP-AR clock combination product, improving on the reliability and robustness of the original products. The following sections consists of a review of the satellite clock combination process, then the method is extended to include the "integer

clock" products, after which the performance of the products are analyzed (Seepersad et al. 2016).

4.2 Satellite clock combination of common clocks

Satellite clock products that do not preserve the integer nature of the ambiguities are referred to as common clocks (as discussed in Section 2.2). It is well-known that combining common clock products is an effective method to address the vulnerabilities an individual AC is susceptible to. In regards to accuracy, the combined clock products have performed comparable to the products from the best AC solution, (Beutler et al. 1995; Kouba and Springer 2001), which is expected, as the strength of satellite combination is in improving reliability and availability of the products and not necessarily accuracy. Clocks can be combined epoch-by-epoch through weighted least-squares (Weber et al. 2007, 2011) or combined sequentially using a Kalman or sequential least-squares filter (Mervart and Weber 2011; Chen et al. 2016).

In the sequential filter approach, clocks estimated by individual ACs are used as observations (dt_a^s) within the adjustment process, where $s = \{1...m\}$ represents a set of m number of satellites. Each observation is modelled as a linear function of three parameters: 1) the combined satellite clock ($\overline{dt}^s$); 2) an AC-specific offset (B_a); and 3) an AC-specific satellite-dependent offset (A_a^s), where, $a = \{1...n\}$ is a set of n analysis centres. The observation equation can be represented as:

$$dt_a^s - \psi_a^s = \overline{dt}^s + B_a + A_a^s \tag{4.1}$$

where ψ_a^s is a consistency correction which is time varying and AC specific. ψ_a^s aligns the individual AC solutions to the selected reference frame which, in our case, was defined by the IGS combined orbit solution. The consistency correction is computed as follows:

$$\psi_a^s = \frac{(\vec{X}_a^s - \vec{X}_{IGS}^s - \vec{D}_a) \cdot \vec{X}_a^s}{\left|\vec{X}_{IGS}^s\right|} \tag{4.2}$$

where $\vec{X}_a^s$ is the AC satellite position vector, $\vec{X}_{IGS}^s$ represents the IGS combined satellite position vector, and $\vec{D}_a$ is the geocentre offset vector provided by the respective AC. Finally, $\left|\ \right|$ represents the computation of the radius vector with respect to the centre of the Earth (Ferland et al. 2000; Kouba and Springer 2001).

The term B_a in equation (4.1) varies with each AC because of the different timing constraints imposed on the network. Timing constraints are defined by fixing the clock parameter of a reference station. Since it is not possible to estimate one such parameter for each AC, one AC needs to be selected as a timing reference. A_a^s varies based on the different solution-specific ambiguity datum ambiguities and the AC adjustment constraints. A_a^s is unique to each AC and satellite and is considered constant in time. It is used to model different time references for each satellite within each AC solution. In practice, A_a^s is routinely included as shown in Mervart and Weber (2011) and Chen et al.

(2016) in their real-time implementation of satellite combinations of common clocks. A_a^s is included because it absorbs any differently modelled satellite-specific errors. Also, including A_a^s facilitates expanding the satellite clock combination from common clocks to the clock products that enable PPP-AR. In the sequential filter, $\overline{dt}^s$ and B_a were assigned an infinite process noise variance whereas A_a^s were modelled as constant parameters. Table 4.1 summarizes the different estimated parameters in the satellite clock combination and associated constraints.

Table 4.1: Estimated parameters in satellite clock combination and associated constraints.

Parameter	Description	Process noise
$\overline{dt}^s$	Combined satellite clock	∞
B_a	Time reference offset (AC-specific)	∞
A_a^s	Satellite-dependent offset (AC-specific)	0

In the adjustment, there is a total of $n+m+m\cdot n$ unknowns and $m\cdot n$ measurements and, as such, there is a rank deficiency of $n+m$ at the first epoch. To remove this singularity, different terms were held fixed within the system. As mentioned previously, the timing reference (B_a) of one AC must be held fixed. Furthermore, it is required to fix one A_a^s

parameter for each satellite and AC. Presented in Table 4.2 are the fixed terms in the adjustment to remove the system's rank deficiency.

Table 4.2: Fixed terms in the adjustment to remove rank deficiency.

Parameter	Fixed terms	Number of estimated terms
$\overline{dt}^{s}$	0	m
B_a	1	$n-1$
A_a^s	$n+m-1$	$(m-1)\cdot(n-1)$

4.3 Combining clock products that enable PPP-AR

The previous section discussed the combination process of the common clocks. This section focuses on the steps required to combine the integer natured satellite clocks products, DCM and IRC. Rather than transforming the FCB products (as discussed in Section 3.2) into integer natured satellite clocks, the combined products were compared to the FCB products. The approach of comparing the combined products to the FCB products were selected because the FCB products were already generated from IGS combined orbit and clock products. Therefore, while AR strategies are mathematically equivalent, the performance of the FCB products surpassed DCM and IRC as a result of this (as discussed in Section 3.4 as well as illustrated in Figure 3.14 and Figure 3.15). An overview of the combination process of the DCM and IRC is presented in Figure 4.1, where the first step requires accounting for AC specific modelling such as different axis conventions and yaw

manoeuvres during a satellite eclipse (Section 3.5). Accounting for AC specific modelling is critical to ensure the integer nature of the carrier-phase ambiguity is not compromised. The next step combines the widelane products which is followed by the combination of the clock products that enable PPP-AR.

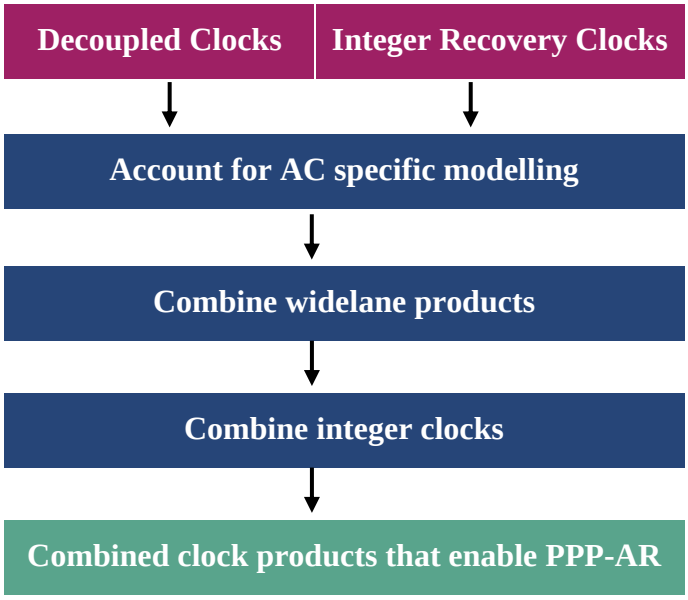

Figure 4.1: Overview of the steps required to combine satellite clocks products that enable PPP-AR.

4.3.1 Combination process of PPP-AR clock products

The combination process of the integer clocks follows exactly the same parametrization and constraints, in addition to the integer constraints imposed on the satellite offset. For the combined products to be integer natured, it is imperative that the reference AC provide products that enable PPP-AR. Presented in equation (4.3) is the alignment of the widelane satellite hardware delay for each AC:

$$\delta^s_{a,WL} = \overline{\delta}^s_{WL} + B_{a,WL} + A^s_{a,WL} \tag{4.3}$$

where $\delta^s_{a,WL}$ is the widelane hardware delay provided by each AC and $\overline{\delta}^s_{WL}$ is the combined widelane hardware delay and $A^s_{a,WL} = \lambda_{WL} N^s_{a,WL}$ with the term N having integer properties. The alignment is necessary to reduce the differences between ACs, and most importantly, maintain the integer nature of the subsequent $A^s_{a,IF}$ parameters. In the second step, presented in equation (4.4), the rounded integer value of $N^s_{a,WL}$ is introduced as an additional correction. The equation for the integer clock combination reads:

$$dt^s_a - \psi^s_b - \frac{f_2^2}{f_1^2 - f_2^2}\lambda_2[N^s_{a,WL}] = \overline{dt}^s + B_a + A^s_{a,IF} \tag{4.4}$$

where

$A^s_{a,IF} = \frac{f_1^2 - f_1 f_2}{f_1^2 - f_2^2}\lambda_1 N^s_{a,L1}$ and $[N^s_{a,WL}]$ represents rounding of the AC-satellite offset.

4.3.2 Combined clock products

In the combination process of IRC and DCM products, each of the ACs were weighted equally. B_{IRC}, A^s_{IRC} (all satellites) and A^1_{DCM} were held fixed as minimal constraints in the adjustment. IRC was arbitrarily selected as the timing reference, and satellite PRN 01 was selected because it had the highest data availability. The results presented in this section were taken from day-of-year (DOY) 178 and 179 of 2016.

The first component analyzed in this section is the effect of yaw manoeuvres on the clock combination process. The expectation is that Block IIR and Block IIF satellites are able to keep their nominal attitude even when orbiting through the penumbra and the umbra. Because of the difficulties in determining the exact moment of exiting the umbra, modelling inconsistencies between ACs can be observed. For example, in Figure 4.2, when PRN 24, a Block IIF satellite, is in the Earth's shadow, discrepancies are present between the IRC and DCM products. According to the Jet Propulsion Lab (JPL) within their ".shad" file (JPL 2016), the time period the satellite transited through the umbra occurred from 03:28:43 to 04:24:09 and 15:27:18 to 16:22:43 and is shaded in green. The limitation of JPL's ".shad" file is that only instances of midnight orbits are provided and it does not include the yaw rate. Highlighted in blue is the information presented in the DCM clock format, which indicates the time period of a critical yaw manoeuvre within the umbra. In the DCM clock format, instances of orbit noon are also provided but not illustrated as consistent modelling occurred during these manoeuvres.

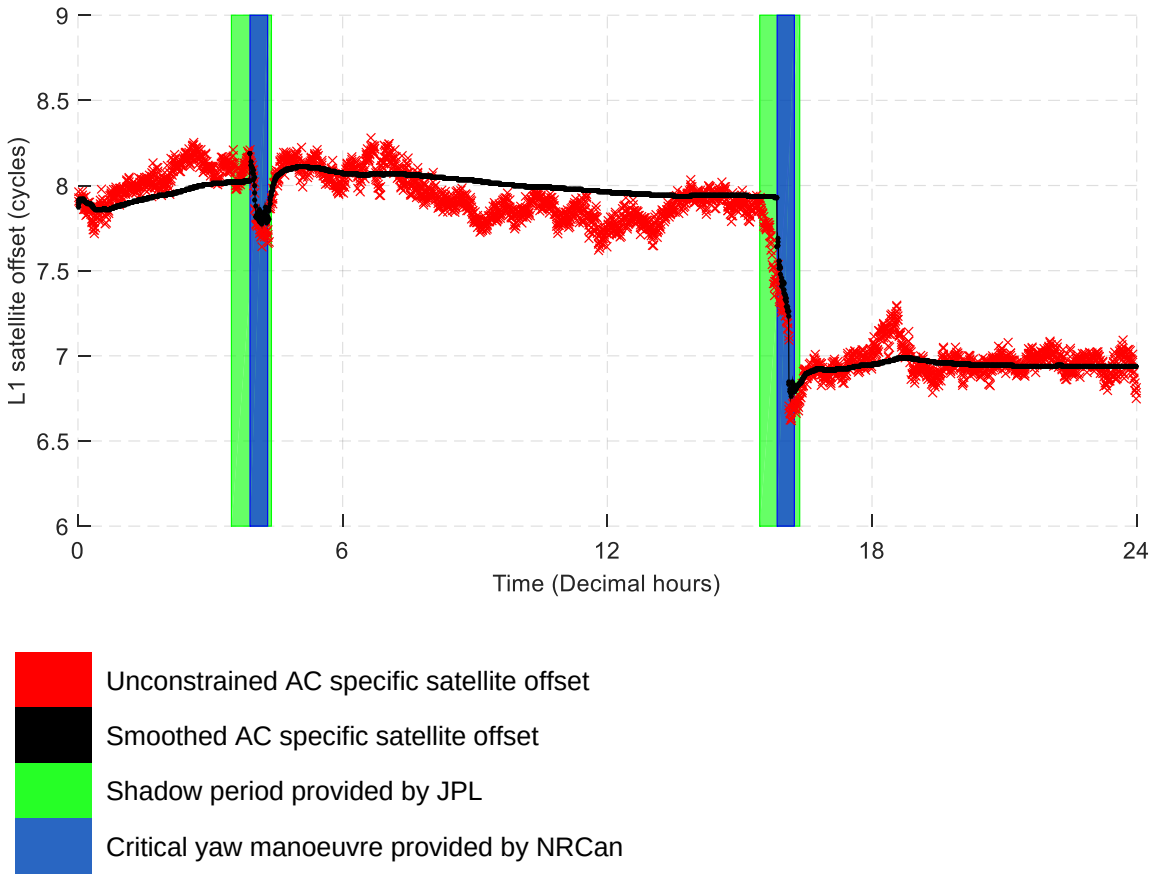

Figure 4.2: Inconsistent error modelling during a satellite eclipse for PRN 24 with respect to PRN 1, Block IIF on DOY 178 of 2016 between IRC and DCM.

Presented in Figure 4.3 is the convergence of the DCM L1 satellite offset. The differences in yaw manoeuvres and antenna axis convention were taken into consideration. During the critical yaw manoeuvres the satellite offset of the eclipsing satellite in the DCM solution was re-initialized.

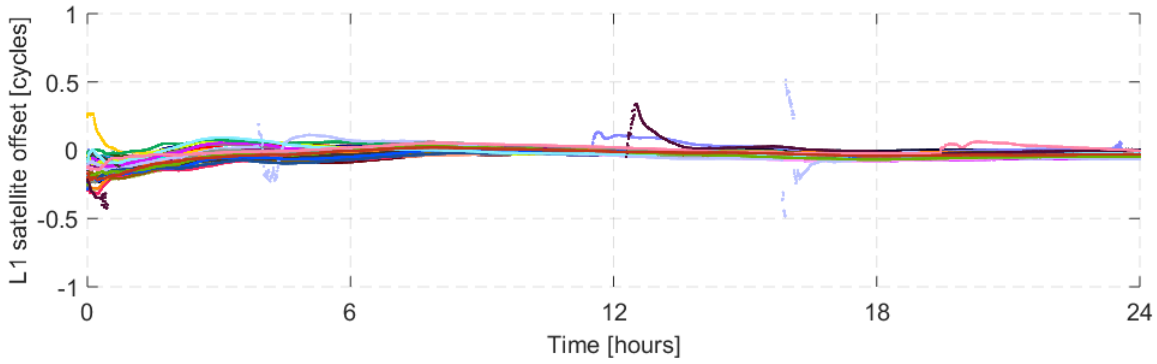

Figure 4.3: Convergence of the forward run of DCM L1 satellite offset with respect to the IRC on DOY 178, 2016 with the differences in yaw manoeuvres and axis convention taken into consideration. Each colour represents a different satellite with the integer component removed from each time series.

As mentioned previously, each AC must adopt a consistent satellite axis orientation definition. When ignoring the different axis conventions adopted by the DCM and IRC products, satellite-dependent offsets for the Block IIR/IIR-M satellites converged to 0.5 cycles as opposed to integer values, as illustrated in Figure 4.4.

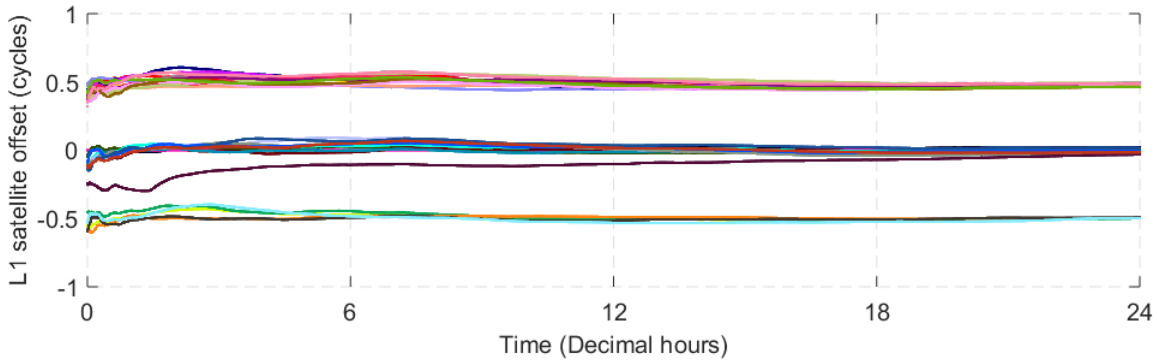

Figure 4.4: Convergence of the DCM L1 satellite offsets with respect to the IRC for DOY 179, 2016 with the differences in axis convention not account for. Each colour represents a different satellite with the integer component removed from each time series.

Hence, a 0.5 cycle correction term is applied to the measurements for ACs that adopted a different convention from the IGS. Presented in Figure 4.5 is the consistent integer natured satellite offset from DCM with respect to IRC on DOY 179, 2016 with an rms error of 0.02 cycles.

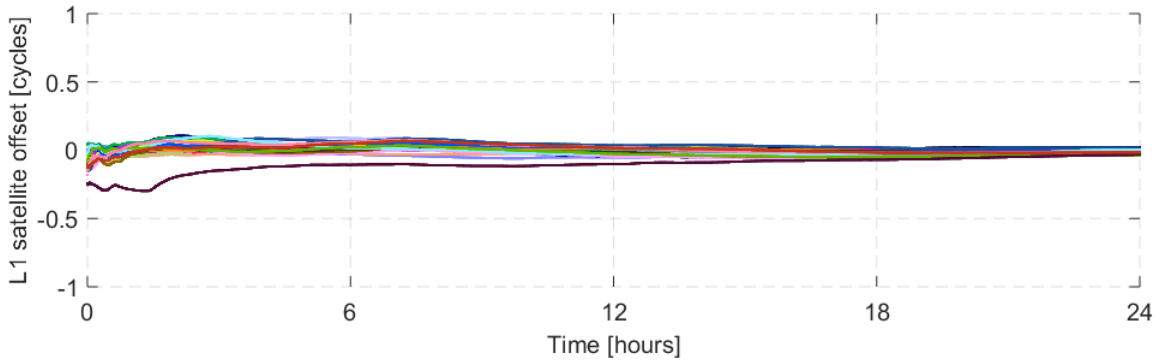

Figure 4.5: Convergence of the DCM L1 satellite offset with respect to the IRC on DOY 179, 2016 with the differences in axis convention account for. Each colour represents a different satellite with the integer component removed from each time series.

Figure 4.6 illustrates an example of the estimated widelane DCM satellite offset with respect to the IRC solution on DOY 178, 2016. Each line represents one satellite with the integer component removed. The final estimates of have an rms error of 0.03 cycles.

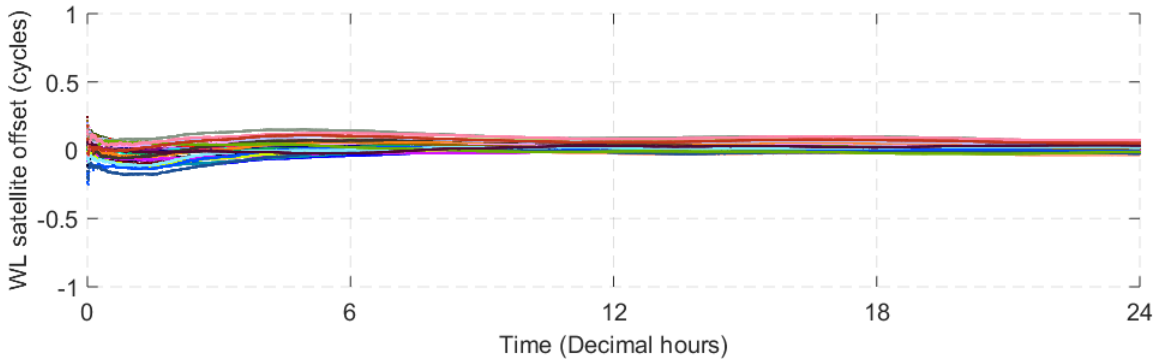

Figure 4.6: Convergence of the DCM widelane satellite offset with respect to the IRC on DOY 178, 2016. Each colour represents a different satellite with the integer component removed from each time series.

Presented in Figure 4.7 is the time reference parameter of the DCM solution (B_{DCM}). Since the term was fixed, this offset effectively represents the offset between the DCM and IRC timing references.

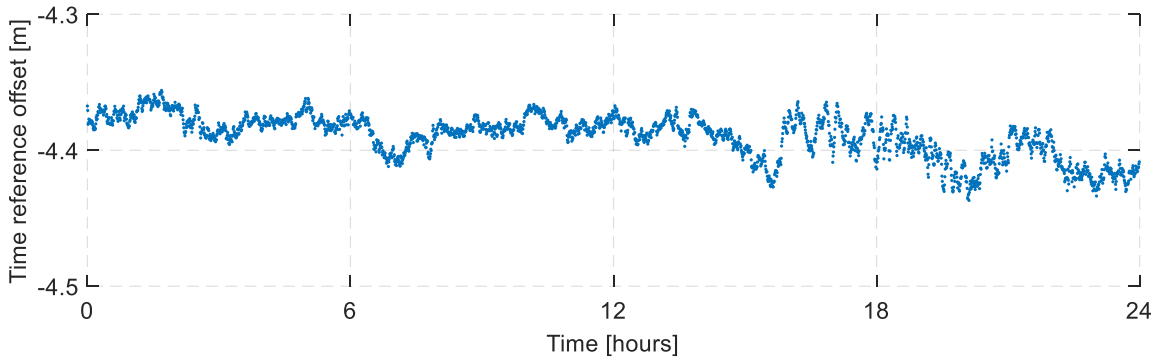

Figure 4.7: Time reference parameter of DCM with respect to IRC on DOY 178, 2016.

Post-fit residuals of the combined IRC+DCM clock with respect to the IRC clock products for DOY 178, 2016 is presented in Figure 4.8 with an rms of 0.42 cm, where 98.85% of the residuals were within 1 cm.

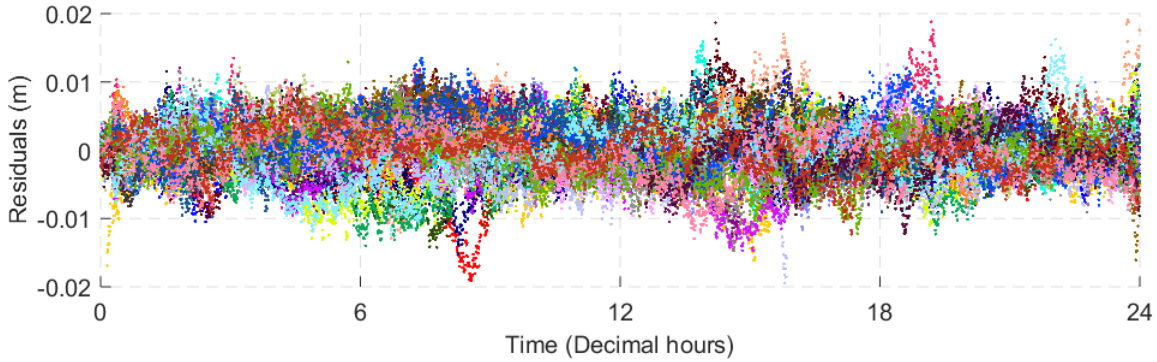

Figure 4.8: Post-fit residuals of the combined clock (IRC and DCM) with respect to the reference clock (IRC) on DOY 178, 2016.

4.4 Aligning IGS common clocks to clock products that enable PPP-AR

As a proof of concept, IGS common clocks were also aligned the IRC integer clocks to allow for ambiguity resolution with the (re-aligned) IGS clocks. Similar to the DCM and IRC combination, B_{IRC}, A^{s}_{IRC} (all satellites) and A^{1}_{IGS} were held fixed as minimal constraints in the adjustment. An infinite weight was assigned to the clocks provided by the IGS, and hence the combined clocks maintain the time variation of the IGS clocks. By assigning an infinite weight and combining the clocks relative to an integer clock solution, the combined clock product has the precision and stability of the original IGS common clocks, while preserving the integer nature of the ambiguities at the user end. Presented in Figure 4.9 is the forward run of the IGS L1 satellite offset estimation with respect to the IRC clocks on DOY 178, 2016. As expected, because the IGS clocks are a combined common clock, satellite offsets are real-valued. Presented in Figure 4.10 is the time reference offset of IGS with respect to the IRC solution. Post-fit residuals of the combined IRC+IGS clock with

respect to the IRC clock products on DOY 178, 2016 is presented Figure 4.11 with an rms of 0.3 cm, where 99.92% of the residuals were within 1 cm indicating the similarity in performance of IRC and IGS clock products.

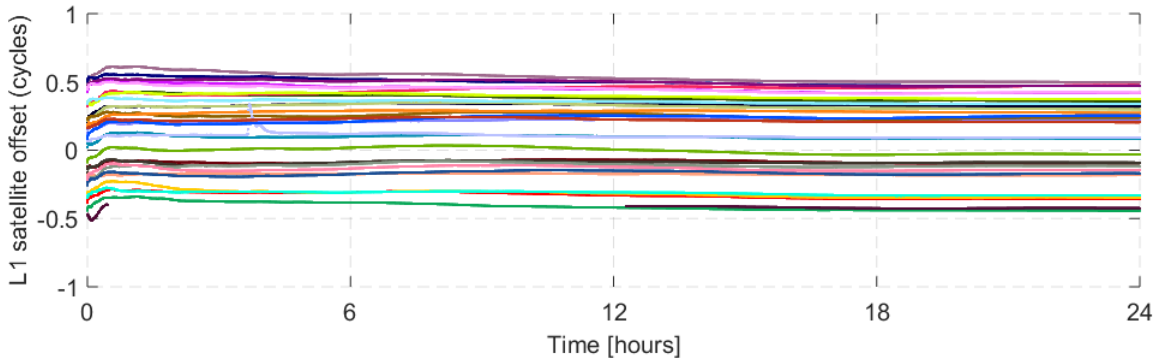

Figure 4.9: Convergence of the forward run of IGS L1 satellite offset with respect to the IRC on DOY 178, 2016. Each colour represents a different satellite with an integer component removed from each time series.

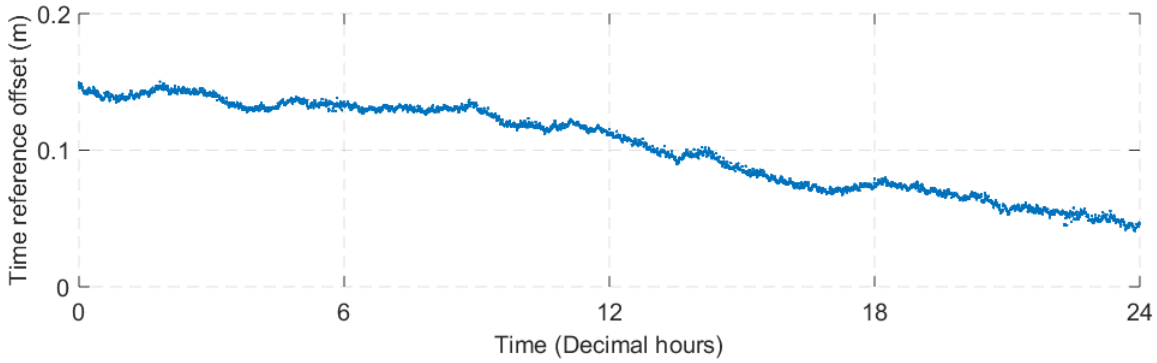

Figure 4.10: Time reference parameter of IGS with respect to IRC on DOY 178, 2016.

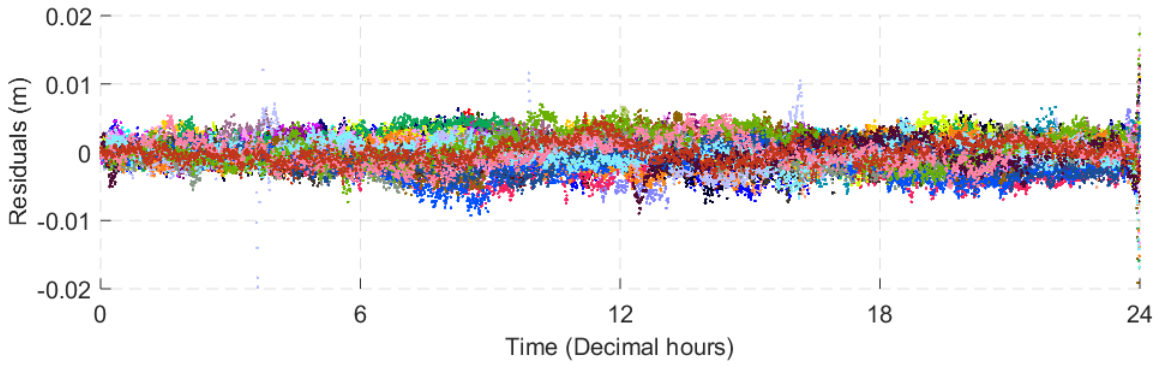

Figure 4.11: Post-fit residuals of the combined clock (IRC and IGS) with respect to the reference clock (IRC) on DOY 178, 2016.

4.5 Performance of combined satellite clock products

The goal of this section is to evaluate the quality of satellite clock combinations that enable PPP-AR in the position domain. The performance was assessed utilizing the same dataset described in Section 3.3 which was comprised of multi-GNSS data from 155 globally distributed stations from DOY 178 to 184 of 2016. Float ambiguity PPP solutions computed with the IGS clocks, (labelled 'IGS') and PPP-AR solutions obtained with the CNES IRC products (labelled 'IRC') are compared. Two sets of combined products are also included in the evaluation: 1) combined satellite clock products that enabled PPP-AR, labelled as 'IRC+DCM' and, 2) The aligned IGS clocks to permit PPP-AR, labelled as 'IGS-AR'. A summary of the different products which are being combined from IGS, CNES and NRCan are presented in Figure 4.12. Also included are the FCB products, labelled 'IGS-FCB' which were reviewed in Section 3.2.2 and the performance was analyzed in Section 3.4. As previously discussed, this set of FCB products was generated utilizing the final IGS products.

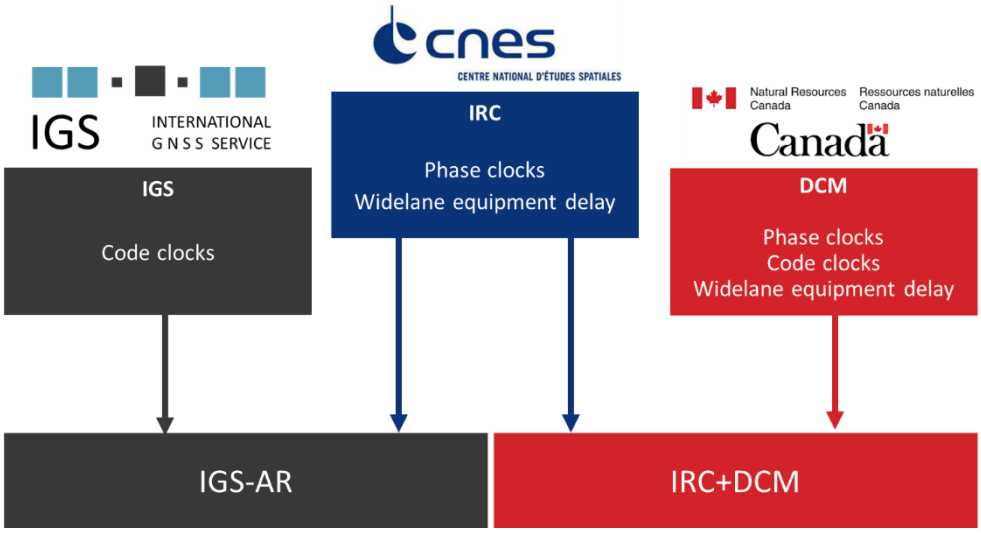

Figure 4.12: Overview of analysis centres used to generate combined products IGS-AR and IRC+DCM

In static mode, position repeatability over the 7 days processed was examined. For each station, the standard deviation of the 7 daily estimates for the northing, easting and up components was computed. These repeatability measures were then averaged over all stations to yield the results presented in Figure 4.13. This process was repeated for every satellite clock product investigated. The impact of ambiguity resolution can clearly be seen in the easting component, where all solutions with ambiguity resolution outperform the standard IGS clock solution in terms of the easting repeatability. Aligning the IGS clocks to the IRC clocks has produced the best solutions, suggesting a benefit from both the robustness of the IGS combination and the integer properties of the integer clocks. Finally, the IRC+DCM solution provides repeatabilities that are marginally better than the IRC solution at the few mm-level. Also, as expected the IGS-FCB products performed similar to the IGS-AR products as they benefited from the robustness of the IGS combination.

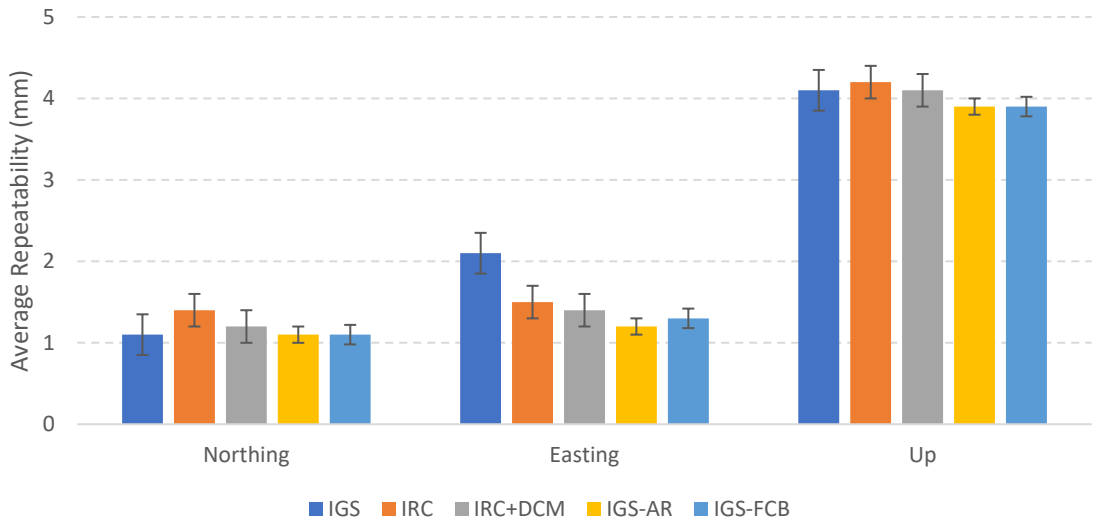

Figure 4.13: Examination of the repeatability of the PPP user solution in static mode utilizing different types of clock products. Statistics are based on GPS data from 155 IGS stations were observed during DOY 178 to 184, of 2016. All units are in millimetres.

Similarly, Figure 4.14 presents the results for kinematic processing. A different evaluation scheme was used in this case: for each daily station processing, the standard deviation of the latitude, longitude and height components were computed. The values for all 155 stations over the 7 days were then ordered and the 90th percentile values were extracted. This method was adopted as solution resets within the day (due to data gaps for example) can impact the mean value. Similar conclusions as in the static case can be made, where the contribution of ambiguity resolution significantly improves the solution. In this case, aligning the IGS clocks to the IRC clocks offered only marginal benefits over the original IRC solution.

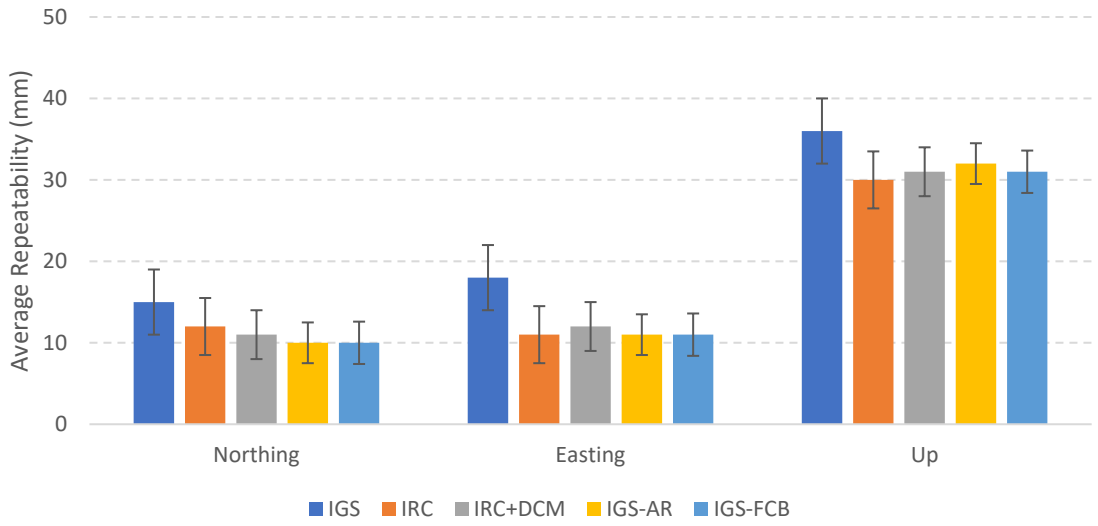

Figure 4.14: Examination of the repeatability of the PPP user solution in kinematic mode utilizing different types of clock products. Statistics are based on GPS data from 155 IGS stations were observed during DOY 178 to 184, of 2016. All units are in millimetres.

4.6 Summary of the benefits of combining AR products

The satellite clock combinations routinely produced within the IGS currently disregard that ACs provide products which enable ambiguity resolution. Users have been expected to choose either an IGS product which is a combined product from multiple ACs or select an individual AC solution which provides products that enable PPP-AR. The goal of the novel research presented was to develop and test a robust satellite clock combination preserving the integer nature of the carrier-phase ambiguities at the user end.

For a satellite clock combination to provide an integer-aligned clock, it is important that the different modelling utilized by the ACs are properly considered in the adjustment process. Two different types of modelling were addressed, namely: 1) different satellite

axis conventions, and 2) differences in modelling of yaw manoeuvres. By not accounting for these differences in the combination process, the underlying integer nature of the clock products were compromised.

For GPS Block IIR/IIR-M satellites, the IGS axis convention and manufacturer specifications are not equivalent. The difference between the two axis representations for Block IIR/IIR-M satellites is the orientation of the X and Y axes. To account for the differences in antenna conventions, a 0.5 cycle correction term must be applied to the clocks for ACs that adopted a different convention from the IGS.

Different ACs have adopted different standards for modelling the yaw manoeuvres during orbit noon and orbit midnight. To account for the inconsistent yaw modelling between ACs. It is critical that additional information such as yaw angle and phase/code satellite hardware delays are provided at the same intervals as the clocks. The yaw information would allow for a phase wind-up correction to be applied to each solution for improved consistency, while the phase/code satellite hardware delays accommodates different product representations, such as FCB. To this end, an updated RINEX clock format is suggested.

Two sets of combined clock products were generated: 1) combined satellite clock products that enable PPP-AR, and 2) IGS satellite clocks aligned to enable PPP-AR. The combined products were evaluated in the position domain by processing GPS data from 155 IGS stations, observed during DOY 178 to 184 of 2016. mm-level differences were noted, which was expected as the strength lies mainly in its reliability and stable median performance and the combined product is better than or equivalent to any single AC's product in the combination process. Aligning the actual IGS satellite clock products yielded

the best PPP-AR results, for both static and kinematic solutions, where mm-level improvements were noted.

CHAPTER 5 REASSESSING THE ROLE OF AMBIGUITY RESOLUTION IN PPP

With the advent of quad-constellation, triple-frequency and external atmospheric constraints being provided to the PPP user, the novelty and focus of this chapter is in the quest to answer the question: Is ambiguity resolution in PPP needed for accuracy or for integrity? To determine if ambiguity resolution in PPP for accuracy or for integrity an examination of the significance between the float and ambiguity resolved PPP user solution is undertaken. Assessment of ambiguity resolution as an integrity indicator has also been an area that has lacked attention. Is the improvement significant enough for applications such as precision agriculture and autonomous vehicles to justify the additional cost and computational complexity of producing a PPP-AR solution?

5.1 Introduction

The utilization of ambiguity resolution in PPP has been primarily focused on high accuracy applications such as geodetic surveying. To re-examine the role of ambiguity resolution in PPP, accuracy specifications from precision agriculture and autonomous vehicles is assessed to determine if the improvement in accuracy between float and resolving GPS ambiguities is significant (Seepersad et al. 2017). Results consist of solution analysis of convergence time (time to a pre-defined performance level), position precision (repeatability), position accuracy (solution error with respect to analysis centre's weekly SINEX solution) and residual analysis. Pre-defined thresholds are based on specifications for lane navigation and machine guidance for agriculture.

A novel component within the realm of PPP-AR is the analysis of ambiguity resolution as a metric to examine the integrity of the user solution. Integrity within the context of the PPP user solution means, the amount of trust that can be placed in the information supplied by the PPP data processing engine. Integrity also relates to the PPP engine's ability to provide timely warnings to users when the solution should not be trusted. Given that in PPP processing, all parameters must be accounted for without multiple solutions (as is in the case with double-differenced static, multi-baseline networks and network RTK), providing integrity information for PPP single receiver estimates is all that more important. Within the context of integrity monitoring, ambiguity resolution will be further examined.

The role of ambiguity resolution depends on what are the user specifications. If the user specifications are at the few cm-level, ambiguity resolution is an asset, as it improves convergence and solution stability. Whereas, if the user's specification is at the few dm-level, ambiguity resolution offers limited improvement over the float solution. If the user has the resources to perform ambiguity resolution, even when the specifications are at the few dm-level, it should be utilized. To have a high probability of correctly resolving the integer ambiguities, the residual measurement error should be less than a quarter of a wavelength (Georgiadou and Kleusberg 1988; Banville 2014; Petovello et al. 2014). Having a successfully resolved and validated solution can indicate to the user increased accuracy, precision and reliability of the user solution thereby increases the amount of trust that can be placed in the information supplied by the ambiguity resolved PPP data processing engine.

5.2 Ambiguity resolution

Ambiguity resolution in PPP requires the equipment delays within the GNSS measurements to be mitigated, which would allow for resolution of the integer nature of the carrier-phase measurements. Resolution of these ambiguities convert the carrier-phases into precise pseudorange measurements, with measurement noise at the centimetre-to-millimetre level compared to the metre-to-decimetre-level of the direct pseudoranges. If the ambiguities could be isolated and estimated as integers, then there would be more information that could be exploited to accelerate convergence to give cm-level horizontal accuracy within an hour of data collection.

5.2.1 Partial Ambiguity resolution

In multi-constellation processing, low elevation satellites will be frequently tracked. These low-elevation ambiguities suffer much more from observation noise, multipath effects and the residual atmospheric delays, and thus have much lower accuracies. Therefore, the likelihood of correctly fixing all ambiguities simultaneously is low. If all ambiguities are fixed simultaneously, the low-elevation ambiguities may influence the search system and make the search result unable to pass the acceptance test.

The challenge of partial ambiguity resolution is finding the largest possible subset of the reliable ambiguities. As a result, different sorting methods have been proposed to fix the largest possible subset of the ambiguities with bootstrapping method. Bootstrapping is a statistical method that resamples the ambiguity candidates to estimate the ambiguity resolved user solution. A partial decorrelation can be applied before the partial ambiguity

resolution to improve the success-rate (Teunissen 2005; Henkel and Günther 2010). The challenge in partial ambiguity resolution is determining the largest possible subset of the reliable ambiguities. Some conventional techniques of the ambiguity subset selection are Sequential fixing Ascending Variance Order (SAVO), Sequential BLewitt fixing Order (SEBLO) method, Sequential Optimum Fixing Order Search (SOFOS) method, and Batch partial ambiguity resolution (Henkel and Gomez 2013; Kamali 2017).

A common approach is the SAVO method (Teunissen 1998), in which float ambiguities are ordered based on their precision. A subset of the most precise is validated first and if the successfully resolved the set of candidates are validated. The remaining subsets of ambiguities with lower precision are bootstrapped. The sequential fixing continues until reaching the ambiguity that can no more be fixed to its nearest integer value. All combinations of independent subsets of ambiguities are then tested, maximizing the number of fixed ambiguities.

There were also more simplistic approaches such as a decision to fix is made when both the formal sigma and the fractional component of the float ambiguity drops below a common threshold. During the early developmental period of PPP-AR, researchers recommended different thresholds such as 0.15 cycles (Collins et al. 2010) and 0.2 cycles (Geng et al. 2010a). The concept of these thresholds was, if the fractional component of the ambiguity term were within a threshold, it would lead to a correctly resolved ambiguity solution. Within the scope of this research, a threshold based only on the elevation angle of the satellite was selected. An elevation threshold of 20° was selected as this elevation cut-off angle was determined as optimal based on multipath analysis presented in

Seepersad and Bisnath (2014b), where typical ground bounce multipath observed with a geodetic GNSS antenna, was pronounced at elevation angles less than 20°. To ensure reliable ambiguity resolution, the error budget should remain below a quarter of a wavelength, namely 10 cm / 4 = 2.5 cm for the ionospheric free combination (Banville 2014).

5.2.2 Resolving and fixing the ambiguities

When determining the integer candidates for an ambiguity resolved solution, there are several different approaches that have been utilized over the decades, these include Cascade Integer Resolution, Fast Ambiguity Resolution Approach (FARA), Fast Ambiguity Search Filter (FASF), Least-squares AMBiguity Decorrelation Adjustment (LAMBDA), Least-Squares Ambiguity Search Technique (LSAST), Optimal Method for Estimating GPS Ambiguities (OMEGA) and Three Carrier Ambiguity Resolution (Kamali 2017). The de facto standard for determining the integer candidates has become the LAMBDA method because of its high success-rate is based on integer least-squares, of which optimality has been proven, that is, highest probability of success. In TCAR and CIR pre-defined ambiguity transformation are used, whereas LAMBDA exploits the information content of the full ambiguity variance-covariance matrix, with statistical decorrelation the objective in constructing the ambiguity transformation. For resolving the ambiguities, TCAR and CIR were designed for use with the geometry-free model. LAMBDA can inherently handle any GNSS model with integer ambiguities and thereby utilize satellite geometry to its benefit in geometry-based models (Teunissen et al. 2002).

The concepts of LAMBDA would not be discussed in further detail here as it has been well documented in literature (Leick 1995; Hofmann-Wellenhof et al. 1997; Teunissen and Kleusberg 2012). To improve the computational deficiencies of LAMBDA, Chang et al. (2005) developed modified LAMBDA (MLAMBDA). MLAMBDA improved the computational speed of LAMBDA, which becomes critical for real-time, multi-GNSS, triple-frequency positioning. The MLAMBDA routine utilized within the PPP engine was obtained from the open source program package RTKLIB (Takasu and Yasuda 2009). The inputs to the MLAMBA function requires the float ambiguity estimates, covariance of the ambiguity terms and the number of sets of integer ambiguities to be returned. The output of the function consists of the number of specified sets of integer ambiguities and the sum of squared residuals of each set of integer ambiguities.

After resolving the ambiguities, there are two main approaches for determining the ambiguity resolved position estimates. These can be performed either functionally (De Jonge and Tiberius 1996) or stochastically (Euler and Schaffrin 1991; Wang et al. 1998). While both approaches are equivalent, the approach by Euler and Schaffrin (1991) presented in equation (5.2) was adopted because it was more flexible from a programming perspective.

Ambiguity resolution can be thought of as a three-step process. After the least-square estimation, the vector of unknown parameters ($\hat{x}$) are sorted according to their meaning utilizing a permutation matrix (Henderson and Searle 1981). The first part consists of all the non-ambiguity terms (e.g., coordinates, clock terms and atmospheric terms), which is

represented by $\hat{x}_1$ and the float ambiguity terms are represented by $\hat{x}_2$ in equation (5.2). After, float ambiguity candidates with the highest likelihood to be successfully resolved are determined and these float ambiguity candidates are constrained utilizing a Boolean matrix (K). K is comprised only of 0's and 1's, where the corresponding candidates to be resolved are assigned a 1. For a total number of ambiguity candidates (r) and a number of integer candidates to be fixed (f), the constraints to be formed is presented in equation (5.1).

$$\mathrm{K}=\left[0, I_r\right] \tag{5.1}$$

Where $0 = \text{zero matrix } (f \times (u - f))$, $I_r = \text{boolean matrix } (r \times f)$ and u is the total number of unknown parameters.

The K matrix allows for constraints to be imposed on a solution after estimation without constraints on the ambiguity parameters, thereby easily permitting epoch-by-epoch fixing. The underlying float solution is maintained independently with the ambiguity-fixed solutions computed separately, as illustrated in Figure 5.1. Epoch-by-epoch fixing is an optimum way of combining sequential least-squares filter with integer state estimation, as well as maintain an independent float solution for comparison purposes. The main benefit of this approach is that the float solution remains uncorrupted by possibly incorrect ambiguity fixes. The downside of epoch-by-epoch fixing is the increased computational load when combined to permanently fixing ambiguity candidates. Permanently fixed

ambiguity candidates allow for reduction of matrix sizes as they are no longer included in state terms and covariances.

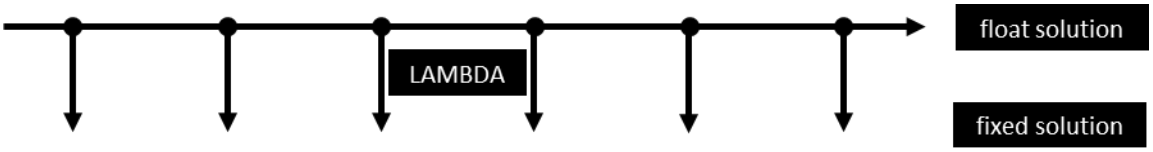

Figure 5.1: Schematic approach to fixing (Collins et al. 2010).

The final step after resolving the ambiguities, involves applying the ambiguity corrections to determine the ambiguity resolved solution $\breve{x}_1$ which is computed utilizing (5.2).

$$\breve{x} = \hat{x} + \mathrm{V}_x \mathrm{K}' \mathrm{V}_{\hat{x}_2}^{-1} (\breve{x}_2 - K\hat{x}) \tag{5.2}$$

where the covariance of the ambiguity candidates is represented by $\mathrm{V}_{\hat{x}_2} = \mathrm{K}\mathrm{V}_x\mathrm{K}'$, and $\hat{x}_2 = K\hat{x}$ is the subset of ambiguities that can be reliably fixed. The covariance of the fixed solution is given by

$$\mathrm{V}_{\breve{x}} = \mathrm{V}_x - \mathrm{V}_x \mathrm{K}' \mathrm{V}_{\hat{x}_2}^{-1} \mathrm{V}_x' \mathrm{K} \tag{5.3}$$

5.3 Ambiguity validation

The integer ambiguity candidates need to be statistically validated before they are accepted as the correct values. Regardless of the ambiguity strategy selected, the most optimal candidates would be determined. The covariance matrix of the real-valued ambiguity parameters can be used as the indicator of the quality of the parameter. Some of the

standard ambiguity validation techniques include Probabilistic rounding region, Success-rate, Ambiguity residual test, Fixed solution residual test, F-Ratio test, Difference test, Projector test.

Of the different tests, the ratio test is the one of the earliest and most popular test to validate the integer ambiguity solution (Blewitt, 1989; Dong & Bock, 1989; Ge et al., 2008; Geng et al., 2012). The ratio is formed by the squared norm of the second-best ambiguity residual vector and the squared norm of the best ambiguity residual vector (Davis, 1991; Tiberius & de Jonge, 1995). This ratio is compared against a certain threshold, the critical value and the integer resolved solution is only accepted if the test pasts (Davis, 1991). This critical value plays a key role since it is the indicator if the two compared solutions are considered to be discriminated with sufficient confidence. Hofmann-Wellenhof et al. (2007) presented a concise overview of different test statics adopted by different researchers. The choice of the critical value may still be regarded as a of a question mark. Euler and Schaffrin (1990) propose a critical ratio value between 5 and 10, depending on the degrees of freedom. Wei and Schwarz (1995b) choose 2, Han and Rizos (1996) propose 1.5, if elevation-dependent weights are used. Leick (2004) states that many software simply use a fixed critical value, for example, 3.

Presented in equation (5.4) is the ratio test

$$If \ \frac{(\hat{x}_2 - \breve{x}_2')\mathrm{V}_{\hat{x}_2}(\hat{x}_2 - \breve{x}_2')}{(\hat{x}_2 - \breve{x}_{\mathbf{2}})\mathrm{V}_{\hat{x}_2}(\hat{x}_2 - \breve{x}_{\mathbf{2}})} \begin{cases} \geq \tau & use \quad \breve{x}_1 \\ < \tau & use \quad \hat{x}_1 \end{cases} \tag{5.4}$$

where τ is the pre-selected ratio threshold and $\breve{x}_2'$ represents the second best set of ambiguity candidates.

In traditional relative positioning techniques such as RTK, after ambiguity resolution is undertaken, the general practice followed is to validate the ambiguities before permanently fixing them. Ambiguity validation was briefly investigated for PPP-AR in Collins (2008), but it was found to be unreliable as it did not correlate with any of the typical validation statistics and the actual positioning results obtained. One possible reason for the reasons for the unreliability of ambiguity validation is, the observation weight matrix used in the processing is it is overly optimistic, as it ignored the correlation between the linear combination of the observables (Han 1997; Geng et al. 2010b; Teunissen and Kleusberg 2012).

5.4 Assessment of the role of ambiguity resolution in PPP

While much research effort has been applied to improving the accuracy of PPP-AR coordinate solutions and the duration of data collection needed to achieve such accuracies, little work has been published on the integrity of PPP-AR solution. Integrity is the measure of the trust that can be placed in the information supplied by a navigation system (Ochieng et al. 2003). It includes the ability of the system to provide timely warnings to users when the system should not be used for navigation. Given that in PPP-AR processing all parameters have to be accounted for, without multiple solutions as is the case with double-differenced static, multi-baseline networks and network RTK, providing integrity information for PPP single receiver estimates is all that more important. While it has been

illustrated in literature (Geng 2010; Shi 2012; Teunissen and Khodabandeh 2015) that PPP-AR is equivalent to a double-differenced solution using a global network, the solution is more sensitive to localized error sources, such as atmospheric error sources and multipath.

Integrity is typically defined in PPP by internally determining realistic measurements of solution precision and also by internally detecting and removing of outlier measurements (Ochieng et al. 2003; Seepersad and Bisnath 2013; Jokinen et al. 2013a). It is important to have integrity monitoring during data processing as it is the only time when all the information used to form the position solution is present for in depth analysis. In the presented work, PPP integrity indicators include post-fit and integer-fit residuals, processing filter convergence and parameter estimation covariance. Each is discussed and developed as a means of providing integrity to the PPP solutions. Presented in the following subsections are the different integrity indicators that have been identified and how they are used in PPP.

To determine if ambiguity resolution in PPP for accuracy or for integrity is an intricate one. While commonly known that ambiguity resolution improves solution accuracy and stability and it is also critical for satisfying user specifications at the few cm-level. Less frequently discussed, is if the accuracy specification is at the few dm-level, such as 10 cm and 20 cm horizontal, what role does ambiguity resolution play?

5.4.1 Convergence

The use of PPP presents advantages for many applications in terms of operational flexibility and cost-effectiveness. One major limitations has always been relatively long

initialization period as carrier-phase ambiguities converge to constant values and the solution reaches its optimal precision. PPP convergence depends on a number of factors such as the number and geometry of visible satellites, user environment and dynamics, observation quality, and sampling rate. As these different factors interplay, the period of time required for the solution to reach a pre-defined precision level will vary. Utilizing PPP-AR would accelerate the overall solution convergence to give cm-level horizontal accuracy after 1 hour or less. Utilizing GPS-only PPP-AR, Collins et al. (2008) and Laurichesse et al. (2009) saw improvements in hourly position estimates by 2 cm horizontal error, compared to 10 cm for the float PPP solution and Geng et al. (2010a) saw noticeable hourly improvements from 1.5, 3.8 and 2.8 cm to 0.5, 0.5, 1.4 cm for north, east and up, respectively. AR usually serves as an ideal and direct indicator of a successful initialization, as correct AR should lead to continuous centimetre-level positioning accuracy in real-time PPP

To examine the issue of the user being aware if the solution has truly converged, accuracy specifications of 20 cm and 10 cm was selected to represent the upper and lower bounds of the accuracy specifications for autonomous navigation used in lane navigation (Schumann 2014) and machine guidance for agriculture (Wang and Feng 2009). As a bench mark, an accuracy specification of 2.5 cm was also included, accuracy specification of network RTK (Trimble 2018). A stringent definition of convergence was established where the solution only attained convergence when it stayed within the accuracy threshold. Presented in Figure 5.2 is an example of the computation of the convergence time using a threshold of 10 cm horizontal error.

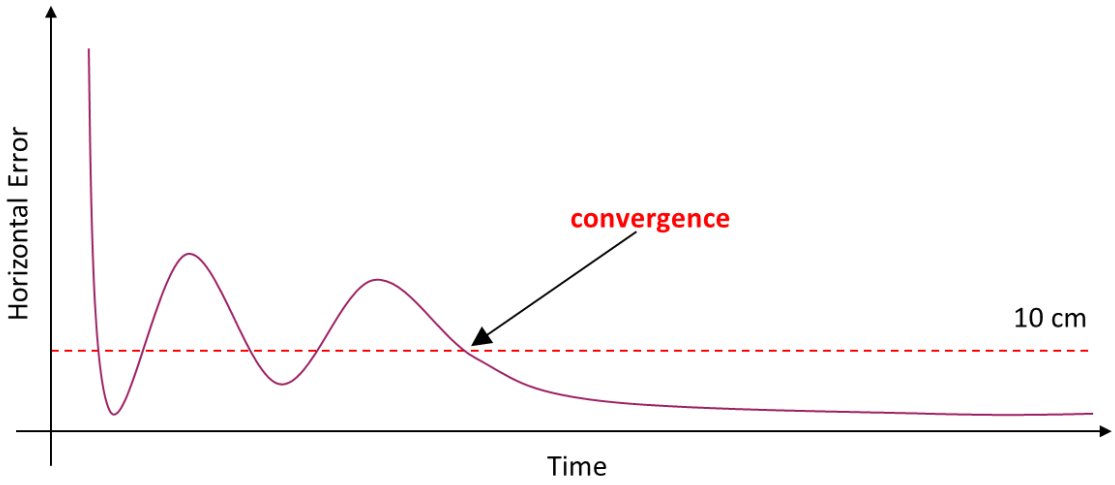

Figure 5.2: Definition of convergence.

Presented in Figure 5.3 is the cumulative histogram examining the time required for 50%, 68% and 95% GPS data to attain a 20 cm horizontal threshold. For the float solution, convergence times of 5, 10 and 40 minutes were required for 50%, 68% and 95% GNSS data to converge. In contrast, the fixed solution required 10 minutes for 50% and 68% of the data, respectively, to converge and 45 minutes for 95% of the data to converge. No improvements were noted when utilizing the fixed solution at a 20 cm horizontal threshold.

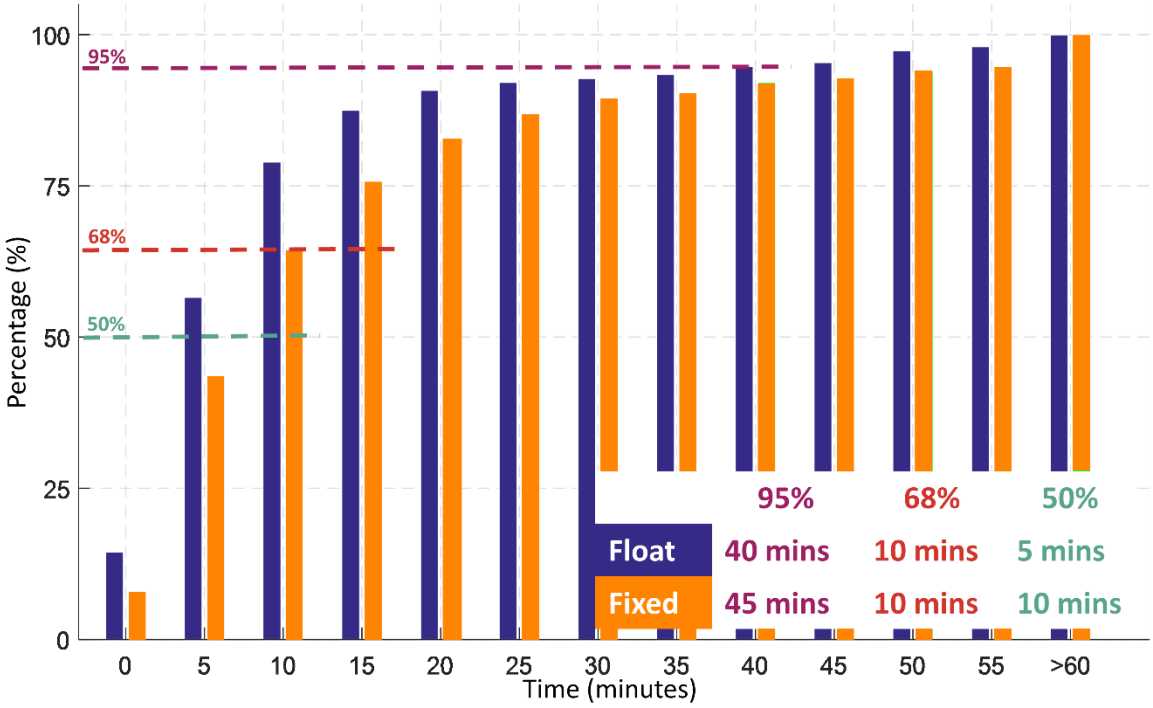

Figure 5.3: Cumulative histogram illustrating the required convergence of time to attain 20 cm horizontal for the float and fixed solutions.

Next, a tighter threshold of 10 cm horizontal was examined, presented in Figure 5.4. For the float solution to attain a 10 cm horizontal accuracy threshold, 15, 20 and 60 minutes for 50%, 68% and 95% respectively. For the fixed solution, improvements over the float solution becomes more apparent as 10, 15 and 60 minutes is needed for 50%, 68% and 95% of the data, respectively, to converge. As expected, the role of ambiguity resolution for accuracy becomes more apparent as the threshold is tightened. Improvements in convergence of the fixed solution occurs, because at dm-level position accuracy it is

possible to successfully resolve the underlying carrier-phase ambiguity term. Also, the rate of convergence of the float PPP solution typically slows down at the few cm to dm-level.

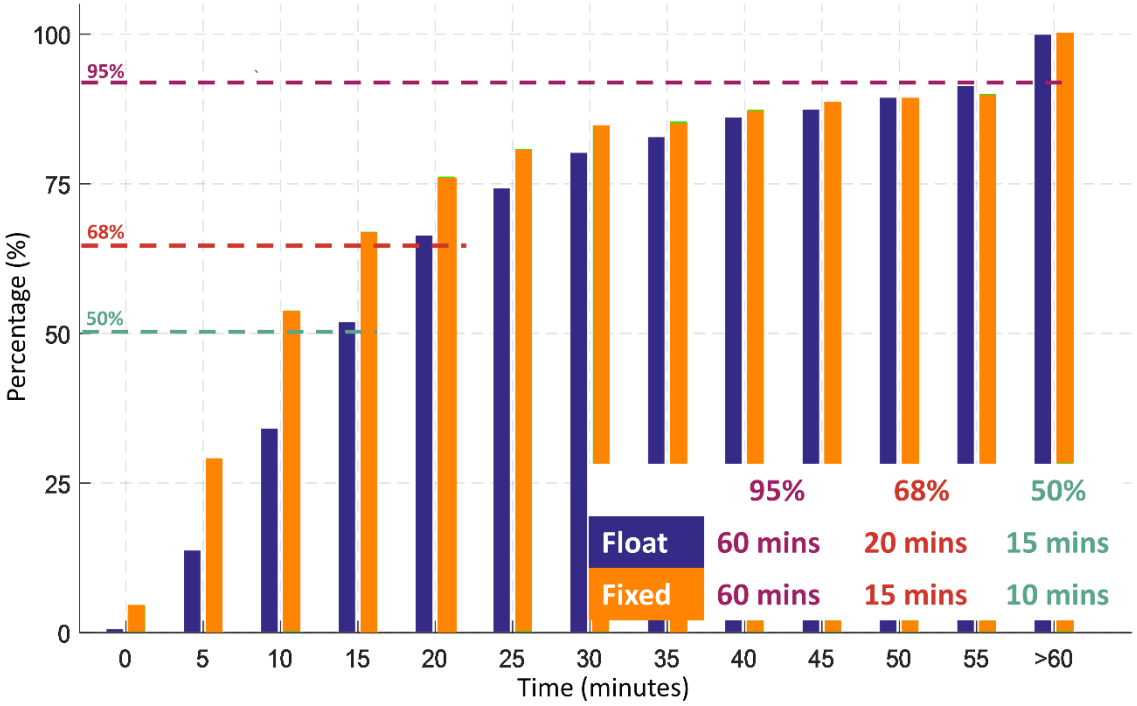

Figure 5.4: Cumulative histogram illustrating the required convergence of time attain 10 cm horizontal for the float and fixed solutions.

Presented in Figure 5.5 is the cumulative histogram examining the time required for 50%, 68% and 95% GPS data to attain a 2.5 cm horizontal threshold. For the float solution, convergence times of 3, 4 and 6 hours required for 50%, 68% and 95% GNSS data, respectively, to converge. In contrast, the fixed solution required 15, 20 and 60 minutes for 50%, 68% and 95% of the data, respectively, to converge. At few cm-level accuracy specifications, PPP-AR becomes a requirement for accuracy as it significantly decreased the convergence time.

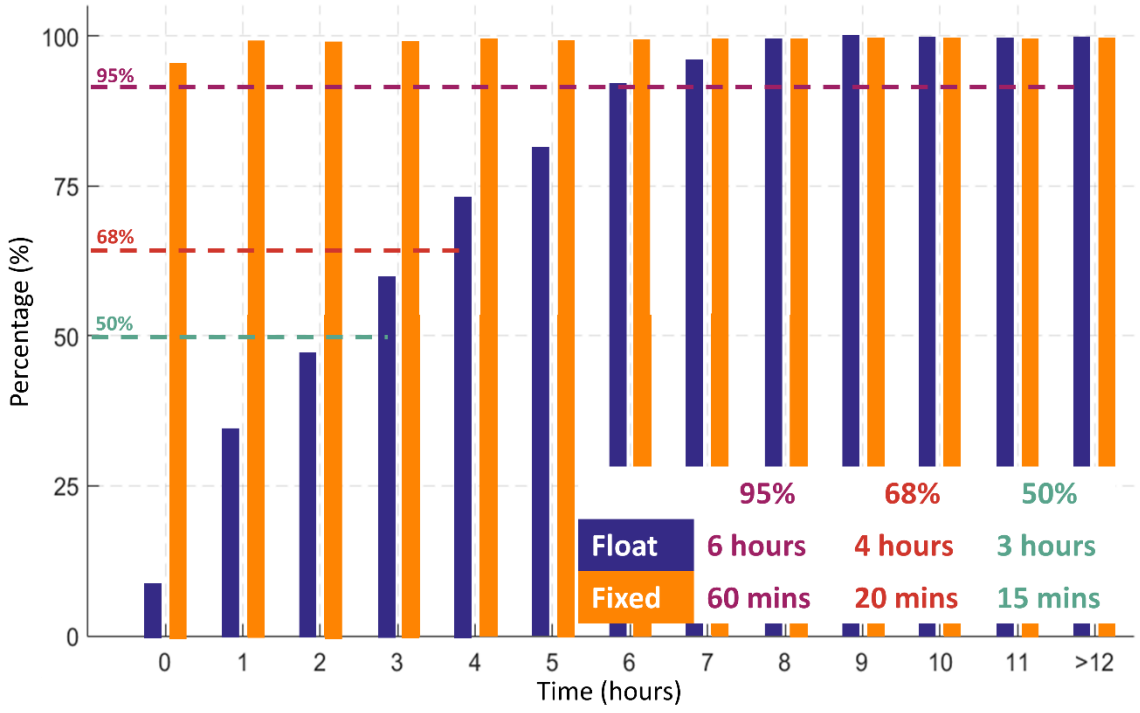

Figure 5.5 Cumulative histogram illustrating the required convergence of time attain 2.5 cm horizontal for the float and fixed solutions.

5.4.2 Position uncertainty

The weighting of the observations are based on the covariance matrix of the observations, which plays a crucial role in the estimation of the covariance of the parameters. The covariance matrix of the position parameters, also known as the position uncertainty will be discussed and assessed in greater detail to determine its reliability to the PPP user. In most cases, the PPP user has no reference solution available. There have been very few studies that address this aspect of integrity monitoring in PPP to answer the questions: How accurate is my epoch PPP position? And, how realistic is the internal PPP uncertainty estimate? What is being asked is how the pseudorange and carrier-phase measurement as

well as the modelled errors affect the estimated parameters. Convergence being the Achilles' Heel in PPP has led to an increase in the reliance on a realistic position uncertainty. The covariance of the estimated position is the main indicator of the solution accuracy, as a reference solution may not always be available. An attempt to address the questions such as how accurate is my epoch PPP position? And how realistic is the internal PPP uncertainty estimate for the float and fixed solution? Integrity was studied by examining the correlation between the determined PPP position error and the position uncertainty scaled to 95%.

The quality of the position uncertainty is defined by rigorous propagation of the observation uncertainties to the estimates of the unknowns. The observations are expected to be normally distributed and uncorrelated. In practice, due to the existence of biases and unknown and/or ignored correlation in the observations, they are not necessarily normally distributed potentially resulting in unrealistic state uncertainty estimates. For single point positioning, the position uncertainty is typically too optimistic. To ensure reliable position uncertainty is provided to the user, it is required that: 1) The stochastic model of the observations is well defined. The covariance matrix must be propagated with realistic observational variances and covariances. And 2) The systematic effects are completely removed (i.e., the functional model is correct). GNSS processing software typically utilizes elevation dependent weights which may be a contributing factor to overly optimistic position uncertainties. Within the YorkU-PPP engine is a module which incorporates the uncertainties in the satellite orbits and clocks from their covariance matrix into the system

of the observation equations. Such information will modify the covariance matrix potentially creating a more realistic position uncertainty.

Illustrated in Figure 5.6 is the correlation plot comparing the average position uncertainty and error for 155 globally distributed stations in horizontal component. The average position uncertainty as well as the float and fixed position error was taken for epochs at time 1, 5, 10, 15, 20, 25, 30 minutes, and 1 to 6, 12, 18 and 24 hours. For the first hour, the float position uncertainty was overly pessimistic suggesting the error was worse than the error between the estimated position and reference solution. For hours 2-6 and 12-18 a strong positive correlation is seen such that the average position uncertainty realistically depicts the magnitude of the average error in the component as the solution converged further. While at hours 18-24 the average position uncertainty and errors are correlated, the uncertainty becomes optimistic, suggesting the error is smaller than it actually is. In contrast, the position uncertainty of the fixed solution was overly optimistic, indicating that the error was significantly better than the error between the estimated position and reference solution. After 2 hours of processing, the position uncertainty became more realistic in depicting the magnitude of the averaged error.

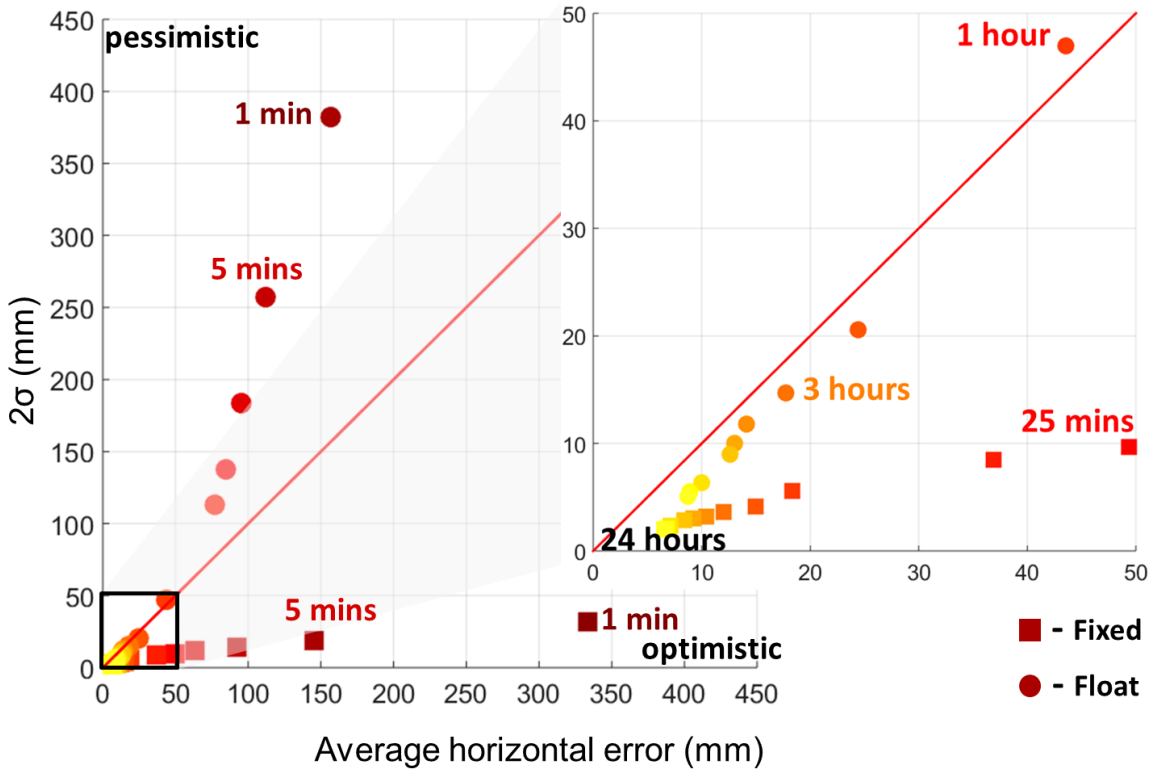

Figure 5.6: Solution integrity for the horizontal component.

5.4.3 Post-fit and integer-fit residuals

In least-squares filtering, the post-fit residuals are a measure of the quality of fit between the observed quantities and the estimated quantities and the integer-fit residuals indicant when the correct ambiguity candidate has been resolved. They can also be thought of as a measure of the appropriateness of the mathematical model used for the measurement (Anderson and Mikhail, 1998). Residual testing in general assumes that errors in the observations and the residuals are normally distributed (Tiberius et al. 1999). Hence, before statistical tests can be applied it may be necessary to test that the residuals are normally distributed. The familiar bell-shape of the Normal Distribution frequency curve

indicates that relatively large residuals can be expected, although these should occur much less frequently than relatively small residuals (Harvey et al. 1998; Rizos, 1997).

Integer carrier-phase ambiguity resolution is the key to fast and high-precision. It is the process of resolving the unknown cycle ambiguities of the carrier-phase data as integers. Once successfully resolved, the precise carrier-phase measurements will act similar to pseudorange measurements, thus enabling precise positioning. As previously mentioned, the procedure for carrier-phase ambiguity resolution does not only consist of integer ambiguity estimation, but also includes ambiguity validation testing. Such testing is important, considering the increasing integrity demands on PPP.

Presented in Figure 5.7 is the site ALGO DOY 178 of 2016 located at Algonquin Park, Canada, illustrating the differences between the float and fixed solution. The fixed solution consists of the validated solution that passed (accepted) and failed (rejected) the ambiguity validation testing. 81% of the fixed solution passed the validation test and of particular interest is between hours 5.5 and 6 where incorrect ambiguity fixing occurred. The incorrectly fixed solution was correctly identified by ambiguity validation. The sensitivity of ambiguity validation was noted particularly between 15 to 24 hours, where the correctly resolved ambiguity solutions were also rejected.

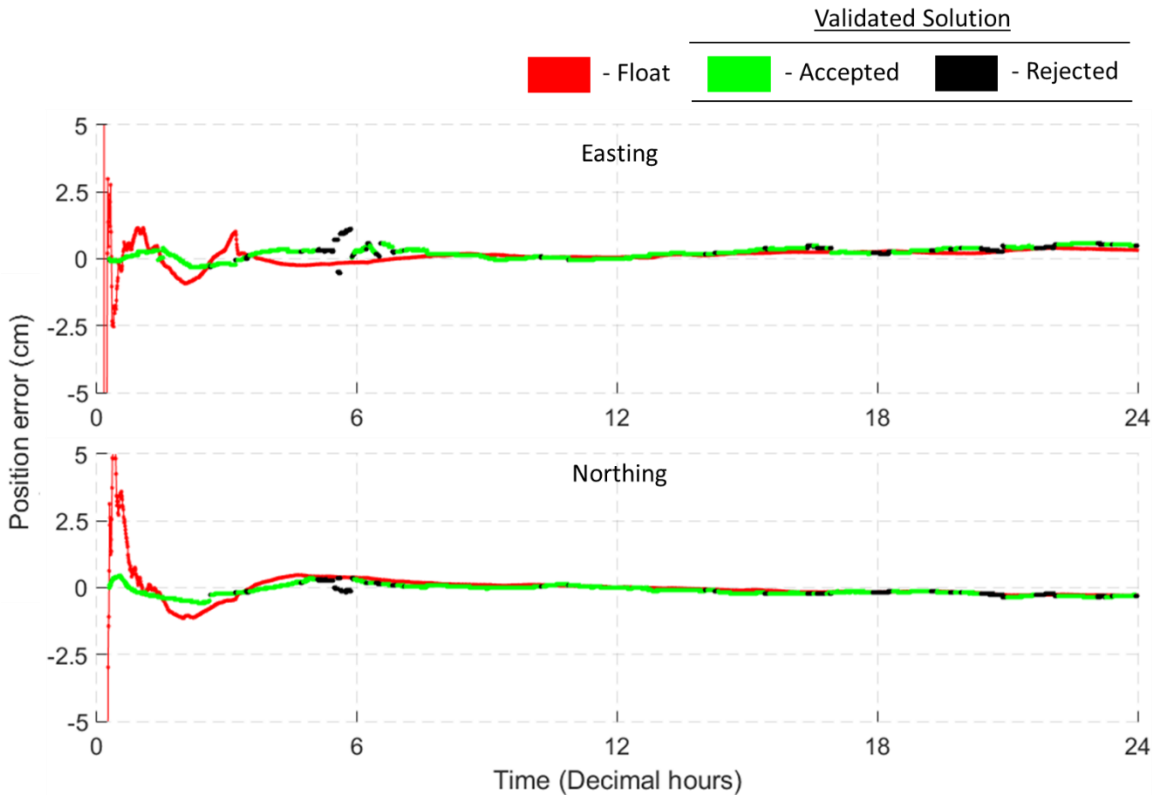

Figure 5.7: Performance of ambiguity validated solution at site ALGO DOY 178 of 2016 located in Algonquin Park, Canada. Upper plot illustrates the easting component and the lower plot is the northing component.

To better understand the underlying problem, present with ambiguity validation in PPP-AR, the performance was compared to long single baseline relative positioning. Ambiguity validation has been typically described as performing more reliable in relative positioning than in PPP-AR. To compare the performance, relative positioning was used to coordinate ALGO and compare the to the PPP performance in Figure 5.9. For the comparison of relative positioning and PPP-AR, two single baselines were established, 1) ALGO with respect to BAIE with a baseline length of 819 km and 2) ALGO with respect to NRC1 with a baseline length of 199 km. The station distribution is presented in Figure 5.8. Long

baselines were selected to ensure atmospheric errors were not correlated. Canadian Active Control System (CACS) stations ALGO, NRC1 and BAIE were selected to minimize localized effects as these are high quality geodetic grade reference stations. For the relative positioning, precise orbits were used and atmospheric errors were managed similar to PPP-AR. The slant ionosphere term was treated as unknown and the zenith tropospheric delays were estimated each epoch with a random walk coefficient of 2 cm/sqrt(hour).

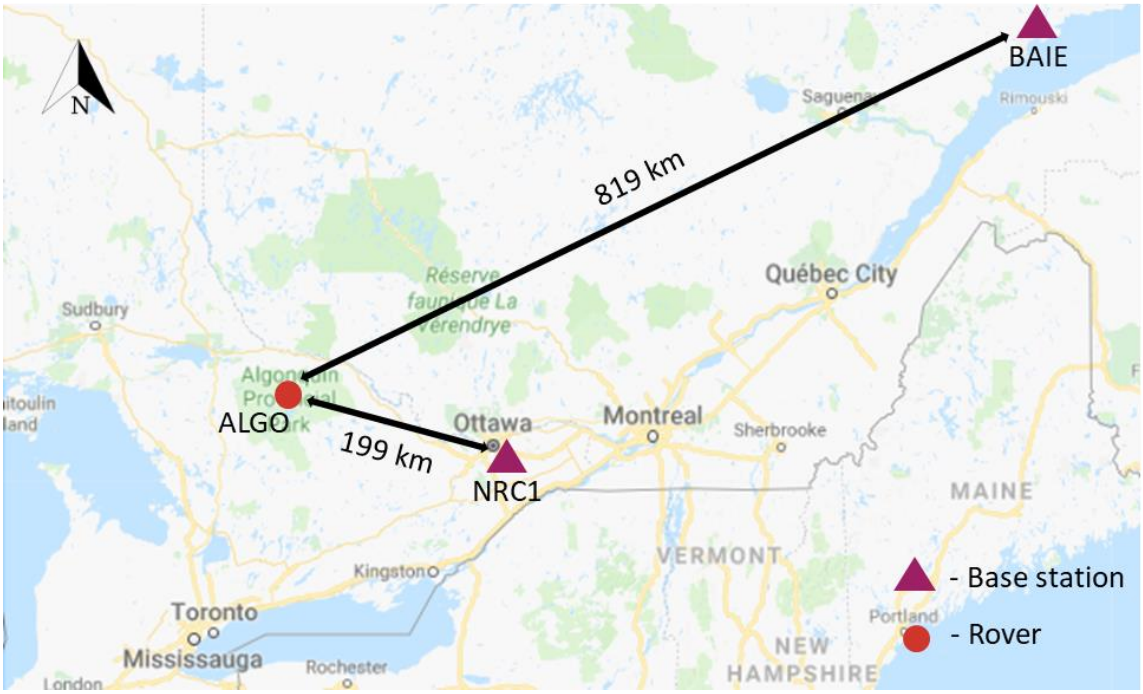

Figure 5.8: Station distribution used to compare the performance of ambiguity validation in single baseline relative positioning and PPP-AR.

Presented in Figure 5.9 is the comparison between the long single baseline relative positioning solution and PPP-AR. Both techniques were utilized to coordinate the station ALGO to examine the performance of ambiguity validation. Sub-plot a) is the horizontal position solution of ALGO with respect to BAIE, sub-plot b) is the ALGO PPP solution,

and sub-plot c) is ALGO with respect to NRC1. The solutions ALGO-BAIE, ALGO PPP and ALGO-NRC1 had an accepted validated solution of 77%, 81% and 83%, respectively. The relative positioning solutions did not experience similar incorrectly fixed ambiguity solutions between 5.5 and 6 hours as ALGO PPP, indicating improvements in the QC of the PPP engine is needed. Of interest, is the similarities of sensitivity of ambiguity validation of all three solutions between 15 to 24 hours in Figure 5.9, where the correctly resolved ambiguity solutions were also rejected. These trends suggest that improvements in atmospheric modelling and more realistic stochastic weights is needed to ensure performance similar to short baseline RTK.

Solution statistics, presented in Table 5.1 were generated by examining each epoch over the 24-hour period, including initial convergence. For all three solutions, ambiguity validation was able to detect initial convergence and identify to the user the float solution was more reliable. This can be seen in the improvement of the summary statistics of the ambiguity resolved solution in contrast to the ambiguity validated solution. Improvements were most notable in the standard deviation, where improvements of 4, 4.5 and 2.9 cm were reduced to 0.6, 0.2 and 0.3 cm for ALGO-BAIE, ALGO PPP and ALGO-NRC1, respectively.

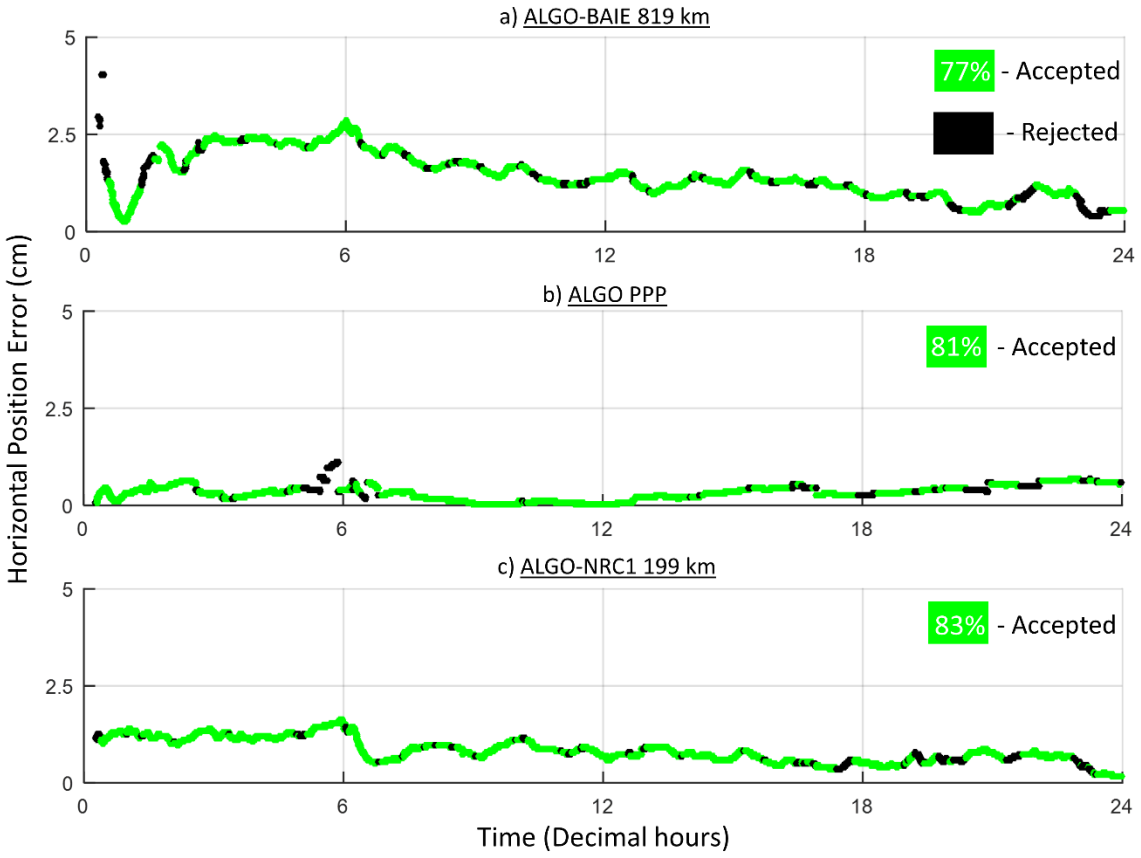

Figure 5.9: Comparison of the ambiguity validated solution between long single baseline relative positioning and PPP-AR. For relative positioning ALGO was coordinated with respect to BAIE with a baseline length of 819 km and with respect to NRC1 199 km. GNSS data from DOY 178 of 2016 was used.

Table 5.1: Summary statistics of ambiguity resolved, and ambiguity validated solutions for the station ALGO. Statistics compares the performance of ambiguity validation in relative positioning and PPP-AR. GNSS data from DOY 178 of 2016 was used. All units are in cm.

	Ambiguity resolved solution			Ambiguity validated solution		
	st dev	mean	rms error	st dev	mean	rms error
ALGO-BAIE	4.0	1.7	4.4	0.6	1.4	1.5
ALGO PPP	4.5	0.7	4.5	0.2	0.4	0.4
ALGO-NRC1	2.9	1.0	3.1	0.3	0.8	0.9

5.5 Conclusions

As have been shown in relative positioning and PPP-AR, ambiguity resolution is critical for enabling cm-level positioning. However, what if specifications where at the few dm-level, such as 10 cm and 20 cm horizontal – what role does ambiguity resolution play? To determine the role of ambiguity resolution in PPP, different accuracy specifications and integrity indicators were examined. These indicators include processing filter convergence, parameter estimation covariance, solution position error and ambiguity validation (residual testing).

Convergence: Similar performance was noted between the float and fixed solutions at the 10 and 20 cm horizontal thresholds. As expected, the role of ambiguity resolution for accuracy only become more apparent as the threshold were tightened from the few dm-level to few cm-level.

Position uncertainty: The covariance matrix of the estimated position is the main indicator of the solution accuracy, as a reference solution may not always be available. Within the first hour, the float position uncertainty was overly pessimistic suggesting the error was worse than the error between the estimated position and reference solution. As the solution converged, a strong positive correlation is illustrated such that the average position uncertainty realistically depicts the magnitude of the average error in the component as the solution converged further. While at hours 18-24 the average position uncertainty and errors are correlated, the uncertainty becomes optimistic. In contrast, the position uncertainty of the fixed solution was overly optimistic, indicating that the error was significantly better than the error between the estimated position and reference solution. After 2 hours of processing, the position uncertainty became more realistic in depicting the magnitude of the averaged error.

Ambiguity validation: Ambiguity validation is important, considering the increasing integrity demands on PPP. Of the different tests, the ratio test, was selected as it is one of the earliest and most popular tests to validate the integer ambiguity. Of the few sites examined, ambiguity validation proved to be a feasible indicator of when a steady state is attained as fixed solutions during initial convergence was rejected. Ambiguity validation in PPP-AR was also compared to single baseline relative positioning. Long baselines were selected to ensure atmospheric errors were not correlated. Sensitivity of ambiguity validation was noted amongst the relative positioning and PPP-AR after 15 hours of processing, where the correctly resolved ambiguity solutions were also rejected. These

trends suggest that improvements in atmospheric modelling and more realistic stochastic weights are needed to ensure RTK-like performance.

The role of ambiguity resolution relies primarily on what are the user specifications. If the user specifications are at the few cm-level, ambiguity resolution is an asset as it improves convergence and solution stability. Whereas, if the user's specification is at the few dm-level, ambiguity resolution offers limited improvement over the float solution. If the user has the resources to perform ambiguity resolution, even when the specifications are at the few dm-level, it should be utilized. To have a high probability of correctly resolving the integer ambiguities, the residual measurement error should be less than a quarter of a wavelength (Georgiadou and Kleusberg 1988; Banville 2014; Petovello et al. 2014). Having a successfully resolved and validated solution can indicate to user the solution strength and reliability.

CHAPTER 6 CONCLUSIONS AND RECOMMENDATIONS FOR FUTURE RESEARCH

Techniques such as single baseline RTK and network RTK have enabled centimetre-level position accuracy but require localized base stations. PPP eliminates the need for a localized infrastructure as it capitalises on a sparse global network to attain decimetre-level performance, but it typically requires approximately 30 minutes convergence. The length of time it takes to reach the optimal solution has been a major disadvantage for the broader use of the PPP technique. The existing convergence period was due primarily to the carrier-phase ambiguities being initialized by the pseudorange observables. Advancements over the past decade in PPP ambiguity resolution has enabled the resolution of GPS ambiguities to integers, but convergence time is still in the order of 10 to 15 minutes to attain centimetre-level accuracy.

6.1 Research Conclusions

The advent of PPP-AR provided the bridging gap between PPP and RTK as it enabled ambiguity resolution within a single localized GNSS receiver by capitalizing on correction terms provided from a network of GNSS receivers. An appropriate description of PPP-AR is, it is a state space relative positioning technique, as all error terms are mitigated relative to a global distribution of receivers. To enable PPP-AR the equipment delays present within the carrier-phase and pseudorange measurements need to be accounted for. Currently, there are three common approaches to PPP-AR with publicly available data: 1)

Decoupled Clock Model 2) Fractional Cycle Biases model 3) Integer Recovery Clock model.

In light of the different techniques to perform PPP-AR, the focus of this research was to leverage these different products to improve the reliability of the user solution. The research objectives focused on 1) The re-design of the traditional PPP-AR model to an uncombined representation, 2) Examination of the interoperability of the PPP-AR products, 3) Development a combination process of the PPP-AR products, and 4) Re-examination the role of PPP ambiguity resolution.

6.1.1 Uncombining the PPP representation

The standard practice in PPP use to be to linearly combine two pseudoranges and two carrier-phases to produce ionosphere-free linear pseudoranges and carrier-phase combinations, which eliminated the ionosphere delay (to the first order). Originally the ionosphere delay was considered a nuisance parameter within the positioning community. As such, the linear combination was favoured in contrast to the estimation of the slant ionosphere delay, this model is referred to as the conventional PPP model, which provides the user a float-only (ambiguity unresolved) solution. After which the PPP model evolved as research begun to focus on mitigating convergence time. To isolate the ambiguities and estimate them as integers, the PPP model was expanded to include the Melbourne-Wübbena linear combination and decomposition of the ionosphere ambiguity into a widelane and L1 ambiguity with an approximate wavelength of 86.2 and 10.7 cm, respectively.

With the resolution of the ambiguities, it was soon realized that capturing the integer natured ambiguities were not the only key required to unlocking instantaneous cm-level PPP convergence. As with relative positioning, it was a two-step process, requiring the elimination of the atmospheric terms which permitted fast convergence of the float ambiguity term and elimination of the hardware delays which enabled access to the integer ambiguity term. Researchers opted for the decomposition of the Melbourne-Wübbena linear combination into its constituents, the narrowlane code and the widelane phase. With a priori slant ionosphere information being introduced, instantaneous cm-level convergence was attainable.

With the introduction of multi-GNSS and multi-frequency PPP, some researchers were forming more linear combinations than the number of underlying measurements. At this juncture in PPP's evolution, it became more intuitive to adopt a more elegant way of processing GNSS data using the uncombined observations, where the slant ionosphere delays are estimated as unknown parameters which also permitted easier scalability with the growing number of frequencies and constellations. Processing of the uncombined observations within the least-squares solution meant the estimated state terms directly represent the physically observables atmospheric effects and receiver dependent equipment delays while providing equivalent performance of combined measurement models.

6.1.2 Interoperability of the PPP-AR products

Interoperability of the PPP-AR products is important, as it can increase the availability, continuity and reliability of the user solution while offering equivalent performance, in

regard to precision and accuracy. Interoperability of the products is possible because the PPP-AR mathematical model is equivalent. The different PPP-AR products contain the same information and would allow for a one-to-one transformation, thereby enabling interoperability of the PPP-AR products. The PPP user can transform the independently generated PPP-AR products to seamlessly integrate within their PPP user solution. The seamless integration of the transformed products allows the PPP user to have multiple solutions, which will increase the reliability of the solution for e.g., real-time processing. During real-time PPP processing, if there was an outage in the generation of the PPP-AR products, the user can instantly switch streams to a different provider.

To examine the interoperability of the different PPP-AR products GNSS data from 155 globally distributed stations were processed from DOY 178 to 184 of 2016 provided by the IGS. PPP-AR products were obtained from the Analysis Centres, Centre national d'études spatiales, Natural Resources Canada and School of Geodesy and Geomatics at Wuhan University. Equivalent performance was noted utilizing the different methods. Of the three PPP-AR solutions, FCB products had the highest accuracy. This is attributed to the products being generated using final IGS orbit and clock products, which are a combined product from multiple ACs. Where as DCM products are generated using rapid orbit and clocks and IRC products utilize final GRG orbit and clocks. To confirm this, FCBs generated using GRG orbit and clock products were also examined and comparable performance was observed between the FCBs and IRC products. While feasible, there were challenges when processing the different PPP-AR products. These challenges were due to the same conventions not being followed between the network and user solution for e.g.,

different satellite antenna convention. The differences in conventions are also important when combining multiple PPP-AR products. Within the user solution, it is expected that the IRC products will become the standard product to utilize as it requires minimal changes to pre-existing software architecture, because of the alignment of the pseudorange and carrier-clock. Whereas for real-time processing the DCM products is anticipated to become the standard approach as it makes no assumption about the temporal variability of the equipment delays thereby minimizing the possibility of incorrectly fixed ambiguities parameters. A summary of the different conventions is presented in the following section.

6.1.3 Combining the PPP-AR products

The satellite clock combinations routinely produced within the IGS currently disregard the fact that Analysis Centres (such as Centre national d'études spatiales, Natural Resources Canada and School of Geodesy and Geomatics at Wuhan University) provide products that enable PPP-AR. Users have been expected to choose either a robust combined solution or select an individual AC solution that provides products which allow PPP-AR.

For a satellite clock combination to provide an integer-aligned clock, it is important that the different modelling utilized by the ACs are properly considered in the adjustment process. Two different types of modelling were addressed, namely: 1) different satellite axis conventions, and 2) differences in modelling of yaw manoeuvres. By not accounting for these differences in the combination process, the underlying integer nature of the clock products were compromised.

For GPS Block IIR/IIR-M satellites, the IGS axis convention and manufacturer specifications are not equivalent. The difference between the two axis representations for Block IIR/IIR-M satellites is the orientation of the X and Y axes. To account for the differences in antenna conventions, a 0.5 cycle correction term must be applied to the clocks for ACs that adopted a different convention from the IGS.

Different ACs have adopted different standards for modelling the yaw manoeuvres during orbit noon and orbit midnight. To account for the inconsistent yaw modelling between ACs. It is critical that additional information such as yaw angle and phase/code satellite hardware delays are provided at the same intervals as the clocks. The yaw information would allow for a phase wind-up correction to be applied to each solution for improved consistency, while the phase/code satellite hardware delays accommodates different product representations, such as FCB. To this end, an updated RINEX clock format that includes the yaw information is suggested.

Two sets of combined clock products were generated: 1) combined satellite clock products that enable PPP-AR, and 2) IGS satellite clocks aligned to enable PPP-AR. The combined products were evaluated in the position domain. mm-level differences were noted, which was expected as the strength lies mainly in its reliability and stable median performance and the combined product is better than or equivalent to any single AC's product in the combination process. Aligning the actual IGS satellite clock products yielded the best PPP-AR results, for both static and kinematic solutions, where mm-level improvements were also noted.

6.1.4 Re-examining the role of ambiguity resolution

As have been shown in relative positioning and PPP-AR, ambiguity resolution is critical for enabling cm-level positioning. However, what if specifications where at the few dm-level, such as 10 cm and 20 cm horizontal – what role does ambiguity resolution play? To determine the role of ambiguity resolution in PPP, different accuracy specifications and integrity indicators were examined. These indicators include processing filter convergence, parameter estimation covariance, solution position error and ambiguity validation (residual testing). The role of ambiguity resolution depends on what are the user specifications. If the user specifications are at the few cm-level, ambiguity resolution is a requirement as it improves convergence and solution stability. Whereas, if the user's specification is at the few dm-level, ambiguity resolution offers limited improvement over the float solution. If the user has the resources to perform ambiguity resolution, even when the specifications are at the few dm-level, it should be utilized. To have a high probability of correctly resolving the integer ambiguities, the residual measurement error should be less than a quarter of a wavelength. Having a successfully resolved and validated solution can indicate to user the solution strength and reliability.

6.2 Research recommendations for the near future

The PPP GNSS measurement processing approach was originally designed to greatly reduce computation burden in large geodetic networks of receivers by removing the need for network baseline processing. The technique was favoured for applications in remote areas or regions with little terrestrial infrastructure, including the absence of GNSS

reference stations. Given PPP's characteristic use of a single receiver for precise positioning has allowed processing technique to make inroads precise positioning and navigation is required. To allow PPP to become the de-facto standard for high-precision GNSS data processing, three main areas require further investigation: real time PPP-AR with (ultra) low GNSS receiver and antenna, improving the stochastic modelling and multiple low-cost sensor integration with PPP GNSS measurement processing.

6.2.1 Real time PPP-AR with low GNSS receiver and antenna

Traditionally, low-cost GNSS positioning was equated to single-frequency positioning but with a strong demand for low-cost precise positioning existing within the mass market has led to a redefinition of what low-cost positioning means. Ultra-low-cost positioning became possible with the announcement of multiple-frequency and multi-constellation tracking chips from manufactures such as Broadcom Corporation, Qualcomm Inc., u-blox AG, Unicore Communications Inc., SkyTraq Technology, Inc. and STMicroelectronics. Integration of low-cost chips with real-time SSR products will further allow accessibility of accuracy to the mass market. Mass market precise positioning will be expected to demonstrate convergence and accuracy performance rivalling that of the most demanding current precise positioning applications. With advancement in low-cost hardware for measurement tracking, creates inroads into novel areas of research with PPP. Lower cost hardware will result in increased measurement noise and multipath due to reduction in hardware cost, architecture and size of the receiver and antenna. Increased measurement noise and multipath coupled with less precise real-time SSR products (in contrast to post-

processed) would require further analysis of the performance and reliability of PPP-AR. Increased residual errors would make it more challenging to fix raw ambiguity terms and may require fixing linear combinations of the ambiguity terms.

6.2.2 Improving the stochastic model

In order to obtain optimal estimates from a least-square solution, both a mathematical model, also called a functional model, and a stochastic model should be correctly defined. The functional model describes the relationship between measurements and unknown estimates. On the other hand, the stochastic model represents the statistical characteristics of the measurement that is mainly provided by the covariance matrix for the measurements. Stochastic modelling has typically taken the back burner in regards research foci within the PPP GNSS measurement scope. While understandable, as eliminating PPP convergence has been the elusive goal; advancements in ambiguity resolution and utilizing a priori ionospheric information has led to elimination of the Achilles' Heel of PPP when utilizing geodetic quality data. Such advancements has resulted in the limitations of the current stochastic schemes adopted with most PPP GNSS measurement engine of be more visible, especially in regard to ambiguity validation. In practice, the stochastic models of GPS measurements are mainly based on considerable simplifications. In current stochastic models it is usually assumed that all pseudorange measurements and all carrier-phase measurements have the same variance and they are statistically independent. The common practice of if the raw GNSS measurements are statistically independent in space and time, and have the same accuracy, is undoubtedly unrealistic. The result of over simplification

of the stochastic model is presented in Section 5.4.2, whereby the precision associated with position estimates obtained from GNSS processing software is unrealistic. This is due to an incomplete definition of the stochastic model which has neglected heteroscedastic, space- and time-correlated error structure of the GPS measurements. The measurements obtained from different satellites cannot have the same accuracy due to varying noise levels. Also, the raw measurements are spatially correlated due to similar observing conditions for these measurements. In addition, the time correlations may exist in the measurements because the systematic errors such as multipath, as well as satellite orbit and clock errors change slowly over time. Also, available uncertainties which can be utilized to populate the covariances are typically neglected. For example, included within satellite products are the uncertainties associated with the orbits, clocks and AR products and within the receiver the signal-to-nose ratio is available. Traditionally, an unrealistic position uncertainty has been of lower priority due to the applications such as control surveying where accuracy and precision took precedence. As PPP GNSS measurement processing techniques are being in adopted in mass market applications such as autonomous navigation, the importance of solution reliability and integrity are becoming even more critical.

6.2.3 Low-cost, multi-sensor integration

Complimentary to the growth of low-cost GNSS receivers described in Section 6.2.1 and the importance of improving the stochastic model described in Section 6.2.2 there is also the necessity to include more low-cost, multi-sensor integration within the PPP

augmentation. Optimized navigation algorithms and efficient user processing engines will be a priority as the capabilities of low-cost equipment continue to increase and low-cost integrated sensor solutions are required for mass-market applications. With the growth in the number of constellations and frequencies available to the user, has led to improvements in the user solution, especially in challenging environments such as urban canyons, but what about GNSS denied environments?

GNSS-INS integration refers to the use of GNSS satellite signals in the correction of a solution from an Inertial Navigation System (INS) or vice versa. The two systems are reliant on each other, compensating for the limitations of the other. The topic of GNSS-INS integration is not novel as it has been studied extensively in literature over the past decades, but, low-cost multi-sensor integration requires additional research if it is to be utilized within the mass market as it requires a better understanding of the sensitivity, reliability and integrity in challenging environments is needed. Low-cost, multi-sensor includes accelerometers, gyroscopes, pressure sensors, RFID, MEMS atomic clocks and controller area network (which is a serial bus system used in vehicles). Coupling of multiple sensors such as a MEMS atomic clocks can lead to improved performance especially in the up component of a GNSS only PPP solution. Improved performance of the GNSS solution with a MEMS atomic clocks can be used to constrain the low-cost IMUs especially in applications with lower dynamics such as pedestrian applications and a subset of unmanned aerial vehicles.

6.2.4 A priori atmospheric corrections

The key component to enable (N)RTK-like performance of centimetre-level accuracy within a few minutes is a priori atmospheric corrections in the form of tropospheric and ionospheric information together with PPP-AR. The core challenge in atmospheric modelling has always been the localized variability of the ionosphere and troposphere. At low latitudes scintillations of GNSS signals are associated with the equatorial anomaly are frequent events whereas at mid-latitudes they are rare and related typically to geomagnetic storms. At high latitudes the ionosphere is influenced by magnetospheric processes. Whereas with the troposphere, the challenge has always been the reliable modelling of the wet component as the troposphere contains 99% of water vapor in the atmosphere and the water content varies significantly based on localized geographic conditions. Such high atmospheric variability has always required dense terrestrial infrastructure to enable reliable (N)RTK-like performance. An important question that affects the adoption rate of PPP is how much terrestrial infrastructure would be required in terms of reference stations spacing to deal with spatial and temporal decorrelation of errors? Also, what is the required accuracy for the a priori tropospheric and ionospheric models to have (N)RTK-like performance with PPP in terms of initial solution convergence and solution accuracy.

As industry, academia and government transition towards SSR dissemination of products, additional analysis is the required to determine the most efficient atmospheric models in terms of bandwidth and reliability to transmit such information. An aspect that has not been sufficiently investigated within literature if it would be possible to produce a wide-area

PPP solution that performs like (N)RTK or will PPP users have to settle for a hybrid solution?

REFERENCES

Abbot R, Counselman C (1987) Demonstration of GPS orbit determination enhancement by resolution of carrier phase ambiguity. Eos Trans AGU 68:1238

Aggrey JE (2015) Multi-GNSS precise point positioning software architecture and analysis of GLONASS pseudorange biases. MSc Thesis, York University

Anderson JM, Mikhail EM, Anderson J (1998) Surveying: Theory and practice. WCB/McGraw-Hill Boston

Banville S (2014) Improved convergence for GNSS Precise Point Positioning. PhD Thesis, University of New Brunswick

Banville S (2016a) Unified PPP-AR Processing. In: Blackdot GNSS. https://www.blackdotgnss.com/2016/11/06/unified-ppp-ar-processing/. Accessed 20 Nov 2016

Banville S (2016b) GLONASS ionosphere-free ambiguity resolution for precise point positioning. Journal of Geodesy. doi: 10.1007/s00190-016-0888-7

Banville S, Collins P, Lahaye F (2013) GLONASS ambiguity resolution of mixed receiver types without external calibration. GPS Solutions 17:275–282. doi: 10.1007/s10291-013-0319-7

Banville S, Collins P, Zhang W, Langley RB (2014) Global and regional ionospheric corrections for faster PPP convergence. Navigation 61:115–124

Bar-Sever YE (1996) A new model for GPS yaw attitude. Journal of Geodesy 70:714–723

Bertiger W, Desai SD, Haines B, et al (2010) Single receiver phase ambiguity resolution with GPS data. Journal of Geodesy 84:327–337. doi: 10.1007/s00190-010-0371-9

Beutler G, Kouba J, Springer T (1995) Combining the orbits of the IGS Analysis Centers. Bulletin Geodesique 69:200–222

Beutler G, Rothacher M, Schaer S, et al (1999) The International GPS Service (IGS): an interdisciplinary service in support of earth sciences. Advances in Space Research 23:631–653

Bisnath S, Aggrey J, Seepersad G, Gill M (2018) Innovation: Examining precise point positioning now and in the future. GPS World. March.

Bisnath S, Collins P (2012) Recent developments in precise point positioning. Geomatica 66:103–111

Bisnath S, Gao Y (2009) Current state of precise point positioning and future prospects and limitations. In: Observing our changing earth. Springer, pp 615–623

Blewitt G (1989) Carrier phase ambiguity resolution for the Global Positioning System applied to geodetic baselines up to 2000 km. Journal of Geophysical Research: Solid Earth 94:10187–10203

Bock Y, Abbot RI, Counselman CC, et al (1985) Establishment of three-dimensional geodetic control by interferometry with the Global Positioning System. Journal of Geophysical Research: Solid Earth 90:7689–7703

Bock Y, Gourevitch SA, Counselman III CC, et al (1986) Interferometric analysis of GPS phase observations. Manuscripta geodaetica 11:282–288

Bock Y, Nikolaidis RM, Jonge PJ, Bevis M (2000) Instantaneous geodetic positioning at medium distances with the Global Positioning System. Journal of Geophysical Research: Solid Earth (1978–2012) 105:28223–28253

Britting KR (1971) Inertial Navigation Systems Analysis. Artech House

Cai C, Gao Y (2007) Precise point positioning using combined GPS and GLONASS observations. Journal of Global Positioning System 6:13–22

Cai C, Gao Y (2013) Modeling and assessment of combined GPS/GLONASS precise point positioning. GPS Solutions 17:223–236. doi: 10.1007/s10291-012-0273-9

Caissy M, Agrotis L, Weber G, et al (2012) The International GNSS Real-Time Service. In: GPS World. http://gpsworld.com/gnss-systemaugmentation-assistanceinnovation-coming-soon-13044/. Accessed 8 Aug 2016

Center for Orbit Determination in Europe (2016) Differential Code Biases (DCB). In: Astronomical Institute. http://www.aiub.unibe.ch/research/code___analysis_center/differential_code_biases_dcb/index_eng.html. Accessed 3 Feb 2016

Chang XW, Yang X, Zhou T (2005) MLAMBDA: a modified LAMBDA method for integer least-squares estimation. Journal of Geodesy 79:552–565

Chen L, Song W, Yi W, et al (2016) Research on a method of real-time combination of precise GPS clock corrections. GPS Solutions. doi: 10.1007/s10291-016-0515-3

Choy S, Zhang S, Lahaye F, Héroux P (2013) A comparison between GPS-only and combined GPS+GLONASS Precise Point Positioning. Journal of Spatial Science 58:169–190. doi: 10.1080/14498596.2013.808164

Chuang S, Wenting Y, Weiwei S, et al (2013) GLONASS pseudorange inter-channel biases and their effects on combined GPS/GLONASS precise point positioning. GPS Solutions 17:439–451. doi: 10.1007/s10291-013-0332-x

CNES (2015) Le site du Centre national d'études spatiales. https://cnes.fr/

Cocard M, Bourgon S, Kamali O, Collins P (2008) A systematic investigation of optimal carrier-phase combinations for modernized triple-frequency GPS. Journal of Geodesy 82:555–564

Collins JP (1999a) Assessment and development of a tropospheric delay model for aircraft users of the global positioning system. MSc Thesis, University of New Brunswick

Collins P (2008) Isolating and estimating undifferenced GPS integer ambiguities. In: Proc. ION NTM. pp 720–732

Collins P (1999b) An overview of GPS interfrequency carrier phase combinations. Geodesy and Geomatics Engineering Report, University of New Brunswick

Collins P, Bisnath S (2011) Issues in ambiguity resolution for Precise Point Positioning. In: Proceedings of the 24th International Technical Meeting of the Satellite Division of The Institute of Navigation (ION GNSS 2011). pp 679–687

Collins P, Bisnath S, Lahaye F, Héroux P (2010) Undifferenced GPS ambiguity resolution using the decoupled clock model and ambiguity datum fixing. Navigation 57:123–135

Collins P, Lahaye F, Bisnath S (2012) External ionospheric constraints for improved PPP-AR initialisation and a generalised local augmentation concept. In: Proceedings of the 25th International Technical Meeting of the Satellite Division of The Institute of Navigation (ION GNSS 2012). pp 3055–3065

Collins P, Lahaye F, Heroux P, Bisnath S (2008) Precise point positioning with ambiguity resolution using the decoupled clock model. In: Proceedings of the 21st international technical meeting of the satellite division of the Institute of Navigation (ION GNSS 2008). pp 1315–1322

CSNO TARC (2018) System basic information. In: China Satellite Navigation System Management Office Test Assessment Research Center : Test and Assessment Research Center of China Satellite Navigation Office. http://www.csno-tarc.cn/system/basicinfo. Accessed 12 Jun 2018

De Bakker PF (2016) On User Algorithms for GNSS Precise Point Positioning. TU Delft, Delft University of Technology

De Jonge P, Tiberius C (1996) The LAMBDA method for integer ambiguity estimation: implementation aspects. Publications of the Delft Computing Centre, LGR-Series 12:1–47

Defraigne P, Baire Q (2011) Combining GPS and GLONASS for time and frequency transfer. Advances in Space Research 47:265–275. doi: 10.1016/j.asr.2010.07.003

Dilssner F (2010) GPS IIF-1 satellite antenna phase center and attitude modeling. Inside GNSS 5:59–64

Dilssner F, Springer T, Gienger G, Dow J (2011) The GLONASS-M satellite yaw-attitude model. Advances in Space Research 47:160–171. doi: 10.1016/j.asr.2010.09.007

Donahue B, Wentzel J, Berg R (2013) Guidelines for RTK/RTN GNSS surveying in Canada. Version 1.1. Canada. Natural Resources Canada. Geological Survey of Canada.

Dong D-N, Bock Y (1989) Global Positioning System network analysis with phase ambiguity resolution applied to crustal deformation studies in California. Journal of Geophysical Research: Solid Earth 94:3949–3966

Dow JM, Neilan RE, Rizos C (2009) The international GNSS service in a changing landscape of global navigation satellite systems. Journal of geodesy 83:191–198

Euler H-J, Schaffrin B (1991) On a measure for the discernibility between different ambiguity solutions in the static-kinematic GPS-mode. In: Kinematic Systems in Geodesy, Surveying, and Remote Sensing. Springer, pp 285–295

European GNSS Agency (2015) Report on the Performance and Level of Integrity for Safety and Liability Critical Multi-Applications. https://www.gsa.europa.eu/sites/default/files/calls_for_proposals/Annex%202.pdf

Feng S, Ochieng W, Samson J, et al (2012) Integrity Monitoring for Carrier Phase Ambiguities. Journal of Navigation 65:41–58. doi: 10.1017/S037346331100052X

Feng Y (2008) GNSS three carrier ambiguity resolution using ionosphere-reduced virtual signals. Journal of Geodesy 82:847–862

Ferland R, Kouba J, Hutchison D (2000) Analysis methodology and recent results of the IGS network combination. Earth, planets and space 52:953–957

Forssell B, Martin-Neira M, Harris R (1997) Carrier phase ambiguity resolution in GNSS-2. In: Proceedings of the 10th International Technical Meeting of the Satellite Division of The Institute of Navigation (ION GPS 1997). pp 1727–1736

Gabor MJ, Nerem RS (2002) Satellite–Satellite Single-Difference Phase Bias Calibration As Applied to Ambiguity Resolution. Navigation 49:223–242

Ge M, Douša J, Li X, et al (2012) A Novel Real-time Precise Positioning Service System: Global Precise Point Positioning With Regional Augmentation. Journal of Global Positioning Systems 11:2–10. doi: 10.5081/jgps.11.1.2

Ge M, Gendt G, Rothacher M, et al (2008) Resolution of GPS carrier-phase ambiguities in Precise Point Positioning (PPP) with daily observations. Journal of Geodesy 82:389–399. doi: 10.1007/s00190-007-0187-4

Geng J (2010) Rapid integer ambiguity resolution in GPS precise point positioning. PhD Thesis, University of Nottingham

Geng J, Bock Y (2013) Triple-frequency GPS precise point positioning with rapid ambiguity resolution. J Geod 87:449–460. doi: 10.1007/s00190-013-0619-2

Geng J, Bock Y (2016) GLONASS fractional-cycle bias estimation across inhomogeneous receivers for PPP ambiguity resolution. Journal of Geodesy 90:379–396. doi: 10.1007/s00190-015-0879-0

Geng J, Bock Y, Melgar D, et al (2013) A new seismogeodetic approach applied to GPS and accelerometer observations of the 2012 Brawley seismic swarm: Implications for earthquake early warning. Geochemistry, Geophysics, Geosystems 14:2124–2142. doi: 10.1002/ggge.20144

Geng J, Meng X, Dodson AH, Teferle FN (2010a) Integer ambiguity resolution in precise point positioning: method comparison. Journal of Geodesy 84:569–581. doi: 10.1007/s00190-010-0399-x

Geng J, Meng X, Teferle FN, Dodson AH (2010b) Performance of precise point positioning with ambiguity resolution for 1-to 4-hour observation periods. Survey Review 42:155–165

Geng J, Shi C (2017) Rapid initialization of real-time PPP by resolving undifferenced GPS and GLONASS ambiguities simultaneously. Journal of Geodesy 91:361–374. doi: 10.1007/s00190-016-0969-7

Geng J, Shi C, Ge M, et al (2012) Improving the estimation of fractional-cycle biases for ambiguity resolution in precise point positioning. Journal of Geodesy 86:579–589

Georgiadou Y, Kleusberg A (1988) On carrier signal multipath effects in relative GPS positioning. Manuscripta Geodaetica 13:172–179

Goad CC (1985) Precise relative position determination using Global Positioning System carrier phase measurements in a nondifference mode. In: First Int. Symp. on Positioning with the Global Positioning System, Rockville. pp 347–356

Grimes J (2007) Global Positioning System Precise Positioning Service Performance Standard. Department of Defense, United States of America

Han S (1997) Quality-control issues relating to instantaneous ambiguity resolution for real-time GPS kinematic positioning. Journal of Geodesy 71:351–361

Han S, Rizos C (1999) The impact of two additional civilian GPS frequencies on ambiguity resolution strategies. In: 55th National Meeting US Institute of Navigation," Navigational Technology for the 21st Century", Cambridge, Massachusetts. pp 28–30

Hatch R (2006) A new three-frequency, geometry-free technique for ambiguity resolution. In: Proceedings of ION GNSS. pp 26–29

Hauschild A, Montenbruck O (2014) A study on the dependency of GNSS pseudorange biases on correlator spacing. GPS Solutions. doi: 10.1007/s10291-014-0426-0

Henderson HV, Searle SR (1981) The vec-permutation matrix, the vec operator and Kronecker products: A review. Linear and multilinear algebra 9:271–288

Henkel P, Gomez V (2013) Partial ambiguity fixing for multi-frequency ionospheric delay estimation. Google Patents

Henkel P, Günther C (2010) Reliable integer ambiguity resolution with multi-frequency code carrier linear combinations. Journal of Global Positioning Systems 9:90–103

Héroux P, Kouba J (1995) GPS precise point positioning with a difference. Natural Resources Canada, Geomatics Canada, Geodetic Survey Division

Hofmann-Wellenhof B, Lichtenegger H, Collins J (1997) Global positioning system: theory and practice, 4., rev. ed. Springer, Wien

Hofmann-Wellenhof B, Lichtenegger H, Wasle E (2007) GNSS–global navigation satellite systems: GPS, GLONASS, Galileo, and more. Springer Science & Business Media

IGS (2013) IGS Quality of Service Fact Sheet. In: International GNSS Service. https://kb.igs.org/hc/en-us/articles/201208216-IGS-Quality-of-Service-Fact-Sheet

IGS (2018a) MGEX Product Analysis. In: International GNSS Service. http://mgex.igs.org/analysis/index.php

IGS (2007) IGS Frequently Asked Questions (FAQ). In: International GNSS Service. https://kb.igs.org/hc/en-us/articles/201142366-IGS-FAQ-May-2007

IGS (2018b) About. In: International GNSS Service. http://www.igs.org/about/analysis-centers

IMO (2001) Revised Maritime Policy and Requirements for future GNSS. In: Resolution A.915(22), London, United Kingdom

Jokinen A, Feng S, Schuster W, et al (2013a) Integrity monitoring of fixed ambiguity Precise Point Positioning (PPP) solutions. Geo-spatial Information Science 16:141–148. doi: 10.1080/10095020.2013.817111

Jokinen A, Feng S, Schuster W, et al (2013b) GLONASS Aided GPS Ambiguity Fixed Precise Point Positioning. Journal of Navigation 66:399–416. doi: 10.1017/S0373463313000052

JPL (2016). In: JPL GPS Products. ftp://sideshow.jpl.nasa.gov/pub/JPL_GPS_Products/Final/2016/. Accessed 6 Sep 2016

Jung J, Enge P, Pervan B (2000) Optimization of cascade integer resolution with three civil GPS frequencies. In: Proceedings of the 13th International Technical Meeting of the Satellite Division of The Institute of Navigation (ION GPS 2000). pp 19–20

Kamali O (2017) Enhanced Performance for GPS-PPP by Resolving Bias-free Ambiguities. PhD Thesis, Université Laval

Kaplan ED, Hegarty C (eds) (2006) Understanding GPS: principles and applications, 2nd ed. Artech House, Boston

Kee C, Parkinson BW, Axelrad P (1991) Wide area differential GPS. Navigation 38:123–145

Kouba J (2009) A simplified yaw-attitude model for eclipsing GPS satellites. GPS Solutions 13:1–12. doi: 10.1007/s10291-008-0092-1

Kouba J, Héroux P (2001) Precise point positioning using IGS orbit and clock products. GPS solutions 5:12–28

Kouba J, Springer T (2001) New IGS station and satellite clock combination. GPS Solutions 4:31–36

Kuang D, Desai S, Sibois A (2016) Observed features of GPS Block IIF satellite yaw maneuvers and corresponding modeling. GPS Solutions. doi: 10.1007/s10291-016-0562-9

Lannes A, Prieur J-L (2013) Calibration of the clock-phase biases of GNSS networks: the closure-ambiguity approach. Journal of Geodesy 87:709–731. doi: 10.1007/s00190-013-0641-4

Laurichesse D (2014) Phase biases for ambiguity resolution: from an undifferenced to an uncombined formulation. http://ppp-wizard.net/Articles/WhitePaperL5.pdf. Accessed 1 Jun 2015

Laurichesse D, Blot A (2016) Fast PPP Convergence Using Multi-Constellation and Triple-Frequency Ambiguity Resolution. In: Proceedings of the 29th International Technical Meeting of The Satellite Division of the Institute of Navigation (ION GNSS+ 2016). pp 2082–2088

Laurichesse D, Mercier F (2007) Integer ambiguity resolution on undifferenced GPS phase measurements and its application to PPP. pp 839–848

Laurichesse D, Mercier F, Berthias J-P, et al (2009) Integer ambiguity resolution on undifferenced GPS phase measurements and its application to PPP and satellite precise orbit determination. Navigation 56:135–149

Leandro RF (2009) Precise Point Positioning With GPS A New Approach For Positioning, Atmospheric Studies, And Signal. PhD Thesis, University of New Brunswick

Leick A (1995) GPS satellite surveying, 2nd ed. Wiley, New York

Leveson I (2006) Benefits of the new GPS civil signal. The L2C Study. Inside GNSS 1:42–47

Li B, Feng Y, Shen Y (2010) Three carrier ambiguity resolution: distance-independent performance demonstrated using semi-generated triple frequency GPS signals. GPS solutions 14:177–184

Li J, Yang Y, Xu J, et al (2012) Ionosphere-free combinations for triple-frequency GNSS with application in rapid ambiguity resolution over medium-long baselines. In: China Satellite Navigation Conference (CSNC) 2012 Proceedings. Springer, pp 173–187

Li P, Zhang X (2014) Integrating GPS and GLONASS to accelerate convergence and initialization times of precise point positioning. GPS Solutions 18:461–471. doi: 10.1007/s10291-013-0345-5

Li P, Zhang X, Ren X, et al (2015) Generating GPS satellite fractional cycle bias for ambiguity-fixed precise point positioning. GPS Solutions. doi: 10.1007/s10291-015-0483-z

Li X (2012) Improving real-time PPP ambiguity resolution with ionospheric characteristic consideration. Proc of ION GNSS-12, Institute of Navigation, Nashville, Tennessee, September 17–21

Li X, Li X, Yuan Y, et al (2017) Multi-GNSS phase delay estimation and PPP ambiguity resolution: GPS, BDS, GLONASS, Galileo. Journal of Geodesy. doi: 10.1007/s00190-017-1081-3

Liu T, Yuan Y, Zhang B, et al (2017) Multi-GNSS precise point positioning (MGPPP) using raw observations. Journal of Geodesy 91:253–268. doi: 10.1007/s00190-016-0960-3

Lou Y, Zheng F, Gu S, et al (2016) Multi-GNSS precise point positioning with raw single-frequency and dual-frequency measurement models. GPS Solutions 20:849–862. doi: 10.1007/s10291-015-0495-8

Mervart L, Lukes Z, Rocken C, Iwabuchi T (2008) Precise Point Positioning with ambiguity resolution in real-time. In: Proceedings of ION GNSS. pp 397–405

Mervart L, Weber G (2011) Real-time combination of GNSS orbit and clock correction streams using a Kalman filter approach. In: Proceedings of the 24th International Technical Meeting of The Satellite Division of the Institute of Navigation (ION GNSS 2011). pp 707–711

Mohammed J, Moore T, Hill C, et al (2016) An assessment of static precise point positioning using GPS only, GLONASS only, and GPS plus GLONASS. Measurement 88:121–130. doi: 10.1016/j.measurement.2016.03.048

Montenbruck O, Schmid R, Mercier F, et al (2015) GNSS satellite geometry and attitude models. Advances in Space Research 56:1015–1029. doi: 10.1016/j.asr.2015.06.019

NRCan (2015) Natural Resources Canada. https://www.nrcan.gc.ca. Accessed 19 Jun 2015

Ober P (1999) Towards High Integrity Positioning. In: ION GPS. pp 2113–2120

Ochieng WY, Sauer K, Walsh D, et al (2003) GPS integrity and potential impact on aviation safety. The journal of navigation 56:51–65

Odijk D (2002) Fast precise GPS positioning in the presence of ionospheric delays. PhD Thesis, Delft University of Technology

Parkinson BW, Axelrad P (1988) Autonomous GPS integrity monitoring using the pseudorange residual. Navigation 35:255–274

Petovello MG, Feng S, Ochieng W (2014) How do you trust centimeter level accuracy positioning? In: Inside GNSS. http://www.insidegnss.com/node/4201

Pham H (2006) System Reliability Concepts. In: System Software Reliability. Springer, pp 9–75

Porretta M, Banos DJ, Crisci M, et al (2016) GNSS evolution for maritime an incremental approach. In: Inside GNSS. http://insidegnss.com/auto/mayjune16-WP.pdf

Pullen S (2011) Augmented GNSS: Fundamentals and Keys to Integrity and Continuity. In: Tutorial Presentation, ION GNSS 2011, Portland, Oregon land, Oregon

Renfro BA, Stein M, Boeker N, Terry A (2018) An Analysis of Global Positioning System (GPS) Standard Positioning Service (SPS) Performance for 2017. In: GPS: The Global Positioning System. https://www.gps.gov/systems/gps/performance/2017-GPS-SPS-performance-analysis.pdf

Richert T, El-Sheimy N (2007) Optimal linear combinations of triple frequency carrier phase data from future global navigation satellite systems. GPS solutions 11:11–19

RTCA DO-181 (1983) Minimum Operational Performance Standards for Air Traffic Control Radar Beacon System/mode Select (ATCRBS/modes) Airborne Equipment. Radio Technical Commission for Aeronautics

Schaer S (2016) SINEX BIAS—Solution (Software/technique) INdependent EXchange Format for GNSS BIASes Version 1.00. Swisstopo/AIUB

Schaffrin B, Bock Y (1988) A unified scheme for processing GPS dual-band phase observations. Journal of geodesy 62:142–160

Scherneck H (2013) Ocean Tide Loading Provider. http://froste.oso.chalmers.se/loading//index.html. Accessed 2 Jan 2013

Schmitz M (2012) RTCM State Space Representation Messages, Status and Plans

Schönemann E, Becker M, Springer T (2011) A new approach for GNSS analysis in a multi-GNSS and multi-signal environment. Journal of Geodetic Science 1:204–214

Schumann S (2014) Why we're mapping down to 20 cm accuracy on roads. In: HERE 360. http://360.here.com/2014/02/12/why-were-mapping-down-to-20cm-accuracy-on-roads/

Seepersad G (2012) Reduction of initial convergence period in GPS PPP data processing. MSc Thesis, York University

Seepersad G, Aggrey J, Bisnath S (2017) Do We Need Ambiguity Resolution in Multi-GNSS PPP for Accuracy or Integrity? In: Proceedings of the 30th International Technical Meeting of The Satellite Division of the Institute of Navigation (ION GNSS+ 2017). pp 2204–2218

Seepersad G, Banville S, Collins P, et al (2016) Integer satellite clock combination for Precise Point Positioning with ambiguity resolution. In: Proceedings of the 29th International Technical Meeting of The Satellite Division of the Institute of Navigation (ION GNSS+ 2016), Portland, OR. pp 2058–2068

Seepersad G, Bisnath S (2013) Integrity Monitoring in Precise Point Positioning. In: Proceedings of the 26th International Technical Meeting of The Satellite Division of the Institute of Navigation (ION GNSS 2013). pp 1164–1175

Seepersad G, Bisnath S (2014a) Challenges in Assessing PPP Performance. Journal of Applied Geodesy 8:205–222

Seepersad G, Bisnath S (2017) An assessment of the interoperability of PPP-AR network products. The Journal of Global Positioning Systems 15:4. doi: 10.1186/s41445-017-0009-9

Seepersad G, Bisnath S (2015) Examining the Interoperability of PPP-AR Products. In: Proceedings of the 28th International Technical Meeting of The Satellite Division of the Institute of Navigation (ION GNSS+ 2015),Tampa, Florida. pp 2845–2857

Seepersad G, Bisnath S (2014b) Reduction of PPP convergence period through pseudorange multipath and noise mitigation. GPS Solutions 19:369–379. doi: 10.1007/s10291-014-0395-3

Shi J (2012) Precise point positioning integer ambiguity resolution with decoupled clocks. PhD Thesis, University of Calgary

Shi J, Gao Y (2014) A Troposphere Constraint Method To Improve PPP Ambiguity-Resolved Height Solution. Journal of Navigation 67:249–262. doi: 10.1017/S0373463313000647

Springer T, Beutler G (1993) Towards an official IGS orbit by combining the results of all IGS Processing Centers. In: Proceedings of the 1993 IGS Workshop, held March. pp 24–26

Sturza MA (1988) Navigation system integrity monitoring using redundant measurements. Navigation 35:483–501

Takasu T, Yasuda A (2009) Development of the low-cost RTK-GPS receiver with an open source program package RTKLIB. In: international symposium on GPS/GNSS. International Convention Centre Jeju, Korea, pp 4–6

Teunissen P, Joosten P, Tiberius C (2002) A comparison of TCAR, CIR and LAMBDA GNSS ambiguity resolution. In: ION GPS. pp 2799–2808

Teunissen PJ (1998) Success probability of integer GPS ambiguity rounding and bootstrapping. Journal of Geodesy 72:606–612

Teunissen PJ, Kleusberg A (2012) GPS for Geodesy. Springer Science & Business Media

Teunissen PJ, Odijk D, Zhang B (2010) PPP-RTK: Results of CORS network-based PPP with integer ambiguity resolution. Journal of Aeronautics, Astronautics and Aviation, Series A 42:223–230

Teunissen PJG (2005) Integer aperture bootstrapping: a new GNSS ambiguity estimator with controllable fail-rate. Journal of Geodesy 79:389–397. doi: 10.1007/s00190-005-0481-y

Teunissen PJG, Khodabandeh A (2015) Review and principles of PPP-RTK methods. Journal of Geodesy 89:217–240. doi: 10.1007/s00190-014-0771-3

Trimble (2018) Transforming the way the world works. In: Transforming the way the world works. http://www.trimble.com/positioning-services/centerpoint-vrs.aspx. Accessed 4 Feb 2018

Tu R, Ge M, Zhang H, Huang G (2013) The realization and convergence analysis of combined PPP based on raw observation. Advances in Space Research 52:211–221. doi: 10.1016/j.asr.2013.03.005

U.S. Coast Guard Navigation Center (2008) Federal Radionavigation Plan. In: Navigation Center.
https://www.navcen.uscg.gov/pdf/2008_Federal_Radionavigation_Plan.pdf

US DoD (2001) Global positioning system standard positioning service performance standard. Assistant secretary of defense for command, control, communications, and intelligence

Van Diggelen F (2009) A-GPS: Assisted GPS, GNSS, and SBAS. Artech House

Wang J, Feng Y (2009) Integrity determination of RTK solutions in precision farming applications. In: Proceedings of the Surveying and Spatial Sciences Institute Biennial International Conference 2009. Surveying and Spatial Sciences Institute, pp 1277–1291

Wang J, Stewart MP, Tsakiri M (1998) A discrimination test procedure for ambiguity resolution on-the-fly. Journal of Geodesy 72:644–653

Wang K, Rothacher M (2013) Ambiguity resolution for triple-frequency geometry-free and ionosphere-free combination tested with real data. Journal of Geodesy 87:539–553. doi: 10.1007/s00190-013-0630-7

Wang Q, Chen Y, Zhao J (2012) Analysis and Modeling of PPP Residuals from GPS and GLONASS. In: Sun J, Liu J, Yang Y, Fan S (eds) China Satellite Navigation Conference (CSNC) 2012 Proceedings. Springer Berlin Heidelberg, Berlin, Heidelberg, pp 301–308

Wanninger L (2012) Carrier-phase inter-frequency biases of GLONASS receivers. Journal of Geodesy 86:139–148. doi: 10.1007/s00190-011-0502-y

Weber G, Mervart L, Agrotis L, Stürze A (2011) Real-time Combination of GNSS Orbit and Clock Correctors for Precise Point Positioning. In: IUGG General Assembly, June 2011, Melbourne, Australia

Weber G, Mervart L, Lukes Z, et al (2007) Real-time clock and orbit corrections for improved point positioning via NTRIP. In: Proceedings of ION GNSS 20th International Technical Meeting of the Satellite Division, Fort Worth, TX, USA

Wells D, Lindlohr W, Schaffrin B, Grafarend E (1987) GPS design: undifferenced carrier beat phase observations and the fundamental differencing theorem. Frederiction: Department of Surveying Engineering, University of New Brunswick

Wübbena G (2012) RTCM State Space Representation (SSR) Overall Concepts Towards PPP-RTK. PPP-RTK & Open Standards Symposium, March 12-13 2012, , Frankfurt, Germany

Wübbena G, Schmitz M, Bagge A (2005) PPP-RTK: precise point positioning using state-space representation in RTK networks. In: Proceedings of ION GNSS. pp 13–16

Wuhan University (2017) School Of Geodesy and Geomatics,Wuhan University. In: Wuhan University. http://en.sgg.whu.edu.cn/. Accessed 19 Aug 2017

Yao Y, Zhang R, Song W, et al (2013) An improved approach to model regional ionosphere and accelerate convergence for precise point positioning. Advances in Space Research 52:1406–1415. doi: 10.1016/j.asr.2013.07.020

Zhang B, Teunissen PJG, Odijk D (2011) A Novel Un-differenced PPP-RTK Concept. The Journal of Navigation 64:S180–S191. doi: 10.1017/S0373463311000361

Zhang X, He X (2015) BDS triple-frequency carrier-phase linear combination models and their characteristics. Science China Earth Sciences 58:896–905

Zumberge JF, Heflin MB, Jefferson DC, et al (1997) Precise point positioning for the efficient and robust analysis of GPS data from large networks. Journal of Geophysical Research: Solid Earth (1978–2012) 102:5005–5017